Universidade de Aveiro
2019
Departamento de Eletrónica,
Telecomunicações e Informática

João Bernardo Santos Caiado

Wideband antenna arrays for mmWaves

Agregados de antenas de banda larga para ondas milimétricas

João Bernardo Santos Caiado

Wideband antenna arrays for mmWaves

Agregados de antenas de banda larga para ondas milimétricas

Dissertação apresentada à Universidade de Aveiro para cumprimento dos requisitos necessários à obtenção do grau de Mestre em Engenharia de Eletrónica e Telecomunicações, realizada sob a orientação científica do Professor Doutor João Nuno Pimentel da Silva Matos, do Departamento de Eletrónica, Telecomunicações e Informática da Universidade de Aveiro e do Doutor Tiago Miguel Valente Varum, investigador no Instituto de Telecomunicações.

o júri / the jury

Presidente / President

Professor Doutor Adão Paulo Soares da Silva
Professor Auxiliar, Universidade de Aveiro

Vogais / Examiners comittee

Professor Doutor João Nuno Pimentel da Silva Matos
Professor Associado, Universidade de Aveiro (orientador)
Doutor Daniel Filipe Simões Malafaia
Radar Systems Architect, Vestas Portugal, Lda

Agradecimentos / Acknowledgements

Em primeiro lugar, agradeço aos meus pais por me terem ajudado a chegar até aqui, por todos os sacrifícios que tiveram que fazer por mim, por todo o apoio que me deram e por estarem lá sempre para me incentivar a ser uma melhor pessoa.

A toda a minha família agradeço por me ajudarem a tornar na pessoa que sou hoje e por terem tomado sempre conta de mim, especialmente, ao Gonçalo e o Miguel. Não posso deixar de agradecer à minha avó Bia, por ter tomado sempre conta de mim quando os meus pais não podiam e por estar lá sempre que precisei de alguma coisa.

Aos meus orientadores, o Professor João Nuno Matos e o Dr. Tiago Varum, agradeço por toda a disponibilidade e por todo o apoio dado durante o período da dissertação.

Ao Instituto de Telecomunicações, e a toda a sua equipa técnica, deixo o meu agradecimento por todo o suporte dado durante a realização desta dissertação.

A todos os meus amigos que me acompanharam durante todos estes anos, agradeço toda a amizade e todos os momentos divertidos que passamos, sei que nem sempre fui fácil de aturar, mas vocês foram incríveis e demonstraram ter uma grande paciência. Em especial, agradeço todo o companheirismo que as pessoas nos grupos "quem é o Zé?" e "acaba a tese mariana" demonstraram todos estes anos.

Por último, a todos os que estiveram no laboratório de RF agradeço por alegrarem os dias de trabalho.

Palavras-chave: Ondas milimétricas, agregado logarítmico periódico, 5G, banda larga, agregado microstrip

Resumo

Nesta dissertação foram desenvolvidos sete agregados de antenas de banda larga usando uma estrutura logarítmica periódica. Um dos agregados opera na banda de frequência C, enquanto os restantes operam na zona de frequência das ondas milimétricas.

Os seis agregados construídos para as ondas milimétricas distinguem-se entre si pela altura do substrato usado e pelo número de elementos radiantes que compõem cada um. Assim sendo, para cada uma das duas alturas de substrato estudadas, foram desenvolvidos agregados com cinco, sete ou nove elementos.

A largura de banda foi sempre influenciada pelas alterações feitas e todos os agregados tem um valor diferente para esta característica. No caso do agregado para a banda C o valor obtido foi de 572 MHz. Nos agregados desenvolvidos com um substrato mais fino, e para frequências mais altas, obteve-se 5.388 GHz, 6.873 GHz e 9.266 GHz respetivamente para os agregados de cinco, sete e nove elementos. Por outro lado, usando um substrato mais espesso, estes valores foram melhorados para 6.899 GHz, 8.282 GHz e 12.07 GHz, respetivamente.

Keywords mmWaves, Log-periodic array, Wideband, 5G, microstrip antenna array

Abstract

In this dissertation seven wideband log-periodic arrays were developed. One of the arrays operates in the C band of frequency, while the others operate in the mmWaves band.

The six arrays constructed for the mmWaves distinguish themselves by the height of the substrate and the number of patches. Two different heights were used and for both arrays with five, seven and nine elements were developed.

The bandwidth was influenced by the changes made in the arrays. In the case of the C band array the bandwidth obtained was 572 MHz. In the arrays developed with a thinner substrate, for the mmWaves, the bandwidths obtained were 5.388 GHz, 6.873 GHz and 9.266 GHz, for the five, seven and nine elements arrays, respectively. Comparatively, the arrays made with a thicker substrate enhanced the bandwidth to 6.899 GHz, 8.282 GHz and12.07 GHz, respectively.

Contents

List of Figures

List of Tables

List of Acronyms

3D	:	*Three-dimensional*
4G	:	*Fourth generation of mobile communications*
5G	:	*Fifth generation of mobile communications*
CST	:	*Computer Simulation Technology*
DETI	:	*Departamento de Eletrónica, Telecomunicações e Informática*
EHF	:	*Extremely High Frequency*
FCC	:	*Federal Communications Commission*
IEEE	:	*Institute of Electrical and Electronics Engineers*
IoT	:	*Internet of Things*
IT	:	*Instituto de Telecomunicações*
LEO	:	*Low Earth Orbit*
mmWaves	:	*Millimeter Waves*
VNA	:	*Vector Network Analyser*
VSWR	:	*Voltage Standing Wave Ratio*

Chapter 1

1 Introduction

1.1 Context and Motivation

In modern times, wireless communications are a part of our daily lives, yet none of this would be possible without Maxwell, Hertz, and Marconi[1]. Their contributions in the fields of electricity and magnetism proved the existence of electromagnetic radiation. Such accomplishment confirmed that radio communication could be attainable, and this was the first step in the world of wireless communications systems [1].

The wireless communications definition is a mode of data transmission between two or more devices over a specific distance, and where no cables or wires are required [2]. There are many different types of wireless communications, and all of them consist of broadcasting electromagnetic signals through the air [3].

Using these kinds of systems has some advantages when compared with wired communications. One example of how a person can benefit more from these systems is, for example, when they suffer an accident in a remote area. In this case, the emergency number is always available to ask for help.

Despite having significant advantages, some drawbacks need attention. For instance, hacking a wireless signal is easy. Hence security algorithms were developed to attenuate this problem and prevent privacy attacks. Furthermore, interferences in communications can occur [4].

Antennas are a fundamental element in wireless systems, seeing that it is through them that signals are received and transmitted. However, sometimes antennas are not able to fulfill the requirements desired for a specific type of communication, then, and to achieve these demands, array antennas were developed [5].

Microstrip antennas have become very popular over the years. Some contributing reasons are the fact that these types of antennas are small and compact, which allows easy incorporation into everyday systems [1]. Regardless of this, microstrip antennas have a low gain, and with the fifth generation of mobile communications (5G) just around the corner, and due to higher attenuation in these systems, this characteristic could be a downfall [5]. Howbeit, microstrip arrays can overcome this problem and still have relatively similar dimensions.

Wideband antennas and arrays can be very helpful in 5G. Due to having more bandwidth than other antennas, they can cover some needs of 5G systems, being the most obvious the capability of providing extreme data rates [6].

More and more each day, people try to upgrade the existent wireless communications systems. 5G arrival brings new light to this field of research and intends to provide more benefits when compared with the previous ones.

Despite that, 5G systems need to migrate to the millimeter waves (mmWaves) band, since there is a need for broader bandwidth that it is no longer available in the current frequency spectrum. With that in mind, new structures of antennas and arrays need to be explored to fulfill 5G demands.

1.2 Objectives

This dissertation objective is to produce a viable wideband antenna array that works in the mmWaves band. To achieve this, the array should provide the maximum possible bandwidth, while maintaining both gain and efficiency values constant throughout the range of operation, meaning that the values cannot abruptly change and should be similar in the frequency range. Furthermore, the direction of the main radiation lobe should be maintained apart from frequency, in other words, main lobe position should be the identical at every frequency.

A research was made to understand better the work previously done on this matter. There were many articles found on the subject, but not all of them could be applicable for mmWaves applications. To reach the final array a lower frequency array was developed to find a good structure capable of working in the mmWaves band. Eventually, a reliable solution was found and used to develop the arrays of this dissertation. Lastly, a study was

developed to see different ways to elevate the array performance and take full advantage of the structure used in this dissertation, and create the best wideband array possible, being this the main intention of this dissertation.

1.3 Dissertation Structure

This section presents the structure of this dissertation. Each chapter is briefly explained to give the reader a better insight on what information they present.

This document is divided into the following 7 chapters:

- **Chapter 1** – is the ongoing chapter. It aims to present the topic of this dissertation and frame it in everyday life.
- **Chapter 2** – gives a better knowledge of some necessary concepts of this dissertation. The state-of-art is presented to finalize the chapter.
- **Chapter 3** – describes all theoretical and simulation steps necessary to design the arrays of this dissertation.
- **Chapter 4** – shows the implementation of each array, includes the optimized design parameters of the arrays.
- **Chapter 5** – shows the simulation results of all arrays. It helps to characterize each overall array performance.
- **Chapter 6** – presents all measured results of the arrays and compares them with their simulated results.
- **Chapter 7** – the last chapter of the dissertation. It presents some considerations and conclusions on the work done, as well as some ideas for future improvements.

1.4 Original Contributions

The work done for this dissertation provided the opportunity to publish one scientific paper:

- J. Caiado, T. Varum and J. N. Matos "Ultra-wideband Log-periodic antenna array for LEO Constellations Terminals", submitted and accepted for the Best Student Paper Award of 13º Congresso do Comité Português da URSI.

Chapter 2

2 Overview on 5G and antennas

This chapter aims to give the reader a better understanding of some concepts of this dissertation, as well as some work done on the main focus, wideband arrays. With this in mind, first mmWaves will be introduced, in addition to some reasons for the recent migration to this band. Second, a presentation of arrays and their characteristics is made. To conclude, a state-of-art review regarding wideband arrays is shown to provide a better insight into this technology.

2.1 Millimeter-Waves as a solution for 5G systems

In 1973 the first mobile phone call using a wireless phone was made. This event marks the birth of handheld phones [7]. We have come a long way since that event, and currently, we already use the fourth generation of mobile communication (4G). Each generation has lasted roughly 10 years, and with the beginning of the new decade in 2020, we are expected to reach a new generation, 5G [8].

5G systems are no longer just an idea [9]. The growing number of users in mobile communications and the increase in the data transmission speed, i.e., higher data rate, led 4G systems to their limit [10]. This reality boosted mobile systems to the next level and in this sense, 5G is no longer a trend, it is an imminent reality.

It has been known for a while the desire to implement well-suited systems for the internet of things (IoT) applications [11]. While 4G still has a very important deficient for those applications, the high value of latency (>10 ms), 5G intends to considerably lower this value, and the intention is to achieve 1ms of latency, which is ten times lower [12]. Considering this, much more reliable systems can be accomplished, and concepts like smart cars and other smart cities technologies can be employed.

However, some parameters still need to be worked on to perfect 5G. One of the most discussed topics is the frequency band in which 5G should operate. To increase the speed of data transmission we have two possibilities, either increase spectrum efficiency or the spectrum bandwidth [13]. Looking into both possibilities, increasing the spectrum bandwidth is a more natural and more direct approach when compared with the other one. Nevertheless, wide bandwidth is only available at the mmWave band, so a migration into this band is mandatory to solve the problem.

MmWaves region is considered to be between 30 GHz and 300 GHz and is sometimes called extremely high frequency (EHF) band [14]. This band is underdeveloped, mainly because the federal communications commission (FCC) prohibited its use, making her a solution to create 5G systems. The main advantage of migrating to this band is the wider bandwidth since it can deal with the high data rates in the future of mobile communications [14]. Another factor that plays in favor of the mmWaves is the decrease of component sizes, making them smaller and lightweight means all systems composed will be more compacted.

Although there are definite advantages, there are still some points that can cause problems. This band presents higher free-space loss resulting in weak links. So, weather effects cause more degradation to the transmitted signal, which means the system range can decrease [15]. To surpass these issues high gain antennas and highly directive antenna arrays should be designed, with smaller elements using several elements array is not a problem.

Another point that the 5G systems aimss to improve is the data rates in their communications systems, meaning that the information per second transmitted is going to be enhanced, providing faster communication systems. To achieve this, systems need to cover more bandwidth than ever. One way to solve that problem is through the development of wideband arrays which cover the necessary bandwidth.

Figure 2.1 presents the level of attenuation per kilometer (km) across frequency. In the mmWaves region there are some problematic points, starting at 60 GHz where the attenuation value of 10 dB/km is very high. However, around 30 GHz and 80 GHz the values of attenuation are acceptable and systems can be created in these bands.

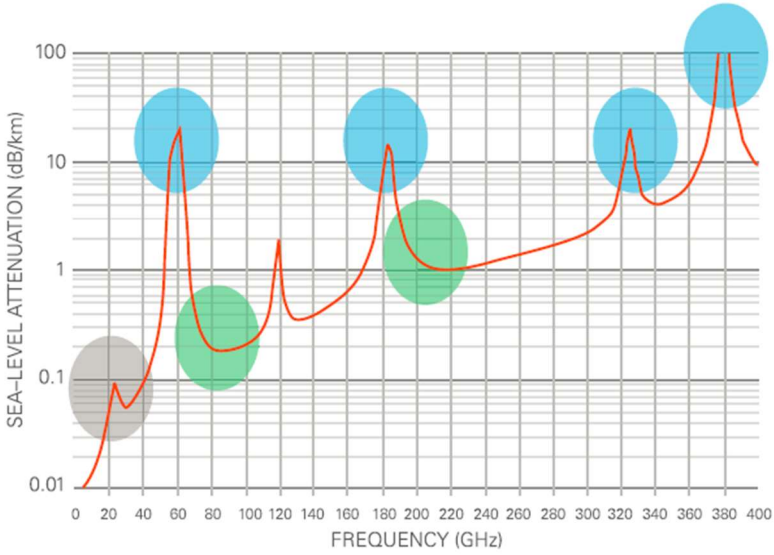

Figure 2.1: Attenuation of a wireless signal as a function of frequency. Adapted from [16].

5G systems, mainly antennas and sensors, are expected to be very small and unnoticeable to people to assure a more connected world, accomplishing IoT. So, antennas for this application should be, besides small, also compact.

2.2 Antenna Arrays: basic concepts

The Institute of Electrical and Electronics Engineers (IEEE) defines an antenna as "*a means for radiating or receiving radio waves.*" [5]. By way of explanation, an antenna is a receiving/transmitting device of the system, being a transitional structure between free-space and guiding device.

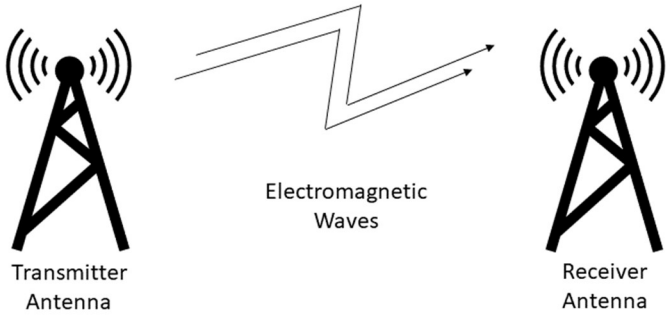

Figure 2.2: Simple diagram of communication between antennas.

Althrough this is antennas pure definition, nowadays, they no longer are a simple transmitting and receiving elements. Their role improved and at this time they become an integral part of wireless systems and help to enhance their overall performance [1].

Even though antennas are essential for wireless systems, there are some constraints that single elements antennas have difficulty to overcome. For instance, after being developed for a specific frequency, most antennas have fixed characteristics, like the radiation patterns, and lack the flexibility to alter these parameters [1]. Another common problem in single element antennas is their low gain, which is a factor to take into account on mmWaves applications. So, one solution to surpass these constraints is to add more elements, creating an antenna array.

An antenna array comprises in many antennas elements that are placed in a determined way to provide the desired characteristics, to achieve those characteristics what can be varied is the feed network and relative position of each patch, this makes them factors to consider in array designing [5].

In spite of correcting some single element problems, antenna arrays are not perfect and possess some handicaps of their own. In some cases, it is necessary to develop complex feeding networks, which makes it harder to adapt an array. Consequently, the bandwidth suffers some limitations with this issue, limiting array capabilities. Despite this, some arrays can overcome this problem, especially in the case of low bandwidth with the design of wideband array [1].

There are many basic configurations an array may adopt. These include collinear arrays, broadside arrays, End-fire arrays, Yagi-Uda arrays, and Logarithmic Periodic (log-periodic) arrays, to mention some [17]. Each one has a specific goal in mind on their design, from high gain to high bandwidth, amongst others. Knowing how these configuration options work allow us to learn more about arrays and to understand how to optimize an array to the various characteristics. Figure 2.3 shows some arrays mentioned before.

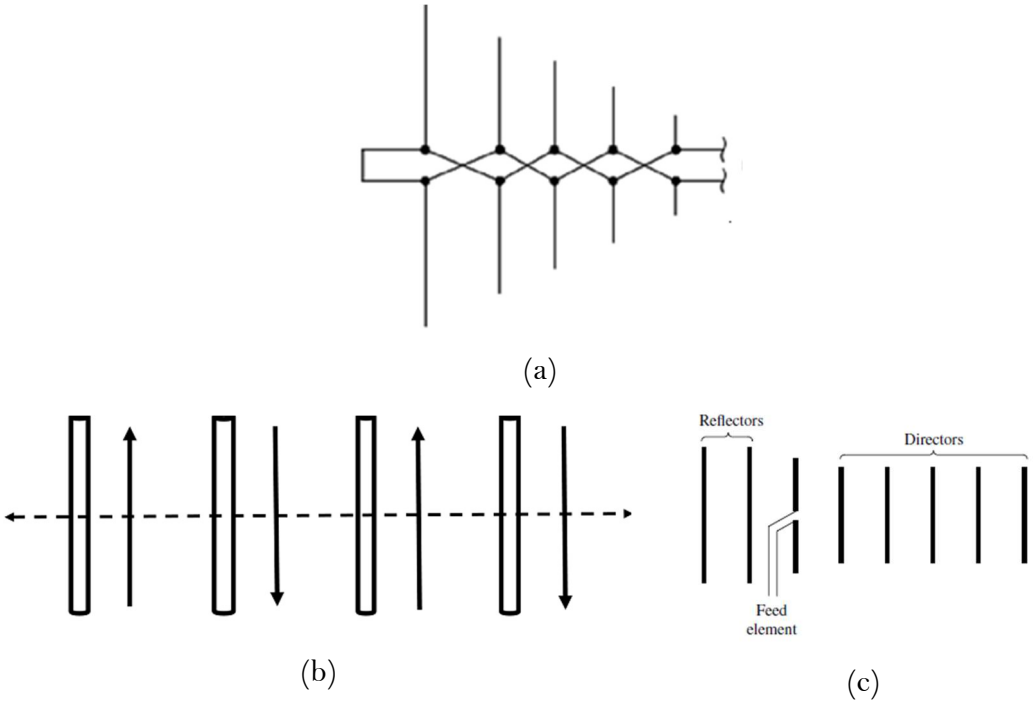

Figure 2.3: Examples of arrays: (a) Logarithmic periodic array; (b) End-fire array; (c) Yagi-Uda array (All adapted from [5]).

2.2.1 Fundamental parameters of an antenna array

Throughout this section, some parameters of arrays and antennas were mentioned without being explained. Therefore, some fundamental parameters that help to evaluate arrays performance will be introduced. There are numerous parameters to be considered. However, only a few of them will be presented:

- **Bandwidth:** Range of frequencies where the characteristics (such as input adaptation, gain, directivity, and more) have good performance when compared with the central frequency characteristics. Regarding this dissertation, to delimitate the range of frequencies, the factor used was S11 lower than -10 dB. This factor is presented in [18].
- **Directivity:** it is the parameter that measures the concentration of an antenna radiation pattern in a particular direction. When the directivity has a higher value, it means that the beam is focused in that specific direction. The directivity value comes in dB, and this is because the value is a ration between radiation intensity of an isotropic antenna, which radiates equally in any direction, and the radiation intensity of an antenna in a specific direction when both radiate the same power.

- **Efficiency:** It is a ratio between power delivered to an antenna and power radiated from an antenna. Sumss up how the losses influence, this may be due to impedance mismatch, dielectric, or even conduction.
- **Gain:** Gives us the power transmitted by an antenna in a specific direction when compared with an isotropic antenna. Although it was a similar definition to the directivity, gain considers antenna losses, while directivity does not.
- **Radiation patterns:** represents the radiation properties as a function of a direction at a fixed distance, it should be a significant enough distance to be considered a far-field, usually represented in a three-dimensional (3D) graph, despite existing other ways to represent them. These properties include Radiation intensity, field strength, power flux density, phase, directivity, or polarization. Figure 2.4 shows some different ways to represent a radiation pattern, including 3D representation.

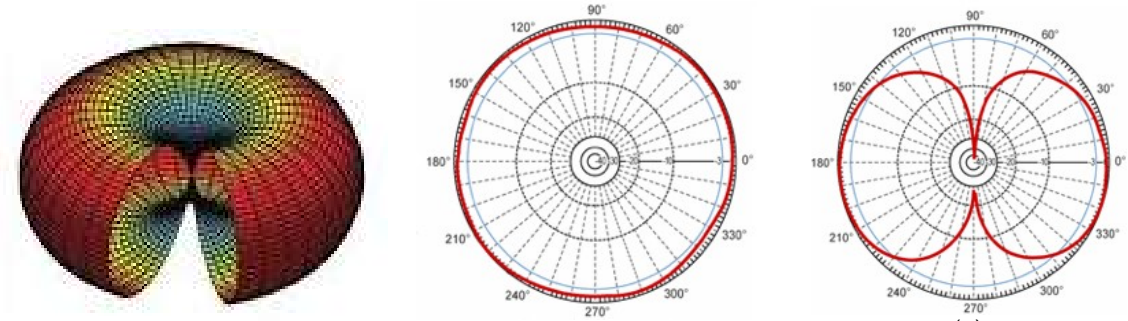

Figure 2.4: Various examples of a radiation pattern representation ; (a) 3D representation; (b) polar representation on plane phi equal 0; (c) polar representation on plane phi equal 90; (figure (a) was adapted from [19], figures (b) and (c) from [20]).

2.2.2 Concept of Wideband

An antenna or an array is always manufactured to work in a certain frequency or band of frequencies. The definition of bandwidth was previously presented. However, the various classifications were not. The Bandwidth of an antenna can be classified into three groups Narrowband, Wideband, and Ultra-Wideband. In the bandwidth there are two bounding points that define the range of operation and are designated as f_h, for upper frequency of the operating band, and f_l for lower frequency of the band. These points have great importance in calculate some characteristics needed to classify the bandwidth. The

Centre frequency or the fractional bandwidth need both points to calculate their values, and these properties distinguish the antenna bandwidth classification. Between all the properties mentioned, the fractional bandwidth is one of the possible criteria used to clarify the classification. The fractional bandwidth is defined as a ratio of the signal bandwidth to the average frequency and is calculated by the equation (2.1) [18].

$$B_f = 2 \text{ x } \frac{f_h - f_l}{f_h + f_l} \tag{2.1}$$

With the result obtained through (2.1) and using the parameters of classification presented in Table 2.1, the array or antenna categorized in one of the three categories presented.

Table 2.1: Classification of a system based on bandwidth covered. (Adapted from [21])

Band Type	Fractional bandwidth
Narrowband	$0.00<B_f\leq 0.01$
Wideband	$0.01<B_f\leq 0.25$
Ultra-Wideband	$0.25<B_f<2.00$

Through those parameters the system is classified in terms of bandwidth characteristic.

2.3 State-of-the-art of wideband antenna arrays

This chapter introduced the concept of wideband as well as the need to migrate to mmWaves. Looking more to what was explained in mmWaves section, especially in the needs of 5G systems, it is seen that to reach the desired data rates systems will require more bandwidth. In other words, wideband arrays and antennas capable of covering a large amount of bandwidth must be designed.

Throughout the years, some ideas were introduced to create wideband arrays. Log-periodic arrays are one of the most popular concepts to develop these kinds of structures. Nevertheless, there are other alternatives. In the following section, log-periodic

arrays will be explored appropriately, given their importance within this dissertation. Firstly, some examples of them will be presented, as well as other approaches to achieve wideband.

Starting with [22]. Here a log-periodic series fed array was designed. It is a simple configuration that consists of a junction of a patch and line as an individual element that is scaled, resulting in a periodic structure (Figure 2.5). Looking into the prototypes developed, it can be observed some interesting results. The simplicity of the array gives a good perception of how periodic structures work. In terms of bandwidth, all prototypes results show they can have an excellent performance in that field. Nonetheless, without a printing and experimental part, it leaves some doubts on how well this would work.

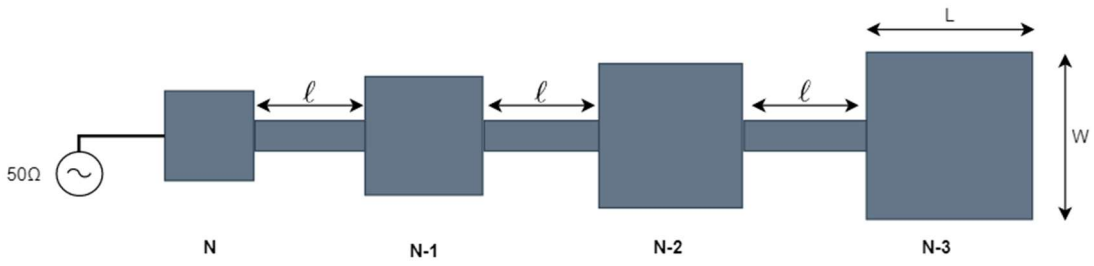

Figure 2.5 - Example of a 4-element array that can be constructed based on the concept in [22].

Another take on log-periodic arrays was presented in [23]. It is very similar when compared to the previous one, being that the only difference is that instead of a square patch the element used is a bow-tie (Figure 2.6). Changing the element shape worsens the bandwidth covered and adding more elements does not enhance this factor. However, S11 seems more stable than before, which may be an advantage. Likewise, there were only simulations to analyse, leaving many doubts about their real performance.

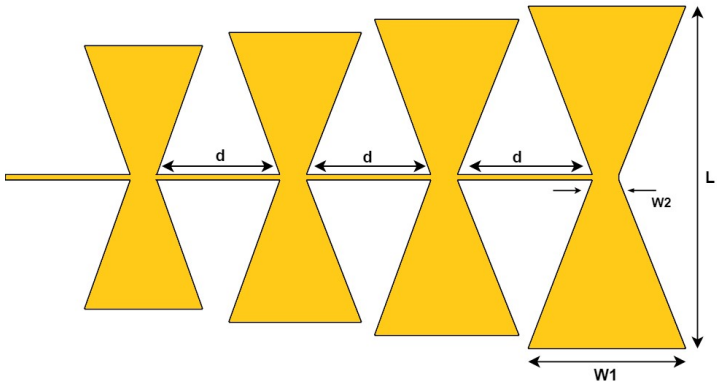

Figure 2.6: Example of an array structure developed in [23].

Continuing in same the topic, in [24] a dipole log-periodic array (Figure 2.7) is presented. Compared to the other two arrays this has some particularities to consider. First, besides the scaling factor between elements, now it is presented a spacing factor that determines how the distance between elements is scaled. Second, each part of the dipoles has an element in the upper layer and one in the lower layer, and a 50 Ω impedance line feeds all of them. Lastly, when evaluating the performance, particularly the bandwidth, instead of observing the S11 graph, the authors choose to simulate the Voltage Standing Wave Ratio (VSWR) graph. By doing this they intend to see the impedance behaviour and prove that this array has a wide impedance bandwidth.

Taking what was described before and examining the results, it can be seen a great impedance performance from 1.4 GHz to 12 GHz. The VSWR value is lower than 2, and this is observed in the simulation and the measurements. Given that in this case gain and efficiency were tested, there are two more parameters to evaluate. Both factors have good agreement between simulation and measurements. In terms of gain, it has an average value of 4.51 dBi that is good for a dipole array with this number of elements, but if applied in the mmWaves band, this characteristic should be enhanced.

In terms of efficiency, on average, its value is 75.32 %, but it decreases with frequency growth. In general, for the purpose application, it has an excellent performance, however, the gain should be enhanced if it was intended to migrate to the mmWaves band.

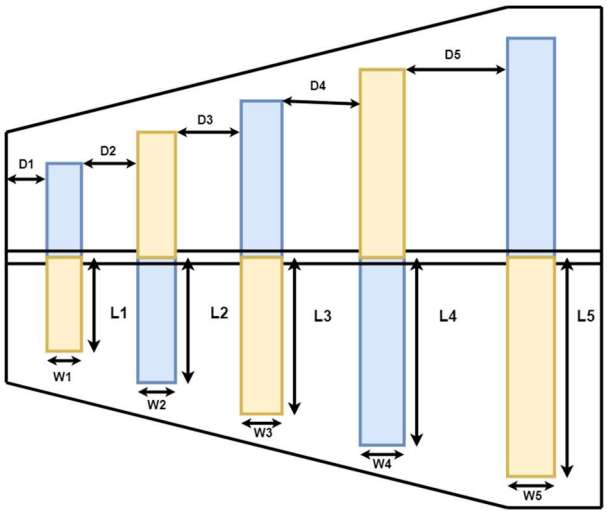

Figure 2.7: Representation of an array designed in [24].

Despite the advantages seen above about log-periodic structures, when implemented in the mmWaves region, these antennas present several limitations. In [25] a new dipole log-periodic array is presented. This structure gathers some of the Yagi-Uda

antennas' characteristics with the log-periodic structures, forming a new array. In essence, it is a log-periodic dipole array with three directors, their size decreases from one to another, helping to improve the gain. One more detail is the fact that each pair of dipoles is separated in the middle and each side is fed individually.

Reflecting on the simulation results, this array covers 5.5 GHz of bandwidth, from 23 GHz to 28.5 GHz, and its gain is higher than 9.74 dBi throughout the frequency band, this means that adding directors proved a valuable choice. Regardless, without implementing and measuring the array, it is uncertain how much will differ the results.

After presenting arrays designed with common logic, it is time to present some different ways to construct a wideband structure. For instance, in [26] an elliptic dipole antenna array was produced. The only peculiar point of this arrays is the fact that in each dipole one side is in the upper layer and the other in the lower layer.

Observing the results, it exists a good agreement between simulation and measurements in all specifications presented. In the VSWR graph its seen a good bandwidth between 1 GHz and 2.5 GHz, considering that is necessary that VSWR is lower than 2.0. Viewing the gain measurements, a small variation occurred throughout the frequency band. Despite that, the smallest value is 14 dB, which is quite good. In general, the array present was good attributes and it would be interesting to implement him in a higher frequency band to see its behaviour.

Furthermore, a wideband array can be created for a specific purpose. One article that demonstrates that is [27], in this case, it was developed a 1x2 U-Slotted wideband array with the objective of energy harvesting. The fundamental element is a rectangular patch, where the slot is applied, this brought some virtues to the performance, at least in the simulations presented. The antenna frequency range varies between 1.46 GHz and 6.15 GHz, while the peak gain is 13.86 dB. Although this result seems appealing, there are some points into take in account.

First, measurements were not performed, and it leaves some doubts on the real performance, especially in the S11, because it seems that between the two peaks the value is too close to -10 dB. Second, the gain is not presented in the same band has the S11 graph. Third, observing the gain, these values are volatile. Ultimately, this array works for its purpose, however, it cannot be applied to mmWaves applications due to some problems in its performance.

In [28] a 2x2 ultra-wideband array was designed to work in see-through-wall scenario. This array has rectangular elements that are fed by a corporate microstrip structure. Also, the ground plane was slotted underneath the placement of each element.

Doing this provided noteworthy results. A bandwidth of 8.2 GHz was achieved, from 2.73 GHz to 10.93 GHz, which is an excellent value. Moreover, the gain varies between 8.5 dBi and 14.6 dBi. Even though there is a variation, their values are high, which makes it easier to insert in a system. In general, it seems like a functional array, despite is missing some measurements to confirm the validity of the simulations.

As stated before, arrays have some advantages over antennas. One clear example of that appears in [29]. This article presents an array based on a wideband antenna. The need for increasing the gain presented by a single element led to the implementation of an array. An omnidirectional modified circular patch was used as an element, and the array feeding network is a modified power divider. This exciting method used to create the array gave some intriguing results. It has a bandwidth of 64%, from 3.1 GHz to 10 GHz, and a gain higher than 7.9 dB. Designing and testing this array at a higher frequency range should be considered to better understand its behaviour.

Not all antenna applications need wideband characteristics, or sometimes it is not the primary need. For example, in [30] accomplishing wideband characteristics was not a priority, yet it was achieved. The primary goal of this array was to possess a high gain. To ensure this a multilayer array was designed. The top layer consists of the patches, while the bottom layer is the feed network, between them is a shared ground plane. To connect the feed network to the patches shorting vias were used. A 4x2 array was designed and tested. Having 15.6 dB of gain is quite good, adding to that a good bandwidth of at least 4 GHz, from 4 GHz to 8 GHz, and it seems like a good solution for a wideband array. Although this is true, as the purpose was not to possess a high bandwidth, it would be interesting to make an array with that objective using this idea.

Despite existing a lot of different forms to create an array, dipole arrays are one of the most popular. For instance, in [31] a new approach to dipole arrays is introduced. This method intends to improve the gain of a typical dipole array. The structure consists of a microstrip series-fed magnetic dipole array, with the peculiarity of each dipole having one edge opened and the other three shortened. Through this concept, both bandwidth and gain improve. The frequency range starts at 5 GHz and stops at 6.7 GHz, about 28.6%, and

an average gain of 10.4 dBi, which is admirable for a dipole array, and could be used for other purposes.

Antennas and arrays can have different types of polarization depending on their applications and their dominant characteristics. In [32] a circularly polarized array is presented. The authors obtained this polarization by cutting the corner of square patches, and then use a sequential-phase feeding network to feed the patches. A 2x2 array was designed and measured with this concept. By using circular polarization there is a new simulation that needs to be made in order to validate the performance, which is an axial ratio simulation.

For an antenna with circular polarization to be considered functional its axial ratio must be lower than 3 dB. So, to be considered a wideband array a correlation between the axial ratio and S11 is necessary. Looking into the results provided by this array and shown in the article, it is observed that between 5.25 GHz and 5.95 GHz is the only band that both S11 and axial ratio are fulfilling their requirements, meaning it covers 700 MHz, which is equivalent to 12.7 % of bandwidth. This value is a little when compared with some of the arrays presented earlier. Nevertheless, it is a workable wideband array, and the gain presented is impressive, about 11.5 dBic, making it a viable array.

Sometimes the application intended for an array imposes some limitations that need to be surpassed. For example, in [33] an array for satellite communications was proposed. In the case of this application, high gain and directional radiation patterns. The designed element for the array is an antipodal Vivaldi element.

Three different arrays were tested to see which would provide better results, each of them with 8 elements. First, a not bent linear array, then a 20 cm diameter-bender array, and to finalize a 30 cm diameter-bended. In terms of bandwidth, all of them operate between 8 GHz and 12 GHz, this is the only frequency band shown. The array considered as the first choice in this article was the 20 cm diameter-bended array because it provides a gain of 17.6 dB without degradation of radiation patterns. Granting all this, it would be interesting to have some measurements to compare with this simulation results to confirm their legitimacy.

Until now, all arrays presented operate at lower frequency bands. However, the objective of the dissertation is to produce an array that operates at the mmWaves band. Thereupon, some examples of works done in this band will be shown to give an idea of some characteristics of the band.

Beginning with [34]. This article has a different approach since it transforms a narrowband Franklin array into a wideband, flexible, and leaky-wave antenna assembly. By doing this they retain the desired gain performance of a typical Franklin array and add the feature of beam steering over a wide bandwidth. Each section of the array is composed of a stub and a patch.

To convert into a wideband array, the lengths of stub and patch were adjusted according to the upper and lower frequency, respectively, meaning they limit their bandwidth. The behaviour between resonances is adjusted by altering patch width, stub width, and the gap between folded stubs. A 6-element array was constructed to test the concept. The frequency range intended was 24 GHz to 30 GHz. Observing the simulation and measurements a slight difference between them. Nonetheless, a bandwidth of 5.4 GHz was achieved, from 24.6 GHz to 30 GHz.

Throughout this band, the gain is higher than 6 dB, with a peak gain of 8.3 dBi at 28 GHz. One point that deserves consideration is the fact that in frequencies above 29 GHz the efficiency decreases to values lower than 40%. Overall, this array has a nice performance and is applicable to mmWaves applications.

Identically to the preceding work, in [35] an array for mmWaves applications is shown. Its design consists of an array that has patches with inset feed and have parasitic patches stacked on top of them. Each element and feed is arranged in an alternating out-of-phase 180-degree rotation sequence that helps to improve the radiation patterns symmetry and decrease mutual coupling.

A 16-element array was simulated and measured to validate the idea. The bandwidth measured was exciting, from 24.35 GHz to 31.13 GHz (24.4%), and its maximum gain of 19.88 dBi demonstrates that this array has good qualities for mmWaves applications, though 16 elements were necessary to achieve these results.

The last array that will be presented in this section is [36]. Similar to both previous arrays, the frequency band of this array is mmWaves band, although this array works at a higher frequency. The array design is a simple array comprising on a 16x8 array with rectangular patches fed with a quarter wavelength transformer in a 1x8 feeding network.

Looking into the simulation results, we see that the bandwidth covered is 5 GHz. In all other arrays presented, if they possess this characteristic it would be quite good, do their lower frequency bands. However, 5 GHz in 80 GHz it is only equivalent to 0.06 of fractional bandwidth.

Nevertheless, if we investigate the previous section, this array is still considered wideband through the definition presented, even though the fractional bandwidth is low. There is only one more parameter presented in the results, which is the gain. The maximum value of that component 14 dBi, which is a good value for that component.

To sum up, there are many ways to design wideband arrays and their development depends on the application for which they are designed. This demonstrates the usefulness of these arrays and how important they are to this field of work.

Chapter 3

3 Design of wideband antenna array

In this chapter, the steps necessary to build the arrays implemented in this dissertation will be described. From theoretical calculations to implementation in Computer Simulation Technology (CST). The design was based on [37][38], with very similar calculations and designs.

3.1 Log-periodic Array Concept

Log-periodic arrays are characterized for their ability to provide broad bandwidth and be directive [39]. However, the bandwidth that these structures can provide depends on numerous factors, including the number of patches or scaling factor.

The log-periodic array was based on the principle of the frequency-independent antenna, which consists of the multiplicity of adjacent cells. This principle states that each cell is scaled in dimensions relative to its adjacent one by a scaling factor, τ, this parameter is constant throughout the array, leading it to become a periodic structure where the ratio factor is based on the frequency logarithm [38]. Taking that into consideration, we can relate the patch length (L), the width (W) and, for this scenario, the inset feed (I_m), of two adjacent elements the following way:

$$\tau = \frac{L_{m+1}}{L_m} = \frac{W_{m+1}}{W_m} = \frac{I_{m+1}}{I_m} \tag{3.1}$$

So, if we multiply or divide all dimensions by τ it scales into itself with element m becoming element $m+1$ and the element $m+1$ becoming $m+2$, and so on. Using this kind of self-scaling properties implies that a factor of τ relates all frequencies (as depicted in

equation (3.1)) and will have the same radiation properties. Considering f_1 as a starting point, the relationship is as follows:

$$f_2 = \tau \times f_1 \tag{3.2}$$

$$f_3 = \tau^2 \times f_1 \tag{3.3}$$

This correlation leads to the following relation:

$$\ln \frac{f_2}{f_1} = \ln \tau \tag{3.4}$$

$$ln \frac{f_3}{f_1} = 2 \times ln \tau \tag{3.5}$$

Proving the existence of a logarithmic relationship between frequencies.

3.2 Theoretical Procedure

3.2.1 Microstrip Antenna Design

For any array patches are fundamental. With that in mind, creating a square patch is a good starting point. This can be accomplished theoretically using equations ((3.6) through ((3.10).

$$\lambda = \frac{c}{f_o} \tag{3.6}$$

$$W = \frac{\lambda}{2} \times \sqrt{\frac{2}{\varepsilon_r + 1}} \tag{3.7}$$

$$\varepsilon_{eff} = \frac{\varepsilon_r}{2} + \frac{\varepsilon_r - 1}{2} \times \frac{1}{\sqrt{1 + 12 \times \frac{h}{W}}} \tag{3.8}$$

$$\Delta L = 0.412 \times \frac{\left(\varepsilon_{eff} + 0.3\right) \times \left(\frac{W}{h} + 0.264\right)}{\left(\varepsilon_{eff} - 0.258\right) \times \left(\frac{W}{h} + 0.8\right)} \tag{3.9}$$

$$L = \frac{\lambda_o}{2 \times \sqrt{\varepsilon_{eff}}} - \Delta L \tag{3.10}$$

In table 3.1 there is a presentation of all parameters needed to calculate a patch and what they represent.

Table 3.1 - Parameters required for the calculation.

Parameter	Description
f_o	Frequency of operation
c	Speed of light in vacuum($3x10^8$ m/s)
λ	Wavelength value at the frequency of operation
ε_r	Relative permittivity
W	Width of patch
h	Dielectric height
ε_{eff}	Effective dielectric constant
ΔL	Length extension caused by the fringing effect
L	Length of patch

Using the above equations, we obtain the patch length, and since the patch needs to be squared, the width value is the same. A representation of the square patch is in Figure 3.1.

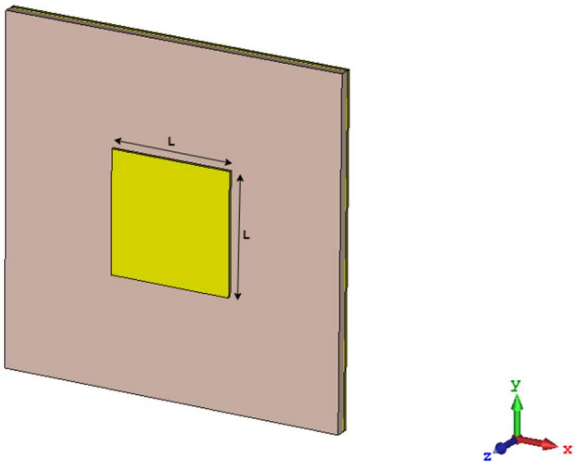

Figure 3.1: Side view of a squared patch.

3.2.2 Antenna feeding

The next step in the array is to design the feed of each patch. This is a particular point on the array since the method used to feed each patch is inset feed. The impedance varies through the patch. The minimum value occurs in the middle (0,0), and in the extremities, it has is maximum. Knowing this, the first thing to do is calculate the patch impedance in its extremities, Z_{in}. We can do that using the following equation:

$$Z_{in} = 90 \times \frac{\varepsilon_r^2}{\varepsilon_r - 1} \times \left(\frac{L}{W}\right)^2 \tag{3.11}$$

After obtaining this value, using equations (3.12 and (3.13, the length of the cut, R_{in} seen in Figure 3.3, can finally be determined.

$$Z_o = Z_{in} \times \cos\left(\frac{\pi \times R_{in}}{L}\right)^2 \tag{3.12}$$

$$R_{in} = \frac{L}{\pi} \times \cos^{-1}\left(\sqrt{\frac{Z_o}{Z_{in}}}\right) \tag{3.13}$$

Here Z_o is the pretended impedance to achieve doing this cut.

Regarding the width, W_c, literature does not present a consensus formula for its determination. For this reason, the value of W_c used was half of the width of the line connected to the patch. This value variates throughout the arrays developed.

One point to keep in mind is that after the first test with inset feed, there a slight deviation occurs in the frequency of operation. This must be taken in account, and adjustments in patch size should be made [5].

After applying the cut, a quarter wavelength is connected to patch, which connects it to the feed line. This quarter wavelength needs to be designed with same the impedance as the rest of the structure, and this happens because both feed line as well as the patch connection point possess the same characteristic impedance. This can be proven through the quarter wavelength equation.

$$Z_{\lambda/4} = \sqrt{Z_{in} \times Z_L} \tag{3.14}$$

As before mentioned, Z_{in} is the impedance of the feed line, Z_L the impedance at patch point connection, and $Z_{\lambda/4}$ is what needs to be dimensioned. Throughout all designs, these three values of impedance will be the same to make a perfect match.

Figure 3.2 and Figure 3.3 illustrate an element created and used on the array and shows all points addressed in this subsection.

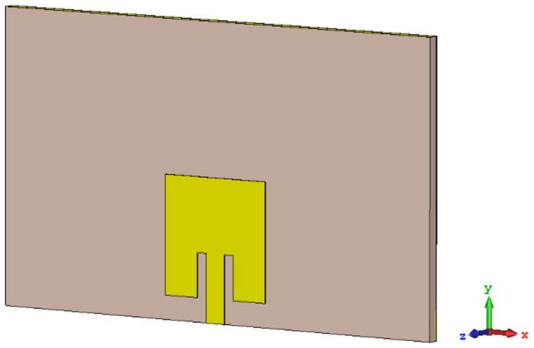

Figure 3.2: Side view of a typical element from the array.

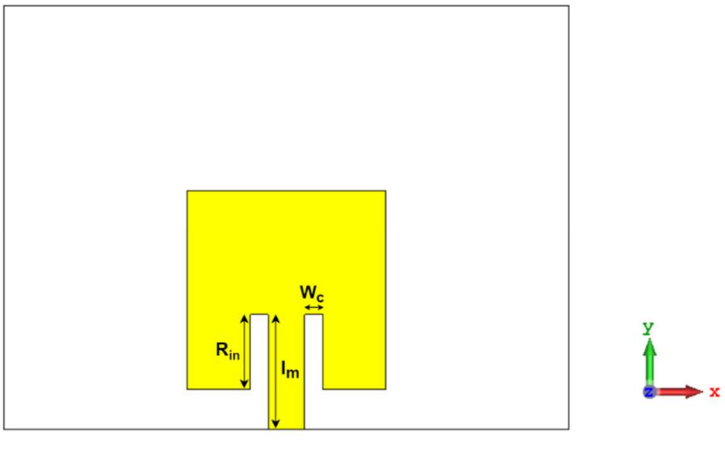

Figure 3.3: Top view from a typical element with the variables.

3.2.3 Array Structure

To turn individual elements patches into an array there is only one thing remaining, the main feed line. This line is used to connect Patches and is defined by the sum of the distance between two consecutive patches (Figure 3.4). So, we need to calculate the distance between them, d_m. To scale these distances, we must have some considerations into account. The most important is *"The distance between element (m) and element (m+1) is determined according to the next higher frequency element of the antenna. The input looking into the next higher frequency must be high impedance before the next element (m+1) is connected to the schematic diagram. In this model the distance between two patches is not necessarily half wavelength and varying periodically."* And it was presented by M.K.A. Rahim in [37]. The previous

quote states that the distance between elements can be problematic. Not only there is no direct formula to calculate these values, but also there is no standard relationship between them that could simplify their design. So, to speed up the designing process, CST optimizer was used to try and achieve the desired results.

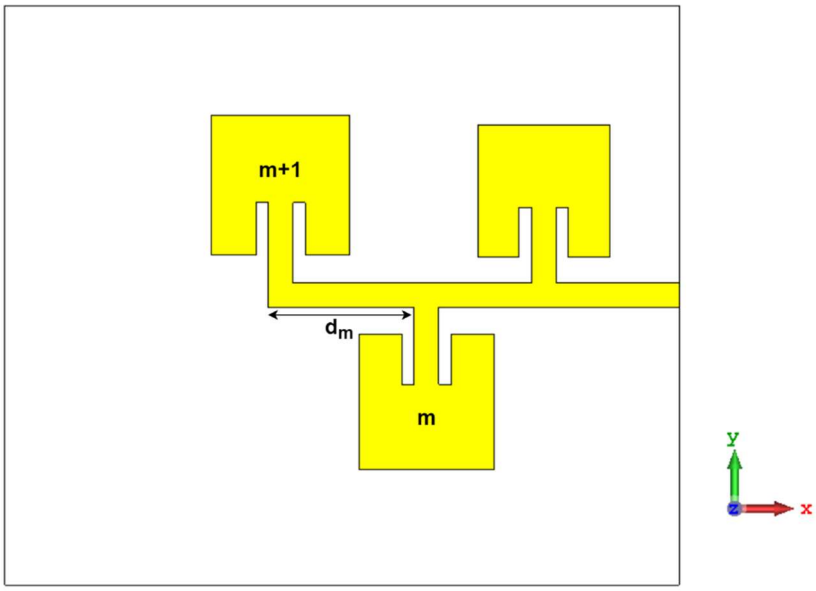

Figure 3.4: Schematic to present the distance.

3.3 CST Process

In the previous section, theoretical calculations and other considerations needed to design the array were presented. This section presents the entire process used in CST to produce the final product.

3.3.1 Patch Simulation

As mentioned in section 3.2.1, a square patch was developed. However, since theoretical calculations are not always reliable, we developed a test to see if calculations match the simulation. This test consisted of producing an element with the same dimensions as in calculations and then adding a half-wavelength line in the centre of one side of the element. The line was added to test the patch in the centre of the substrate, as it would be used frequently. A representation of the structure simulated is in Figure 3.5.

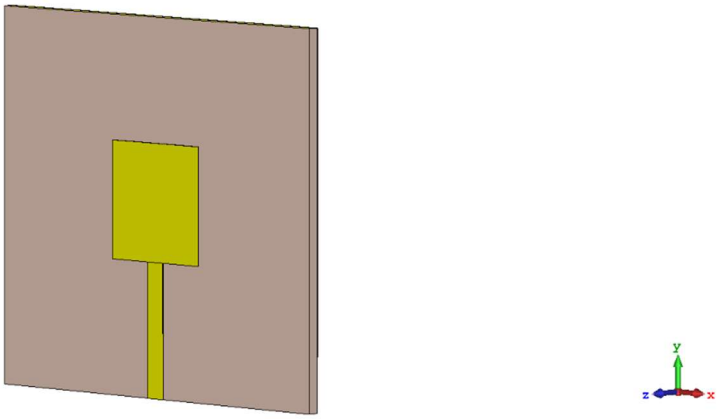

Figure 3.5: Schematic used to test the square patch.

With this test we expect the answers about two problematics. The first consists of observing the frequency of operation, verify if theoretical calculations for the length are correct. Secondly, the simulation tells us the impedance of the patch, which is more reliable than the one obtained theoretically. Moreover, it helps to calculate the inset feed length.

3.3.2 Inset Feed simulation

After having the element ready, we can go to the next step, inset feed. As beforementioned inset feed is designed to reach a specific impedance point of the patch. When simulating this situation, we need to take into account that what is shown on the smith chart must be as close as possible to the desired impedance. In terms of the testing procedure, to see patch impedance at the inset point, we connect a half-wavelength line. This method was chosen because if we connect one side of these lines to a patch of a specific impedance, and at the other point we connect a waveguide port, the impedance seen in port is the same as in the patch. This allows us to have the impedance at that point. Figure 3.6 shows the exact model used in CST to simulate and verify the inset point.

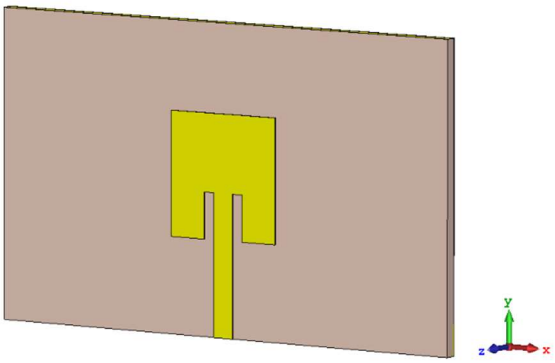

Figure 3.6: Element with inset fed used in tests.

3.3.3 Complete array Simulation

Now that elements are composed, the next step is to form the array. As mentioned before, designing distances between patches is not a straightforward process. To achieve the desired results, it was necessary to conduct optimization of the values of the distances. This can be an impractical and slow process. However, due to lack of information on how to perfect those values, this solution proved to be quite helpful.

CST provides a large variety of optimizers. Since there were several hypotheses from where the best option had to be chosen, it was used the information provided by the website of CST software to learn more about their optimizers, and which one would be better and faster for this situation[40]. After a careful study, the genetic algorithm was chosen because it provided better results whit many variables, a crucial point since the number of distances between elements is numerous and increases along with the number of patches.

After deciding which optimizer to use, there are only two more details before being able to perform a full test. The first is the size limit that the connection lines can have, and the second is the goals that will be imposed on the optimizer. The first case was relatively simple, the maximum size each line can have is half-wavelength, given that the wavelength is related to the lower frequency patch to which the line is attached. The minimum value is typically quarter wavelength except for the line proceeding the last patch. In this case, the lowest value must take into account the fact that the patch cannot leave the substrate plane, becoming a limitation for that specific line.

The second case is straightforward as well. Because of design constraints given by the scaling factor, when defining the targets, since the array is log-periodic, the frequency

of operation of each patch should be one. One last goal is bandwidth, and the objective is to ensure that the array is wideband.

Figure 3.7 shows an example of a 5-element array that was implemented in CST. In this image, it can be observed periodic factor of the patches, and also the non-existent relation of distances between elements.

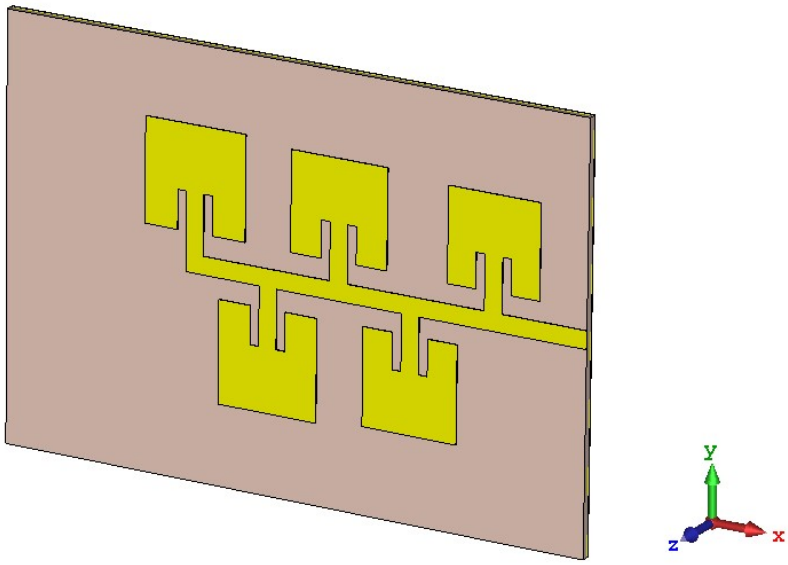

Figure 3.7: Schematic of one array used in the testing phase.

Chapter 4

4 Implementation

In this chapter all arrays developed during this dissertation will be presented, taking into account all of them used chapter 3 designing method, with slight variations between arrays. Each array as a subchapter for itself and contains its theoretical results.

4.1 Wideband array at C-Band

It was said in the previous chapter, that the arrays built were based on articles from other authors. Using this methodology facilitates the development of final work. However, not all articles detail every parameter needed to compose their work or do not present some results necessary to make some comparisons. So, to understand how the array is designed and to create a logical design method for all arrays, a lower frequency array was constructed, near 5 GHz, C band. The develop array has a scaling factor of 1.025 and five patches.

4.1.1 Substrate

Creating a microstrip antenna without a substrate is impossible. In that regard, choosing an adequate substrate for each antenna is very important. A substrate with low losses and permittivity that is constant throughout the frequency are some of the factors that should be taken into consideration upon selection. In this first array, the substrate used was Rogers RO4725JXR, this substrate has low losses and at the frequency of operation has a constant permittivity value which is good. The main characteristics of the material are shown in Table 4.1:

Table 4.1: Rogers RO4725JXR substrate characteristic taken from [41].

Characteristic	Value	Units
ε_r	2.55	-
h	0.78	mm
tan(δ)	0.0026	-
Copper thickness	17.5	μm

Where ε_r is Dielectric constant, h is the substrate's thickness, and tan(δ) is the loss tangent of material.

4.1.2 Array design

As explained before, each element is developed individually. Every parameter needs to be optimized to guarantee that all patches work at their specific frequency. To start these adjustments, the first thing that needs to be observed is the impedance of each patch. This factor influences some posterior calculations, mainly inset feed. Therefore, by doing these simulations and using the values obtained the inset feed calculations will be more accurate, and fewer adjustments will be needed.

In Table 4.2, both the theoretical impedance value and the result obtained in the simulation for all patches are presented, as well as respective frequency of operation.

Table 4.2: Comparison between the calculated and simulated impedance of each patch.

Frequency of operation (GHz)	Z_{in} (Theoretical) (Ω)	Z_{in} (Simulated) (Ω)
4.759	235.11	333.08
4.878	235.32	331.74
5.000	235.53	328.32
5.125	235.76	327.52
5.253	235.99	325.75

A difference between theoretical and simulated values exists. However, in terms of calculations this difference proves to be relevant and, due to that, the values used for the proceeding calculations were the simulated ones.

Although the width and length were used in the previous simulation, their value is only presented in this segment. This is because by performing inset feed, the frequency of operation suffers a small shift, and it is necessary to readjust width and length, showing both values is unnatural.

Regardless, using the value mentioned above of impedance simulated, it was determined the length of inset, and then optimized to achieve optimum point. Table 4.3 shows all parameters of each element. Both the length of patch and length of the cut have their theoretical calculations presented in order to provide a comparison between calculations and simulation results.

Table 4.3: Presentation of the values of each parameter of all elements.

Frequency (GHz)	L=W (Theoretical) (mm)	L=W (optimized) (mm)	R_{in} (theoretical) (mm)	R_{in} (optimized) (mm)	W_c (mm)	I_m (mm)
4.759	19.421	19.430	7.251	6.850	1.045	10.770
4.878	18.938	18.940	7.065	6.730	1.045	10.450
5.000	18.466	18.480	6.877	6.490	1.045	10.260
5.125	18.006	18.030	6.702	6.440	1.045	9.950
5.253	17.556	17.590	6.529	6.181	1.045	9.800

Observing the table, it is seen a good agreement between theoretical and optimized values of length, even though that the length of cut has a slightly more significant difference between both values whereas the length of patch values are almost the same.

In Figure 4.1, a graph with the reflection coefficient (S11) simulation results of each patch is presented, still using a half-wavelength line. For each frequency, the S11 minimum is near -40 dB, which means that the adaptation is good, and it gives some expectations to see the behaviour of the full array.

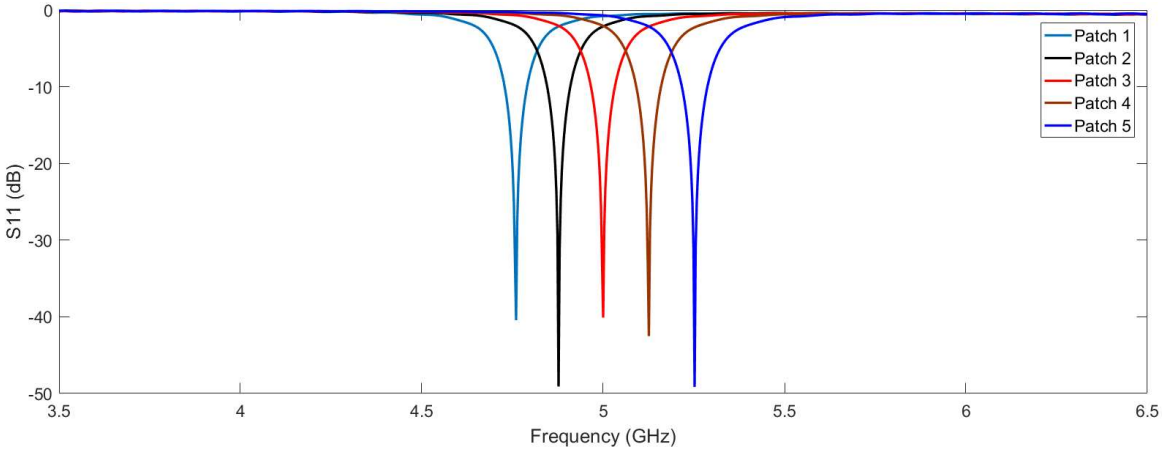

Figure 4.1: S11 of each patch created for the 5-element array.

After pulling off each adaptation, the next step is joining them to create the array. All patches are connected to the main feed line. In this case, the impedance of the line is 50 Ω. It was said in the previous chapter that there is no logical relationship between distances and that reason led to the usage of an optimizer to calculate the best values for each distance. So, in Table 4.4 shows the best values of each distance obtained through optimization.

Table 4.4: Distances between elements of the array.

	Distance (mm)
Patch 1 to Patch 2	18.983
Patch 2 to Patch 3	20.297
Patch 3 to Patch 4	19.867
Patch 4 to patch 5	18.406
Patch 5 to feed	15.333

The first thing to notice in the table is the lack of relation between distances. There is no logical connection between them. With this nonexistence of coherence, using the optimizer proved a correct solution. Figure 4.2 represents the full array tested in CST. In this simulation the space needed for the connector was already inserted to assure that the array response is not influenced.

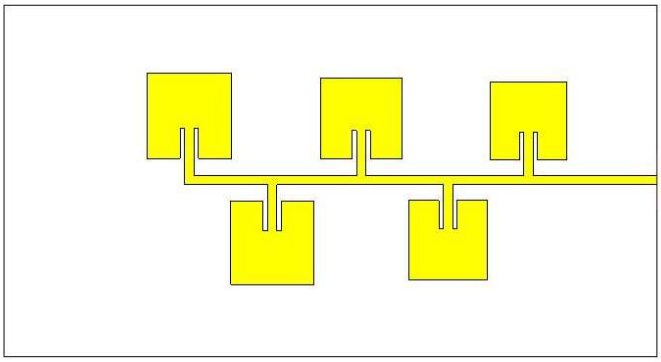

Figure 4.2: C band array simulated in CST.

4.2 Arrays for mmWaves applications: Thinner substrate

In this dissertation it is intended to study the influence of the substrate's height in the production of antenna arrays. In this sense, by using the same dielectric substrate, with two different heights, six antenna arrays were designed, three for each case.

Typically, antenna arrays produced with thicker substrates tend to have higher gains. On the other hand, the overall performance of the array in terms of bandwidth and log-periodic response might be affected by this change.

Consequently, this analysis allows to discover which substrate can be used to construct log-periodic structures in order to bring out their fullest performance.

The arrays produced for mmWaves applications have a scaling factor of 1.04 and with a central frequency of 28 GHz. These characteristics are maintained throughout the arrays developed with the different substrates to make a fair comparison between the results obtained.

4.2.1 Substrate

Similar to the other array, the first topic to be mentioned is the substrate. It was used the Rogers RO4350B. A suitable substrate possessing excellent characteristics of operation in the mmWaves band. Its characteristics are presented in Table 4.5.

Table 4.5: Rogers RO4350B substrate characteristic used during this simulation [42].

Characteristic	Value	Units
ε_r	3.48	-
h	0.254	mm
tan(δ)	0.0037	-
Copper thickness	17.5	μm

Where ε_r is relative permittivity, h is the substrate's thickness, and tan(δ) is the loss tangent of material. This substrate has a more constant permittivity at higher frequencies and maintains a low loss factor.

4.2.2 5-element array

For this section of mmWaves wideband arrays, three different arrays were designed. As explained before, all of them have the same scaling factor of 1.04. So, the only thing that variates throughout designs is the number of elements.

For this first array, the number of elements chosen was five. This allows a small comparison with the previously designed array. Testing this array is a start since the objective is to provide as much bandwidth as possible and for that to happen, elements will be added to enhance the bandwidth.

Applying the same process as before, the impedances of each patch were simulated to be further used to calculate the insertion length. After calculating the theoretical value and through simulation, these values were obtained and are shown in table 4.6.

Table 4.6: Comparison between the calculated and simulated impedance of each patch of a 5-element array for mmWaves applications.

Frequency of operation (GHz)	Z_{in} (Theoretical) (Ω)	Z_{in} (Simulated) (Ω)
25.88	326.57	330.62
26.92	327.56	328.77
28.00	328.62	337.64
29.12	329.75	348.96
30.28	330.94	362.53

Comparing both values, a small variation between values is observed. Nevertheless, using both values in the equation of the patch would give similar values. To proceed to the next step, it was decided that the value of impedance used throughout calculation was the simulated Z_{in}.

Proceeding with the design, the next step is making each element of the array. As the same case as preceding array, these structures were designed to have a 50 Ω feeding line, and consequently a quarter wavelength of 50 Ω and insertion point where the patch has 50 Ω.

Adjusting the various parameters at higher frequencies becomes a little more complicated. Table 4.7 shows every single factor of an element for each frequency and compares some with their theoretical value.

Table 4.7: Values of the variables needed to design an element.

Frequency (GHz)	L=W (Theoretical) (mm)	L=W (optimized) (mm)	R_{in} (theoretical) (mm)	R_{in} (optimized) (mm)	W_c (mm)	I_m (mm)
25.88	3.015	3.042	1.113	1.130	0.256	1.749
26.92	2.894	2.924	1.078	1.086	0.256	1.682
28.00	2.777	2.811	1.039	1.046	0.256	1.617
29.12	2.665	2.702	1.003	1.006	0.256	1.555
30.28	2.558	2.598	0.969	0.971	0.256	1.495

Observing table 4.7 some particularities can be detected. First, all patch lengths and length of quarter wavelength transformers have approximately the same factor between them, 1.04. Second, the length of cut is not a periodic value, but this parameter was never intended to be periodic inasmuch as giving a perfect matching point, in this case, to be as close as 50Ω as possible.

Another point that deserves acknowledgement is the width of cut, W_c, this value is the same for every single element, and in this case, the value is half of a 50Ω impedance line width.

After showing these factors, Figure 4.3 shows each frequency S11 value.

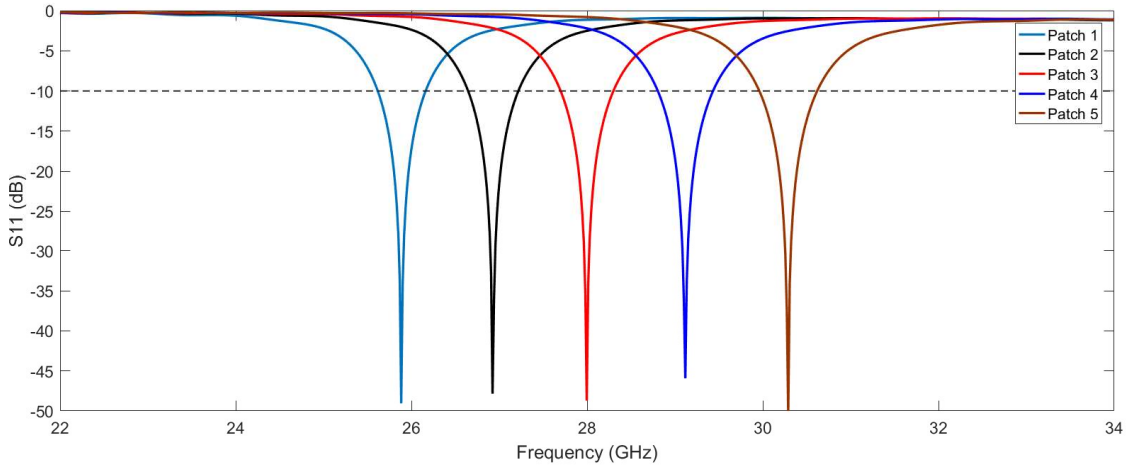

Figure 4.3: Individual S11 of each Patch.

At every frequency of operation, a good adaptation was achieved. This means that the value of impedance achieved with inset is close to 50 Ω.

With all these parameters optimized and the patches providing good S11 joining them to form an array is the following stage. Using CST optimizer window values of distances between patches were uncovered. Table 4.8 shows these values.

Table 4.8: Optimized values of the distances between patches.

	Distance(mm)
Patch 1 to Patch 2	3.2118
Patch 2 to Patch 3	3.0508
Patch 3 to Patch 4	2.8138
Patch 4 to patch 5	2.5145
Patch5 to feed	2.6122

After obtaining these values a full simulation of the array was performed, a representation of this array is in Figure 4.4, the simulation contemplated the holes and space needed to insert the connector to make a full comparison with the arrays that will be subsequently presented.

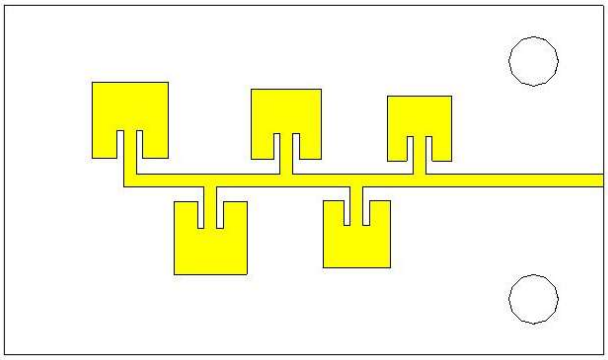

Figure 4.4: 5-element array simulated in CST.

4.2.3 7-element array

The 5-element array had good results and proved a reliable solution in its simulations. However, the bandwidth provided is still low. To try and improve this factor, a 7-element array was designed. For this array the five patches previous developed were used and added two more, one at a lower frequency (24.89 GHz) and one at a higher frequency (31.49 GHz), maintaining a factor of 1.04.

Table 4.9: Comparison between the theoretical and simulated impedance for 24.89 GHz and 31.49 GHz.

Frequency of operation (GHz)	Z_{in} (Theoretical) (Ω)	Z_{in} (Simulated) (Ω)
24.89	325.63	338.75
31.49	332.22	378.59

Table 4.9 shows the difference between impedance theoretical and simulated of each patch. For 24.89 GHz the difference between impedances is not significant, it is less than 15 Ω, for 31.49 GHz a higher difference is perceptible, almost 50 Ω. This shows the necessity of performing the simulation to obtain the various impedances.

Table 4.10: Parameters of the designed elements.

Frequency (GHz)	L=W (Theoretical) (mm)	L=W (optimized) (mm)	R_{in} (theoretical) (mm)	R_{in} (optimized) (mm)	W_c (mm)	I_m (mm)
24.89	3.141	3.168	1.176	1.175	0.256	1.819
31.49	2.454	2.500	0.937	0.933	0.256	1.438

In Table 4.10 the parameters of the complementing array are shown. All theoretical and optimized values are in concordance, despite having slight deviations.

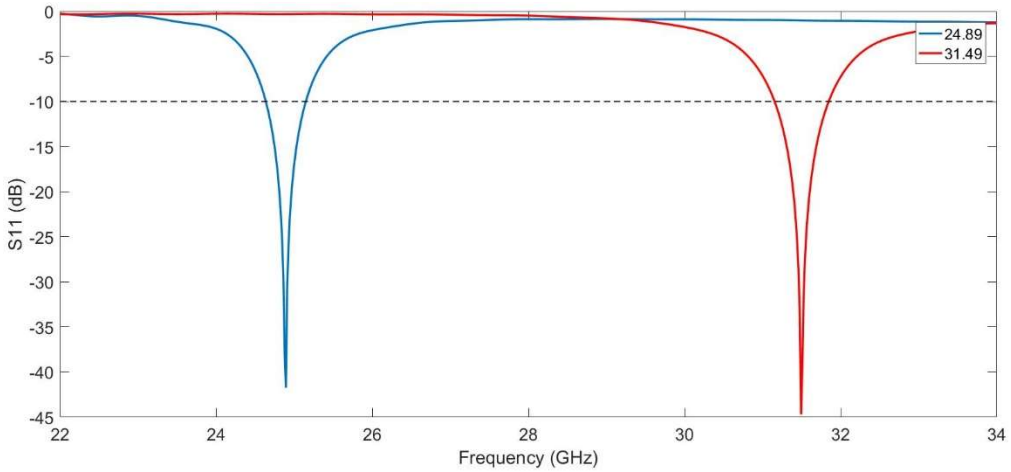

Figure 4.5: S11 of the patches added to form the 7-element array.

In Figure 4.5, both patches S11 is presented. Both values are close to -40 dB, which means a good adaptation was made, and that the value of the impedance is close to 50 Ω.

In this case to, transform into an array every distance between patches needs to be optimized again, values used in the 5-element array do not apply to this array.

Table 4.11: Distances between Patches for the 7-element array.

	Distance (mm)
Patch 1 to Patch 2	3.4624
Patch 2 to Patch 3	3.0483
Patch 3 to Patch 4	2.8673
Patch 4 to Patch 5	2.7065
Patch 5 to Patch6	2.5456
Patch 6 to Patch 7	2.3689
Patch 7 to feed	2.5672

Some considerations can be made about these values presented in Table 4.11. First, a lack of logic between values is easily noticed. Second, these distances are all different from the previous ones, which means that it is harder to get an expression or logic to execute in these arrays, meaning that without optimizers these arrays might not be possible to design. Figure 4.6 shows the 7-element array simulated in CST. This simulation contemplates the necessary space and holes to insert the connector.

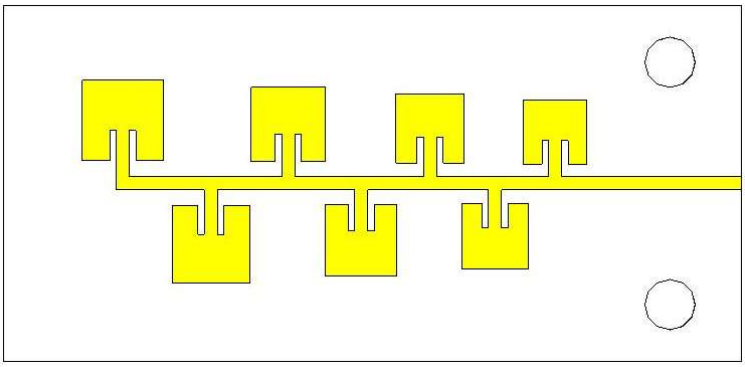

Figure 4.6: 7-element array simulated in CST.

4.2.4 9-element array

After developing the 7-element array and seeing that its performance was good, it was decided to add two more patches to enhance the bandwidth covered, since the objective of this dissertation was to design an array that could cover as much bandwidth as possible.

The added elements operate at the frequencies of 23.93 GHz and 32.75 GHz. The reason for adding one patch at lower and one at a higher frequency is to maintain 28 GHz as the central frequency of the array.

Maintaining the logic described in the design, the first step is to simulate the elements to acquire its impedance.

Table 4.12: Theoretical and simulated impedance of the patches design for the 9-element array.

Frequency of operation (GHz)	Z_{in} (Theoretical) (Ω)	Z_{in} (Simulated) (Ω)
23.93	324.75	353.51
32.75	333.57	385.69

Impedance measured is not the same as expected from theoretical calculations. The results possess a variation in comparison with their theoretical values and verified that by doing this simulation and gather the impedance the next calculations of the inset will be more precise and fewer adjustments will be needed.

Now using values obtained through the simulations, the rest of the values needed to design an element of the array were calculated and optimized through simulations. Table 4.13 presents those values.

Table 4.13: Values for each parameter of the two elements design to complete the 9-element array.

Frequency (GHz)	L=W (Theoretical) (mm)	L=W (optimized) (mm)	R_{in} (theoretical) (mm)	R_{in} (optimized) (mm)	W_c (mm)	I_m (mm)
23.93	3.272	3.295	1.234	1.223	0.256	1.892
32.75	2.354	2.397	0.901	0.897	0.256	1.382

A good agreement between calculated values and optimized values is seen. Throughout all arrays, the width of cut, W_c, was always the same and its value corresponds to half of the width of a 50 Ω impedance line.

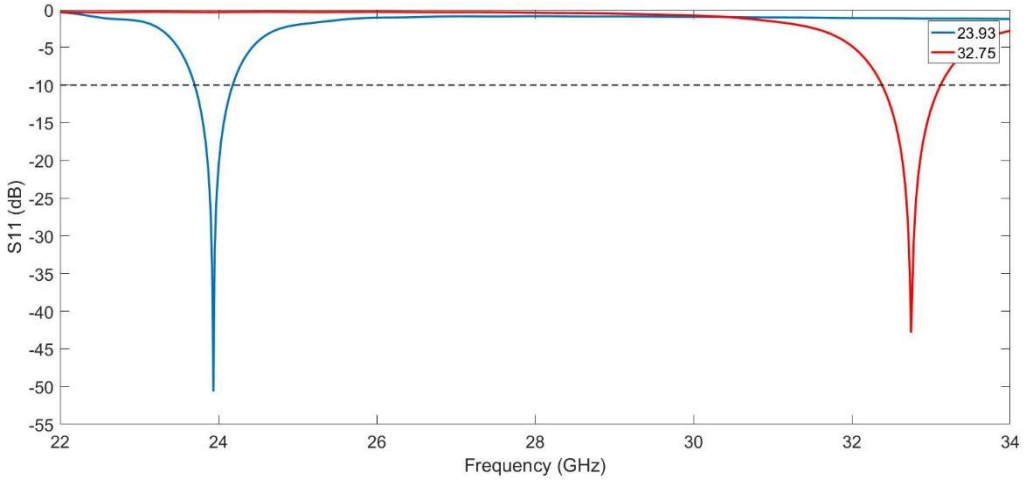

Figure 4.7: S11 of each element added to create the 9-element array.

Figure 4.7 shows the S11 of each element added to create this array. Both have functional adaptations, especially at 23.93 GHz that has an S11 below -50 dB, which means its adaptation is very close to the desired 50 Ω.

Now that all nine elements were designed it's time to produce the final array. As in previous arrays, an optimization was made to find the best distance between patches. Such optimization has the goal of providing wideband characteristics and maintaining the log-periodic characteristic of the array.

Table 4.14: Distance between Patches of the 9-element array.

	Distance (mm)
Patch 1 to Patch 2	3.1550
Patch 2 to Patch 3	3.2821
Patch 3 to Patch 4	2.9203
Patch 4 to Patch 5	2.8510
Patch 5 to Patch6	2.8951
Patch 6 to Patch 7	2.1008
Patch 7 to Patch 8	2.4489
Patch 8 to Patch 9	1.9045
Patch 9 to feed	2.4089

Observing Table 4.14 becomes clear that there is no logic between distances. The values can increase or decrease, and those variations are not constant. Above all, without

using the optimizer these values would be almost impossible to obtain. A representation of this array is shown in Figure 4.8.

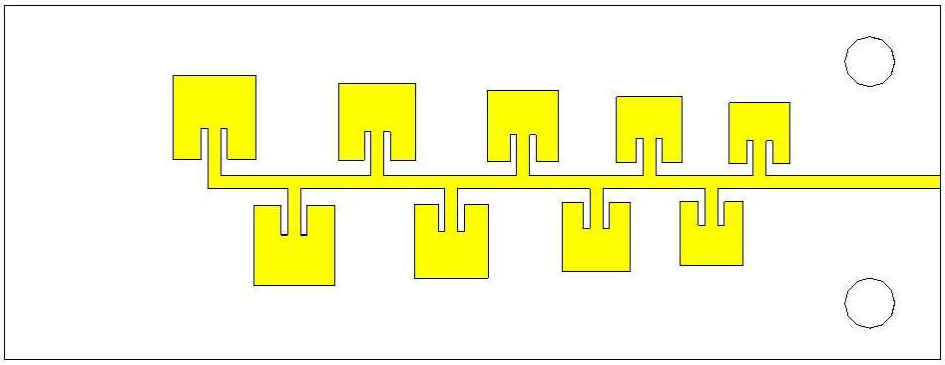

Figure 4.8: 9-element array simulated in CST.

4.3 Arrays for mmWaves applications: Thicker Substrate

Previously three arrays were presented as solutions to be used in mmWaves applications. However, using such a thin substrate might not be the best choice since the gain decreases with this characteristic. So, and to make a comparison with the previous arrays, three new arrays were developed using a thicker substrate to see how some characteristics in the overall performance are affected.

These arrays have the same scaling factor of 1.04 to make a direct comparison with previous ones designed.

4.3.1 Substrate

For this set of arrays, the substrate used was the same as the previous ones presented, but with a significant difference, the thickness of the substrate. By altering this parameter many things will change. Table 4.15 shows the new parameters of the substrate.

Table 4.15: Rogers RO4350B substrate characteristic used to make this array [42].

Characteristic	Value	Units
ε_r	3.48	-
h	0.762	mm
tan(δ)	0.0037	-
Copper thickness	35	μm

As explained before, only the thickness is different. By doing this some structural changes needed to be made. With this change, a 50 Ω line became too wide and influenced the performance of the array. So, instead of using a 50 Ω structure, it was decided that 90 Ω would be used as impedance of reference and then adapted using a quarter wavelength transformer at the centre frequency, the reason for choosing 90 Ω is the fact that a line with this impedance has a width that does not influence the patches operation.

4.3.2 5-element array

Many things will change in the simulations but measuring the impedance of each patch is still the first step to begin the design in CST. In this case, the half-wavelength line impedance is 90 Ω, as in the rest of the simulations throughout these arrays' designs, because it does not influence patch operation, while a 50 Ω line would influence because of its width.

Table 4.16: Comparison between Calculated and simulated impedance of the patches of the 5-element array.

Frequency of operation (GHz)	Z_{in} (Theoretical) (Ω)	Z_{in} (Simulated) (Ω)
25.88	396.40	246.56
26.92	401.65	249.61
28.00	407.22	257.95
29.12	413.12	268.15
30.28	419.35	274.06

Observing Table 4.16, it is clear that exists a difference between the theoretical and simulated value of patch. This difference influences all posterior calculations.

Table 4.17: Parameters of each patch design for this 5-element array.

Frequency (GHz)	L=W (Theoretical) (mm)	L=W (optimized) (mm)	R_{in} (theoretical) (mm)	R_{in} (optimized) (mm)	W_c (mm)	I_m (mm)
25.88	2.7035	2.7869	0.7935	1.1137	0.2200	1.7720
26.92	2.5796	2.6717	0.7609	1.0469	0.2200	1.7000
28.00	2.4606	2.5650	0.7354	0.9872	0.2200	1.6320
29.12	2.3465	2.4622	0.7117	0.9330	0.2200	1.5670
30.28	2.2372	2.3660	0.6841	0.8851	0.2200	1.5050

By doing a careful observation of Table 4.17, it can be seen that the length of the cut value, R_{in}, has a more significant difference between calculated and optimized values than in the previous arrays presented. This may be explained by the fact that the impedances have a more considerable difference between them, meaning an error upon measuring this value.

Length of patch as slight difference between theoretical and simulated value but this can be explained by the variation of R_{in}. As mentioned previously, by doing an inset feed a deviation is caused in the frequency of operation and adjustments are made, and due to the fact that the R_{in} value has a more significant difference in the theoretical and simulated values, this causes a deviation in the length value.

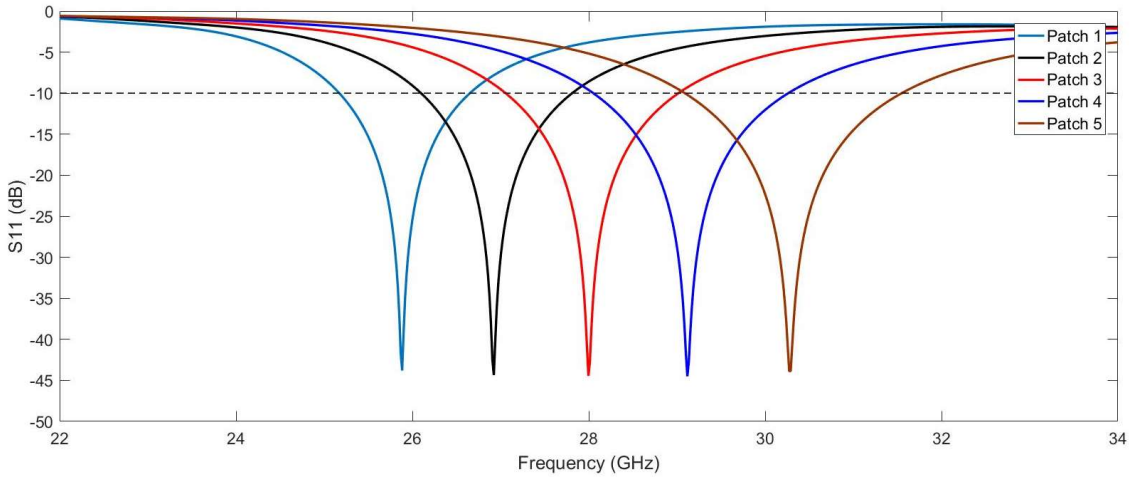

Figure 4.9: Individual S11 of each patch of the 5-element array.

In Figure 4.9 the representation of S11 of each is demonstrated. This simulation was performed with a reference impedance of 90 Ω since it was desired to achieve the 90 Ω

point with inset feed, that is why the S11 results demonstrate such good results, this means that the value of impedance at the frequency is close to 90 Ω.

After finishing the prototype of each element, it is time to construct the full array. Using the optimizer of CST distance between arrays was obtained.

Table 4.18: Distance between patches in the 5-element array.

	Distance (mm)
Patch 1 to Patch 2	2.4471
Patch 2 to Patch 3	1.9537
Patch 3 to Patch 4	2.5927
Patch 4 to patch 5	2.2730
Patch5 to feed	2.6333

Table 4.18 exhibits the values of the distances. No correlation is found between values, proving that even when the impedance of the structure is changed there still no logical way to calculate the distances.

To finish this array there is still one thing missing, transforming the impedance of the structure from 90 Ω to 50 Ω. To do this a quarter wavelength at the central frequency, in this case, 28 GHz, was used to make this adaptation.

This will cause some problems because a quarter wavelength can only be adapted to a specific frequency, and in a wideband array this is a problem since a range of frequencies should be adapted instead of just one. Figure 4.10 shows the final simulated. This contemplates the quarter wavelength transformer and the space necessary for the connector, this was used to assure that the results of the simulation are as close as possible to the measured ones.

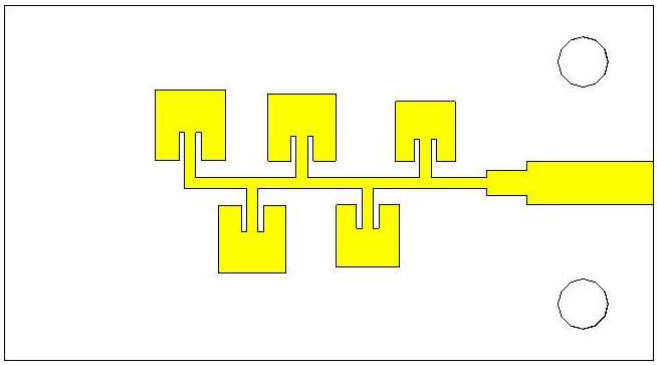

Figure 4.10: 5-element Array simulated.

4.3.3 7-element array

Maintaining the logic presented in the thinner arrays, adding two more patches to enhance bandwidth was the next step.

Seeing that both designing structures presented have the same scaling factor, both patches added operate at the same frequency as those added to create the previously presented 7-element array, meaning that their frequency of operation is 24.89 GHz and 31.49 GHz.

Using the process presented to realize the dissertation array, the first thing to be done is simulating the impedance of each patch at its operating frequency.

Table 4.19: Comparison between theoretical and simulated values of the impedance of the two-element added to form the 7-element array.

Frequency of operation (GHz)	Z_{in} (Theoretical) (Ω)	Z_{in} (Simulated) (Ω)
24.89	391.49	250.47
31.49	425.99	274.48

As expected, the values presented in Table 4.19 are not concordant and have a similar difference between value identical to the difference presented in Table 4.16. This will influence the calculation of the length of the cut, R_{in}.

Table 4.20: Parameters of both patches added to form the 7-element array.

Frequency (GHz)	L=W (Theoretical) (mm)	L=W (optimized) (mm)	R_{in} (theoretical) (mm)	R_{in} (optimized) (mm)	W_c (mm)	I_m (mm)
24.89	2.8310	2.9048	0.8363	1.1853	0.2200	1.8455
31.49	2.1318	2.2734	0.6522	0.8419	0.2200	1.4460

As anticipated, R_{in} values have a difference between theoretical and optimized values, due to the deviation on the impedance, which means that for these arrays' designs, calculating the impedance is not an advantage.

With all parameters of each added patch gathered, their S11 was simulated.

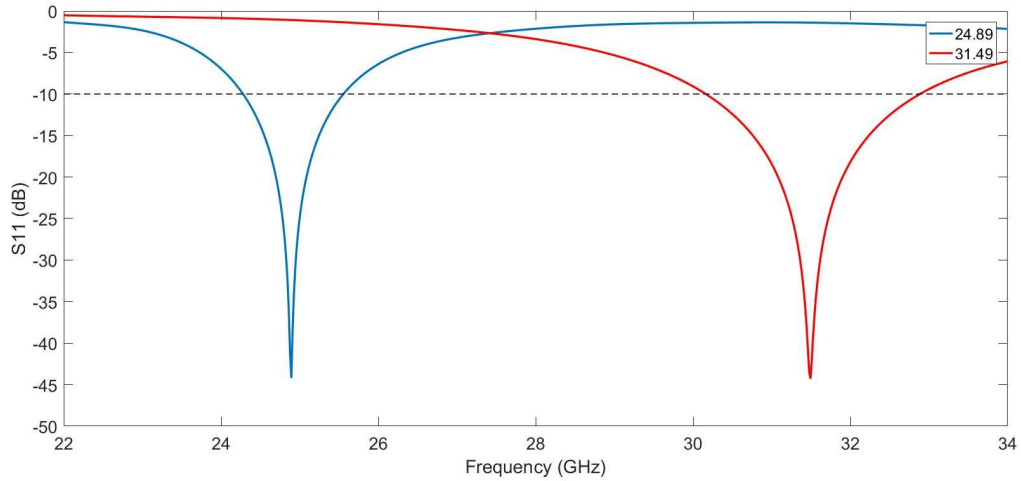

Figure 4.11: S11 of each patch added to form the 7-element array.

Figure 4.11 shows S11 of both patches constructed and added to the array. This simulation was made with a reference impedance of 90 Ω. Knowing this and seeing that the S11 for patches is below -40 dB, meaning that the inset feed was well performed, and the impedance at both patches is close to 90 Ω as intended.

With all patches designed the optimization was performed and the values obtained for each distance are presented in Table 4.21.

Table 4.21: Distance between patches in the 7-element array.

	Distance (mm)
Patch 1 to Patch 2	2.1462
Patch 2 to Patch 3	1.9423
Patch 3 to Patch 4	1.8673
Patch 4 to Patch 5	2.4062
Patch 5 to Patch6	2.1462
Patch 6 to Patch 7	1.8608
Patch 7 to feed	1.5231

After gathering these values, the array was simulated to see its full performance, a representation of the array simulated on CST is in Figure 4.12.

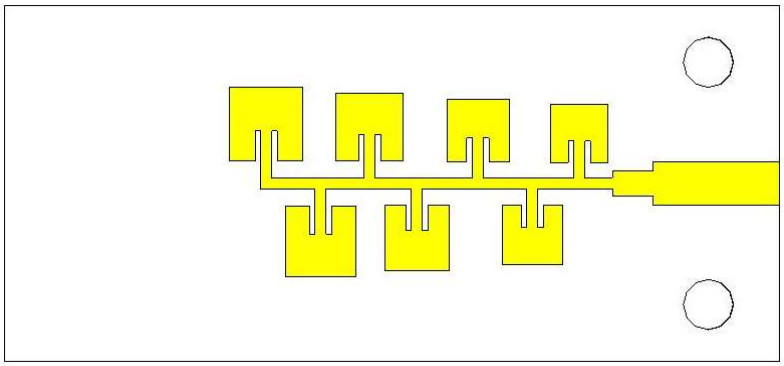

Figure 4.12: 7-element array simulated in CST.

4.3.4 9-element array

To finalize this set of arrays a 9-element array was designed. This array contemplates all previous patches used before and adds two more patches, the same way as in the thinner arrays.

Applying the process defined for this array, the first simulation calculates the impedance of both patches added to create this array.

Table 4.22: Theoretical and simulated impedance of the patches added to create the 9-element array.

Frequency of operation (GHz)	Z_{in} (Theoretical) (Ω)	Z_{in} (Simulated) (Ω)
23.93	387.83	263.59
32.75	433.06	264.53

Table 4.22 presents a comparison of the impedance obtained through calculations and the one obtained in the simulation. Not surprisingly these values are different. It was anticipated since in the previous arrays the impedance also differed.

Although this may be true, a coherence must be maintained, and since all lengths of cut were calculated using the simulated impedance in this array, this will not be different.

Table 4.23: Values for each parameter of the two elements added to complete the 9-element array.

Frequency (GHz)	L=W (Theoretical) (mm)	L=W (optimized) (mm)	R_{in} (theoretical) (mm)	R_{in} (optimized) (mm)	W_c (mm)	I_m (mm)
23.93	2.9350	3.0335	0.8934	1.2574	0.2200	1.9222
32.75	2.0302	2.1850	0.6127	0.8034	0.2200	1.3864

In the same way as the previous arrays, R_{in} has a considerable difference between calculated and optimized. Such is demonstrated in Table 4.23. This happens because of the difference in the impedance. With all these values presented, the elements were simulated, the results are presented in Figure 4.13.

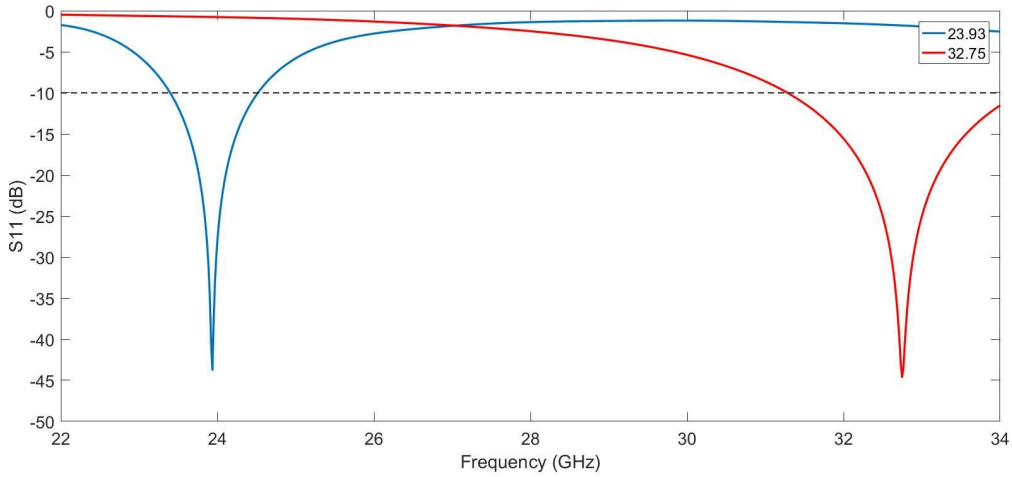

Figure 4.13: S11 of both patches added to create the 9-element array.

The reference impedance used was 90 Ω, that is the reason why the S11 performance is excellent if the reference impedance were changed to 50 Ω the results would be very different. However, by using this reference, a better adaptation is obtained and helps the full array to have a better performance in its S11.

The final step is to join all patches and optimize the distances between elements.

Table 4.24: Distance between Patches of the 9-element array.

	Distance (mm)
Patch 1 to Patch 2	3.0897
Patch 2 to Patch 3	2.6691
Patch 3 to Patch 4	2.2371
Patch 4 to Patch 5	1.9854
Patch 5 to Patch6	2.9972
Patch 6 to Patch 7	2.5228
Patch 7 to Patch 8	2.2080
Patch 8 to Patch 9	2.0550
Patch 9 to feed	1.9809

Through a cautious observation of Table 4.24, it is viewed that the distances do not present a logic between them, and due to this, it is tough to calculate them. After this a quarter wavelength transformer was added to adapt the 90 Ω structure. In Figure 4.14 a representation of the array simulated in CST is given, with the necessary space and holes of the connector.

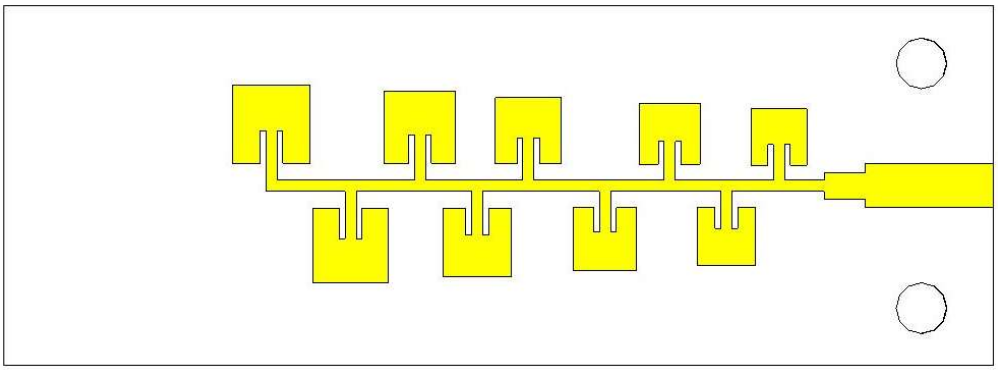

Figure 4.14: representation of the 9-element array simulated in CST.

Chapter 5

5 Simulation Results

This chapter displays the results obtained in CST. Every result need careful evaluation since an array performance is not only evaluated by the S11, but by all the parameters, from the gain to efficiency and even the radiation patterns, all this factor will be presented for every array from the previous chapter.

5.1 Wideband array at C Band Results

In the previous chapter, the various dimensions of the arrays were presented. In this chapter, the simulation results of the various will be presented, in the same order as in the previous chapter. So, to start the C band simulation results will be presented.

5.1.1 Reflection coefficient

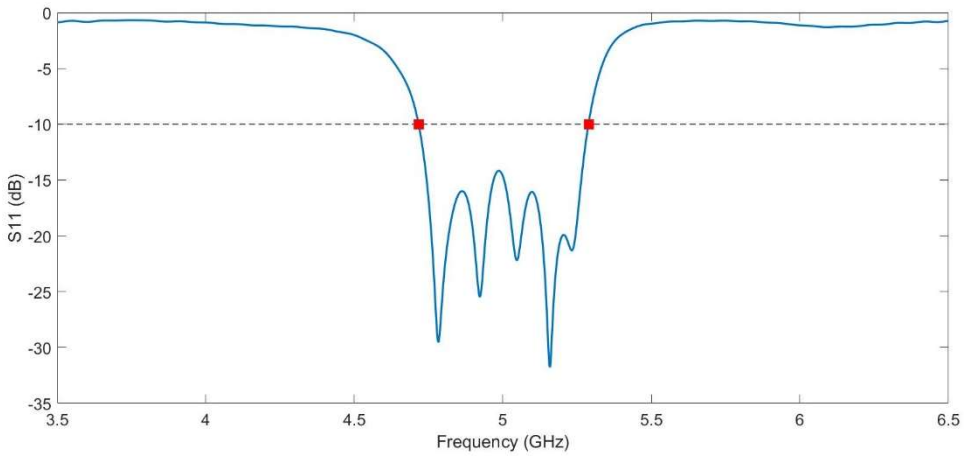

Figure 5.1: Simulated S11 of the array.

Figure 5.1 shows that this array with 5 elements covers approximately 572 MHz, equivalent to 0.114 of fractional bandwidth, starting in 4.716 GHz and finishing at 5.288 GHz. Since the point of creating this structure was to construct a suitable designing method and looking into the results they seem suitable for this simple structure, having fewer elements, only five, and an average scaling factor, 1.025, influenced the bandwidth this array could cover. Nonetheless, these results are good, similar bandwidth performance when compared with [23], and leave a little expectation for its practical work, and for how well they could work in higher frequency bands.

5.1.2 Radiation patterns

An essential factor in an array is its radiation patterns. They give much information about the array, its gain at a specific frequency, angle of direction, sidelobe level and others. However, this is a wideband array, therefore, showing the diagram at only one frequency would limit the information, so three frequencies were chosen to demonstrate the full array capabilities. For this case, the frequencies chosen were 4.8 GHz, 5 GHz, and 5.2 GHz to demonstrate the behaviour of array characteristics throughout the frequency.

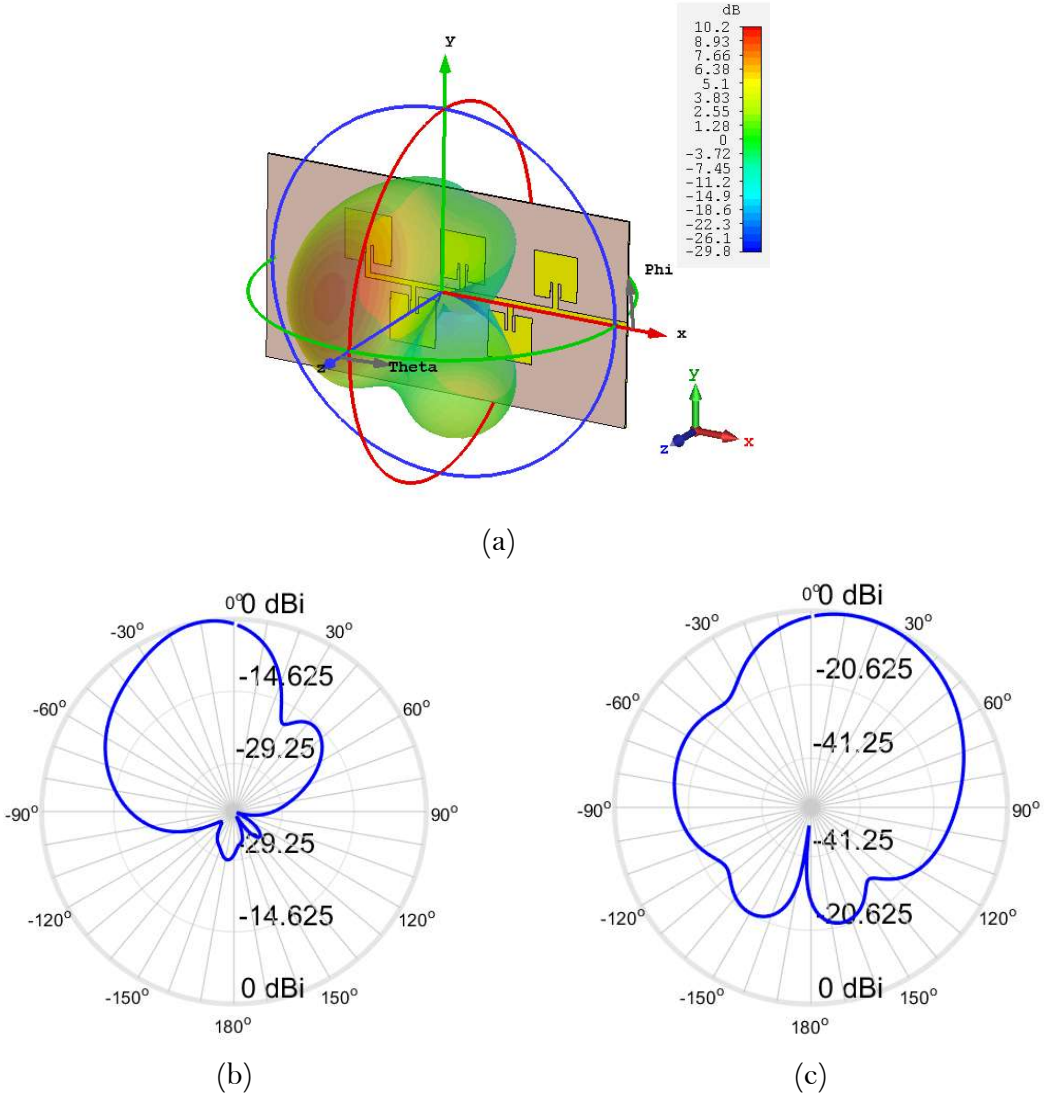

Figure 5.2: Radiation Patterns of the array at 4.8 GHz: (a) 3D representation; (b) φ = 0° plane; (c) φ = 90° plane.

In Figure 5.2 a representation of both 3D diagram and polar diagram of the array at 4.8 GHz are shown. Looking into them, a slight deviation exists in its direction, about -10° in the plane φ = 0° graph and 16° in the plane φ = 90°. Its gain is quite good, 9.497 dBi is an interesting value for these types of arrays, a similar value was presented in [25] and in that case it was necessary the addition of a Yagi-Uda structure, and it could be a good match for mmWaves applications.

One point that gives this array an even better quality is the fact that they have a low sidelobe, the bigger one has -15 dB, which is usually a problem in arrays. With this problem controlled the performance of array its good at this frequency, even though a slight deviation exists in the direction.

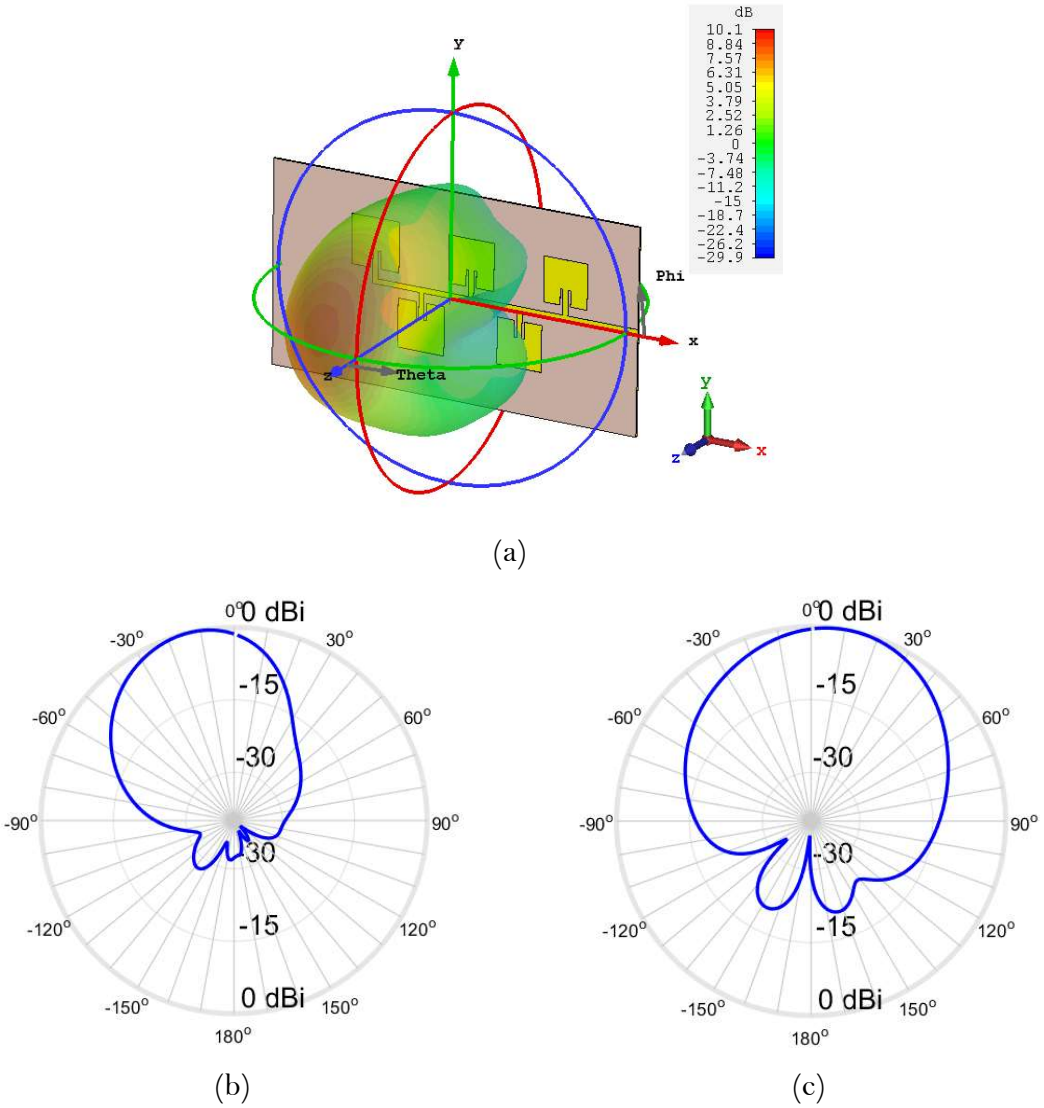

Figure 5.3: Radiation Patterns of the array at 5 GHz: (a) 3D representation; (b) φ = 0° plane; (c) φ =90° plane.

For 5 GHz, the radiation patterns can be observed in Figure 5.3. When compared with the 4.8 GHz patterns, a change in the direction can be observed. Now the direction as a variation of -14° on plane φ = 0°plane and 10° on plane φ = 90°.

Comparing both gains, the value is almost the same. One thing that got enhance was the sidelobe level. The most prominent sidelobe has a power of -20 dB, which is excellent for an array.

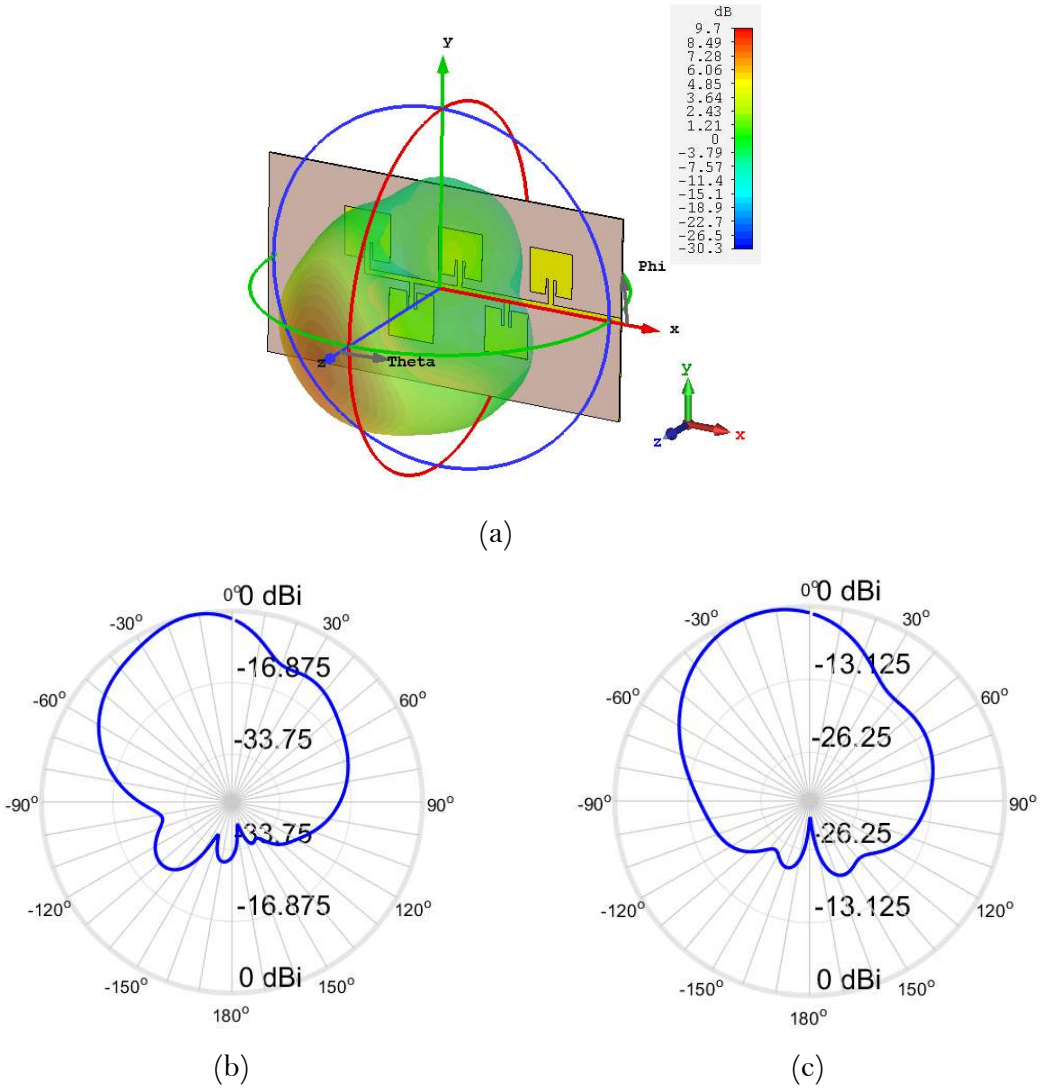

Figure 5.4: Radiation Patterns of the array at 5.2 GHz: (a) 3D representation; (b) φ = 0° plane; (c) φ = 90° plane.

Lastly, 5.2 GHz pattern is shown in Figure 5.4 Looking into the figure, again the angle of direction changes a bit when compared with both previous arrays. Now for plane φ = 0° its angle of direction is -13°, while for plane φ= 90° it is -16°. If only φ = 0° plane was observed, at all three frequencies the array is concordant, however in the plane φ = 90° all three angles of direction differ, nonetheless it's not a noteworthy difference between them.

Checking the gain, its value is 9.7 dBi, maximum, for this frequency, meaning that a 0.4 dBi decrease occurred when compared with 5 GHz. This change is not significant, and the array continues to be well behaved.

Viewing the sidelobes, this value changed to -10.6 dB. This indicates that, at this frequency, the array might some problems in its operation, because of this high value.

Altogether, doing this array proved a valid solution, and gave a good knowledge of how to design these kinds of arrays and, what to expect from their behaviour. Hence, this idea will be used to design all arrays from this dissertation. Some changes between arrays will be done to understand these arrays full capabilities.

5.1.3 Maximum gain and Efficiency over frequency

A necessary characteristic in a wideband array is to perform similarly throughout the frequency range. A good way to verify is to see the behaviour of the maximum gain and efficiency throughout the frequency. If these characteristics are stable, it means that this array has excellent performance, if there are abrupt variations, it means that the array has a poor performance. To start the gain is shown in Figure 5.5.

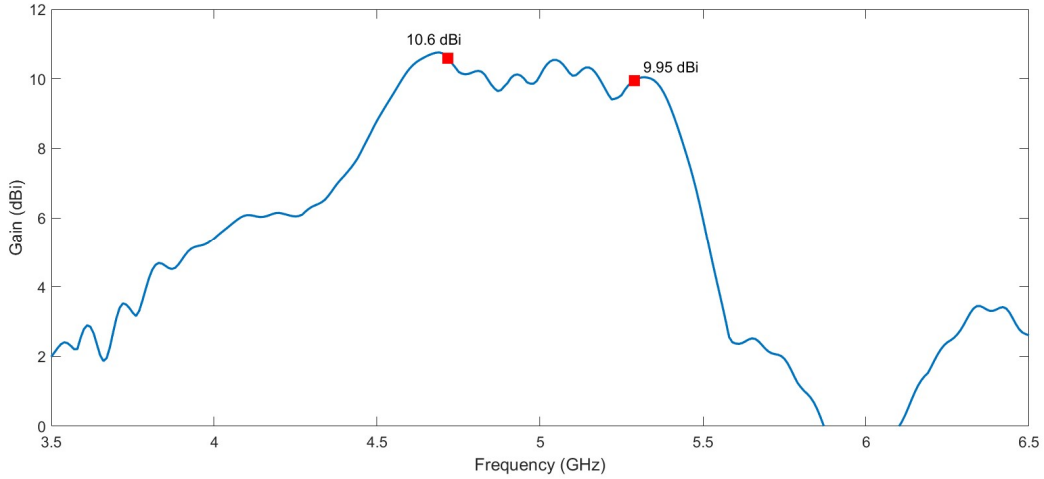

Figure 5.5: Maximum Gain versus Frequency in the C band array.

It is possible to see that in the frequency range, that is delimited by the markers in the figure, the gain is in general stable, and no abrupt variations occur, meaning that in this aspect, the array has good behaviour, if only the gain throughout the band of operation was taken into account these values are very similar to the ones in [25].

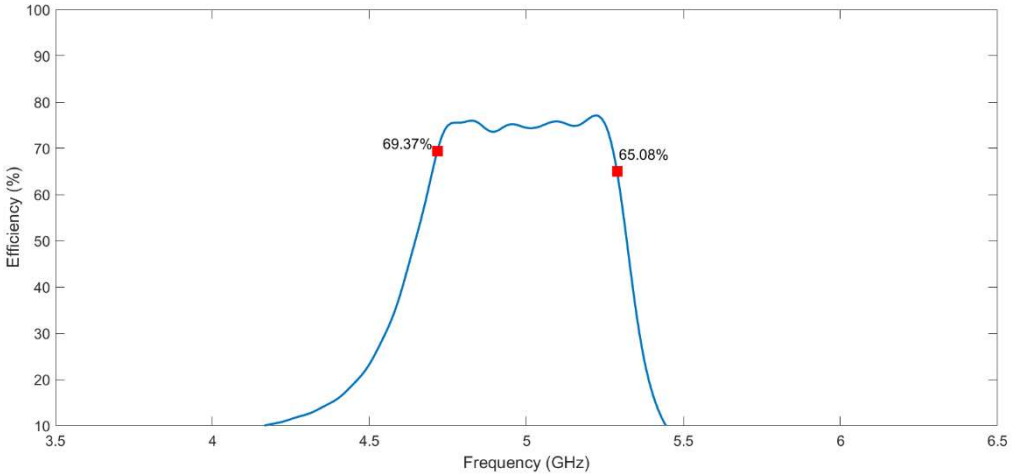

Figure 5.6: Total Efficiency versus Frequency in the C band array.

In Figure 5.6 the total efficiency is presented. Each marker corresponds to a limit of the frequency range. In this aspect the efficiency is reasonably stable, and this value is higher than 60% throughout the band of operation.

Overall, this array has a good performance in the many simulations presented and can be applied in several applications at this band of operation.

5.2 Wideband array at MmWaves: Thinner Substrate case

This section is separated into three subsections, each one containing the results of the antenna arrays presented in the previous chapter.

5.2.1 5-element array

To maintain a logical order, the first array to be presented is the 5-element array.

5.2.1.1 Reflection coefficient

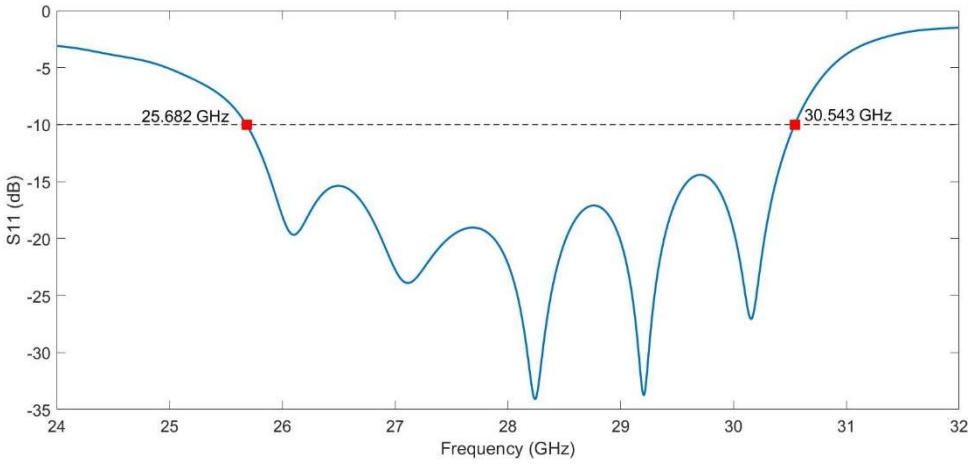

Figure 5.7: S11 of the 5-element array.

Figure 5.7 shows the full behaviour of the array. It is observed that this array covers approximately 4.861 GHz, from 25.682 GHz to 30.543 GHz, which corresponds to a fractional bandwidth of 0.173. This fractional bandwidth is suitable for this array, even though it is less percentage when compared with the previous 5-element array. However, this array has an identical bandwidth performance when compared with the one presented in [34].

One point that deserves comment is the fact that each peak slightly deviates in relation to her working patch. Although this happens, it is not hugely problematic since, at every working frequency, a good S11 value is still achieved, always lower than -15 dB.

5.2.1.2 Radiation Patterns

To continue the characterization of the array the radiation patterns need to be presented. For this array, three frequencies were chosen to better illustrate the array by presenting their patterns. Those frequencies are 27 GHz, 28 GHz, and 29 GHz.

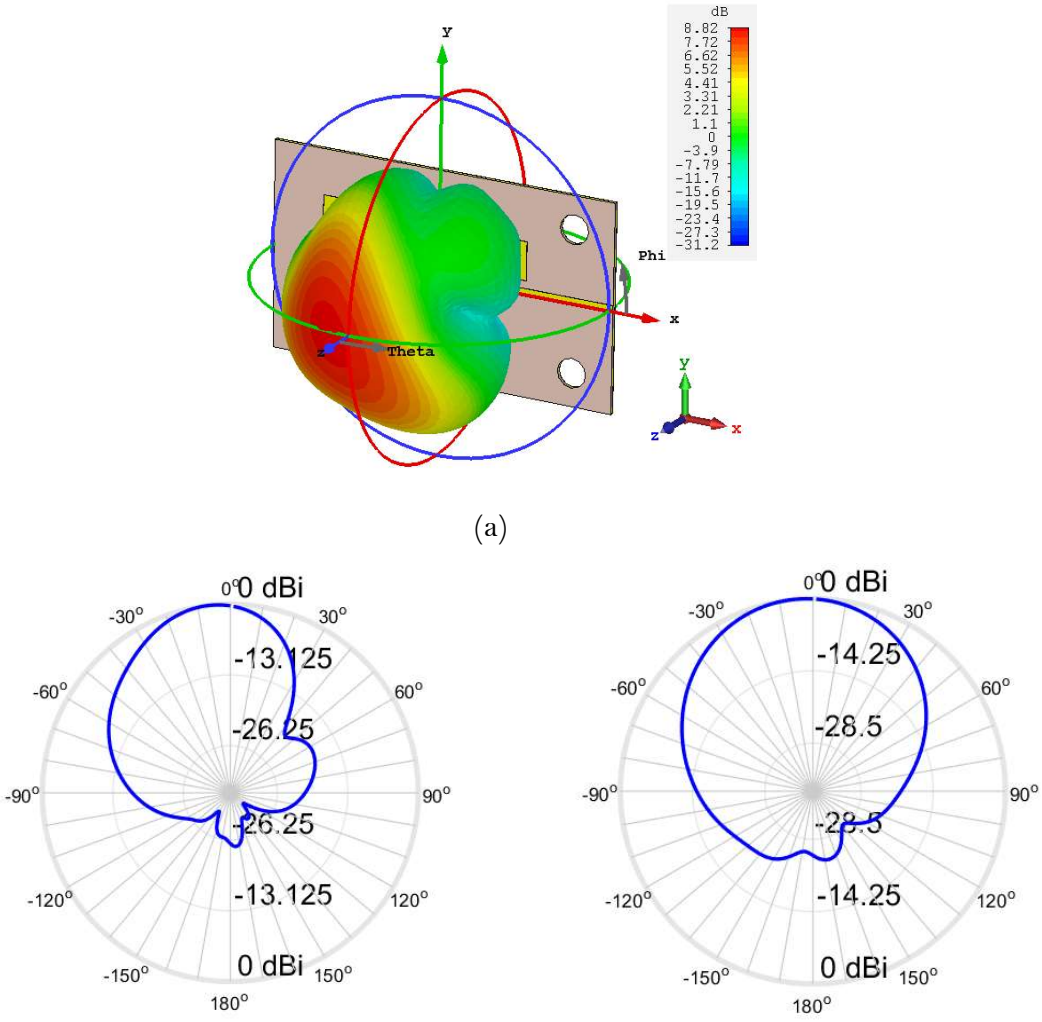

Figure 5.8: Radiation Patterns of the 5-element array at 27 GHz: (a) 3D representation; (b) φ = 0° plane; (c) φ = 90° plane.

For the 27 GHz radiation patterns, a noticeable fact is a maximum gain of 8.82 dBi. When compared with the other 5-element array gain, this value decrease. However, the fact that this array was made with a thinner substrate explains this difference in the parameter.

Another point that is seen is the fact that the angular width of this radiation pattern is broader, meaning that it is a more directive array. Although, the perfect transmitting point is not at the centre of the structure, nonetheless at that point it still possesses good properties.

To finish, consideration is needed for the sidelobe level. As said before an array sidelobe should be as low as possible. In this case, and with the help of CST, the higher

sidelobe level was taken. Its value is -17.8 dB which is a great value, making this a good radiation pattern in general.

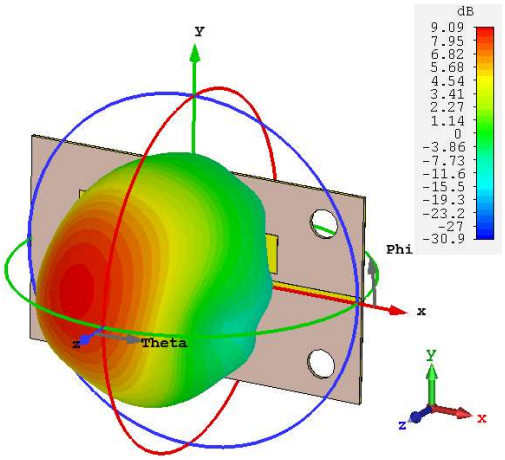

(a)

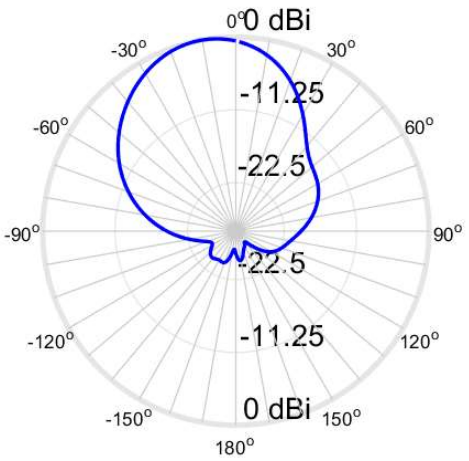

(b)

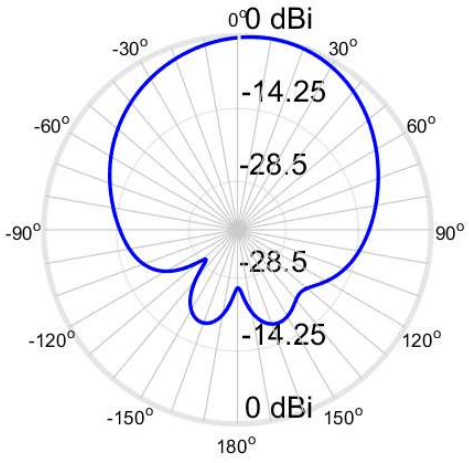

(c)

Figure 5.9: Radiation Patterns of the 5-element array at 28 GHz: (a) 3D representation; (b) φ = 0° plane; (c) φ = 90° plane.

As expected from this array, the gain is reasonably constant, and this can be seen in Figure 5.9, which is the 28 GHz radiation pattern. A maximum gain of 9.09 dBi is presented, which is a close value when compared with the 27 GHz gain.

Both radiation patterns are similar, in spite of existing a slight deviation in the plane of φ = 90°. This means that this array has similar behaviour throughout the frequency, which is desired in a log-periodic array.

For this frequency, the sidelobe level was almost the same and did not present itself as a problem. Its maximum value is -18.1 dB.

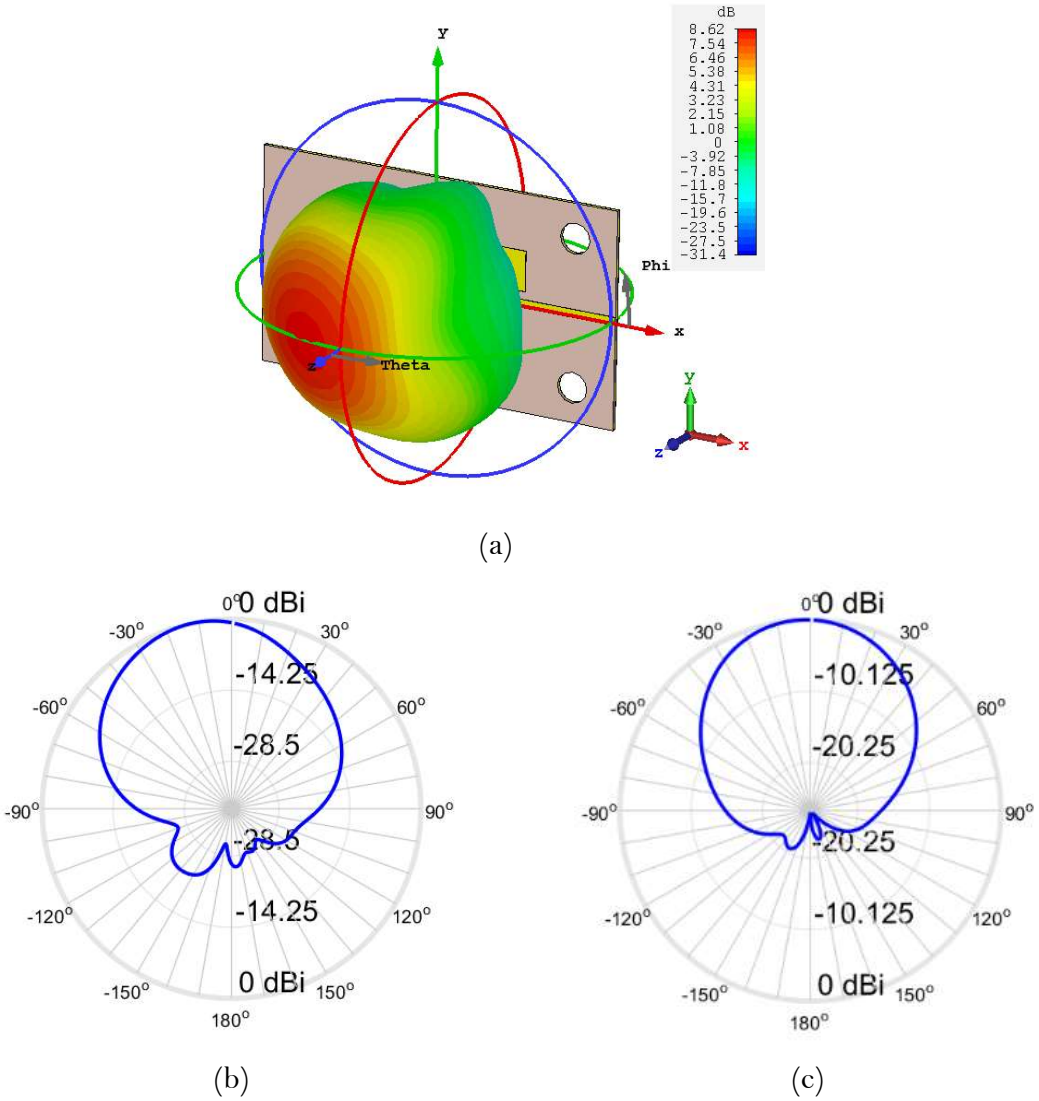

Figure 5.10: Radiation Patterns of the 5-element array at 29 GHz: (a) 3D representation; (b) φ = 0° plane; (c) φ = 90° plane.

The last radiation pattern is for 29 GHz, presented in Figure 5.10. This figure confirms some factors of the log-periodic arrays. Starting with the fact that the gain is similar to both previously presented, its maximum gain is 8.62 dBi. Secondly, the 3D pattern presented is comparable to both presented earlier, and even in the direction where it possesses the maximum point of transmission. As the last factor, its sidelobe is low, -20.9 dB.

5.2.1.3 Maximum Gain and Efficiency over frequency

On account of being a wideband array, two essential factors that deserve some considerations are the gain and efficiency behaviour throughout the frequency range. On the one hand, if the gain is low, the array might not be usable in this band of frequency due

to their high free space losses. On the other hand, if the efficiency is low, this array would waste a much power and might compromise the operation of the system.

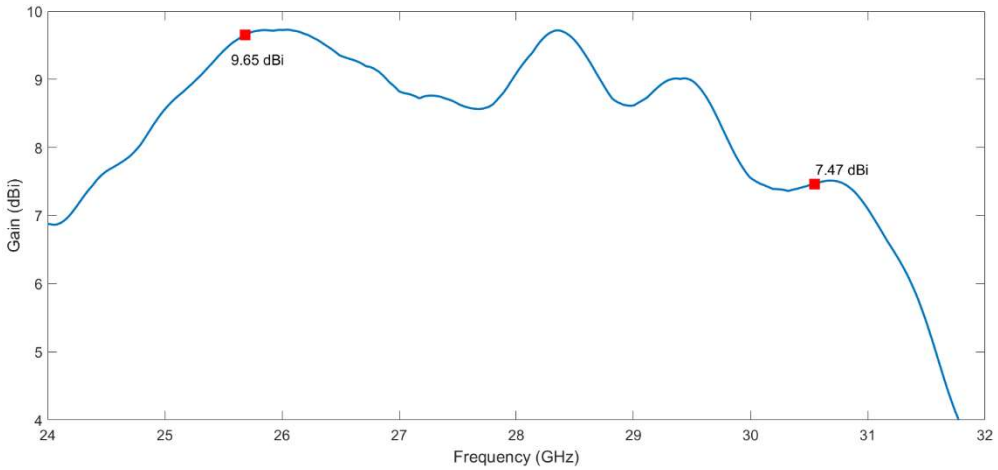

Figure 5.11: Maximum Gain over frequency behaviour in the 5-element array.

Figure 5.11 presents gain performance. Its behaviour is not stable and variates throughout the band of operation. There are two markers in the figure. One presents the gain at 25.682 GHz and the other at 30.543 GHz. With the help of the markers, it can be seen that the gain is higher than 7.47 dBi throughout the frequency range, which is good, it is better when compare with the gain presented in [34].

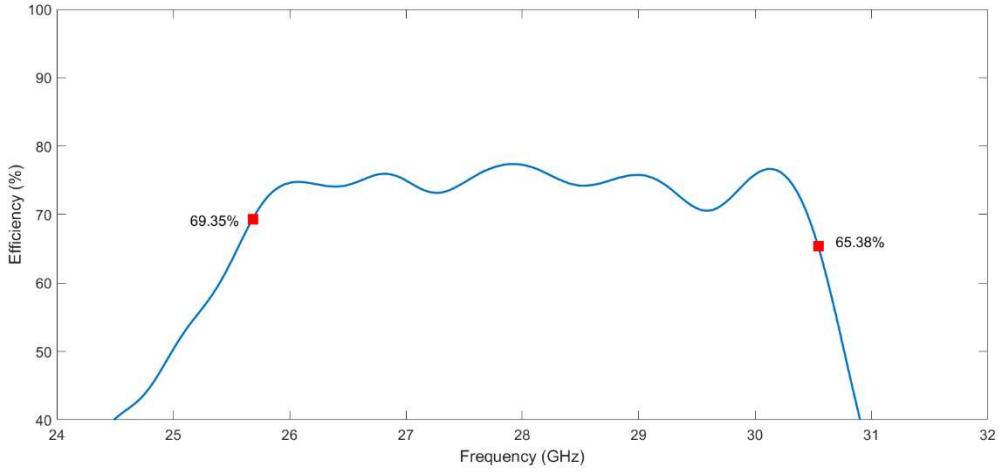

Figure 5.12: Total efficiency over frequency in the 5-element array.

Figure 5.12 shows the performance of the total efficiency throughout the frequency. The markers delimitate the frequency range in which the array works, the efficiency is higher than 63.44 %, and between 26 GHz and 30 GHz is over 70 %, meaning that this array, performs well throughout the frequency band comparing with [34].

5.2.2 7-element array

Preserving the same order, the next array is the 7-element array.

5.2.2.1 Reflection coefficient

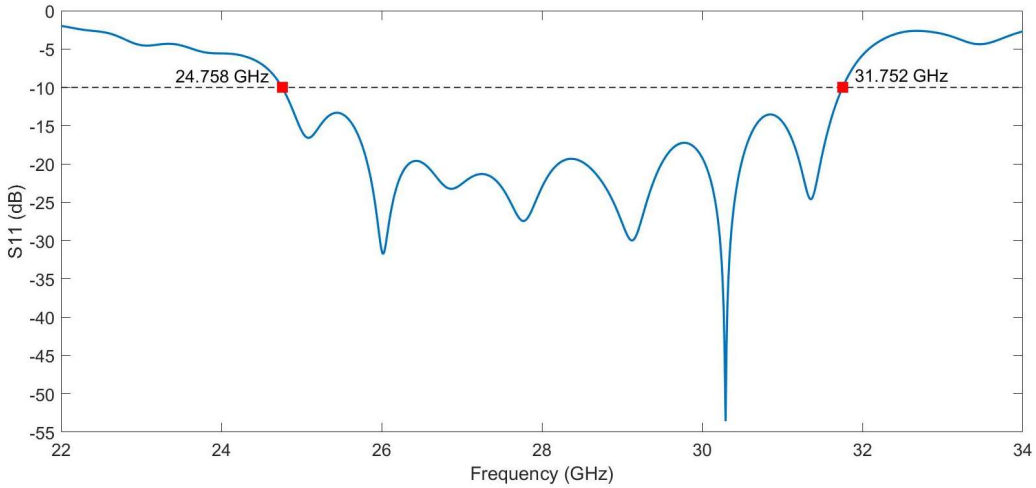

Figure 5.13: S11 of the 7-element array.

Throw an observation of Figure 5.13 an improvement is seen in terms of bandwidth. A fractional bandwidth of 0.248 was obtained with this configuration, from 24.758 GHz to 31.752 GHz, which is equivalent to 6.994 GHz of bandwidth covered. Taking into consideration the fractional bandwidth of this array he is considered a wideband array. However, it was very close to being considered an ultra-wideband array.

5.2.2.2 Radiation Patterns

Equally to the preceding arrays, three frequencies were chosen to evaluate the radiation characteristics of the array, in this case, the same frequencies used in the 5-element array were repeated to make a direct comparison between them.

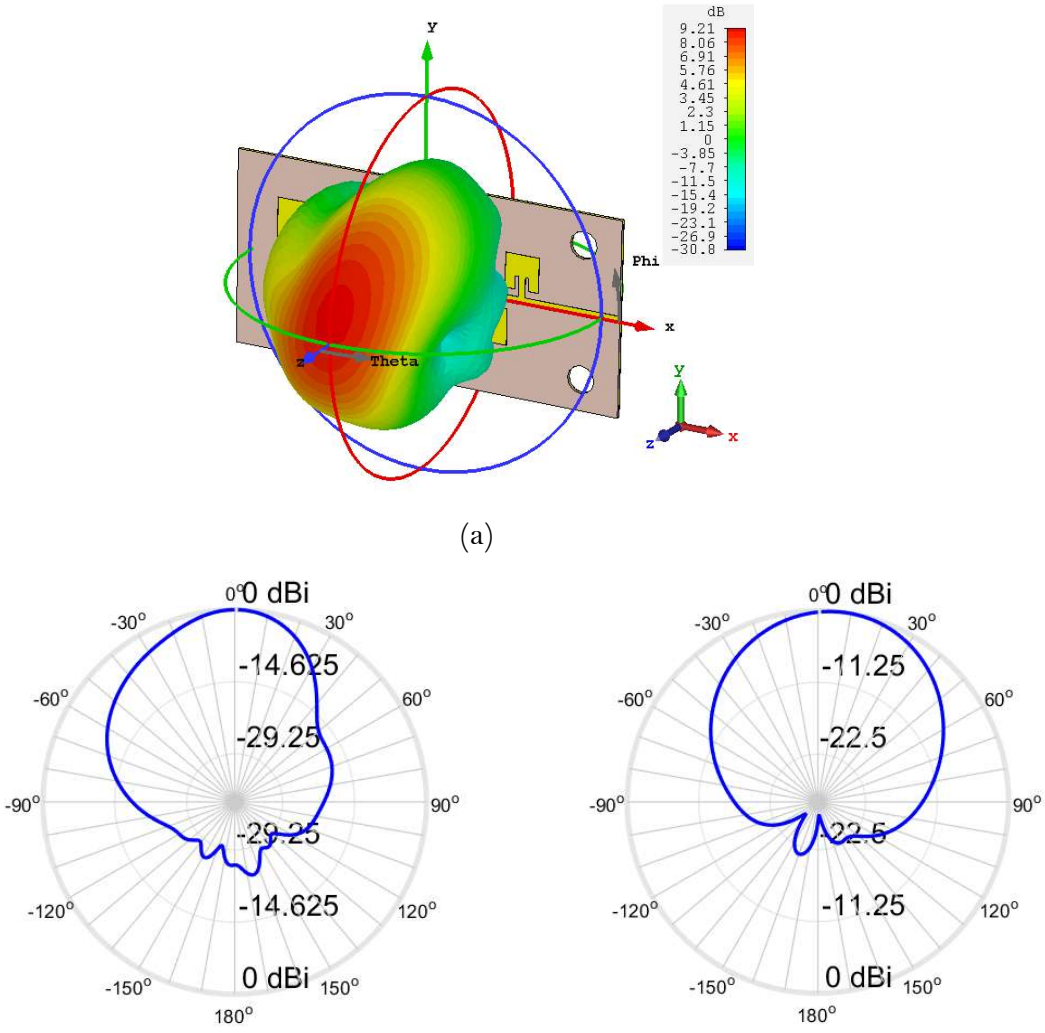

Figure 5.14: Radiation Patterns of the 7-element array at 27 GHz: (a) 3D representation; (b) φ = 0° plane; (c) φ = 90° plane.

Observing Figure 5.14, some considerations can be made. In the first place, the gain maximum is 9.21 dBi, which is very identical to gain presented in the 5-element array. In their direction, at 27 GHz, this array has a direction of transmission close to 0°, which is the desired value.

In this case, the value presented is -21.3 dB, which is low and, due to that, it does not bother the operation of the array.

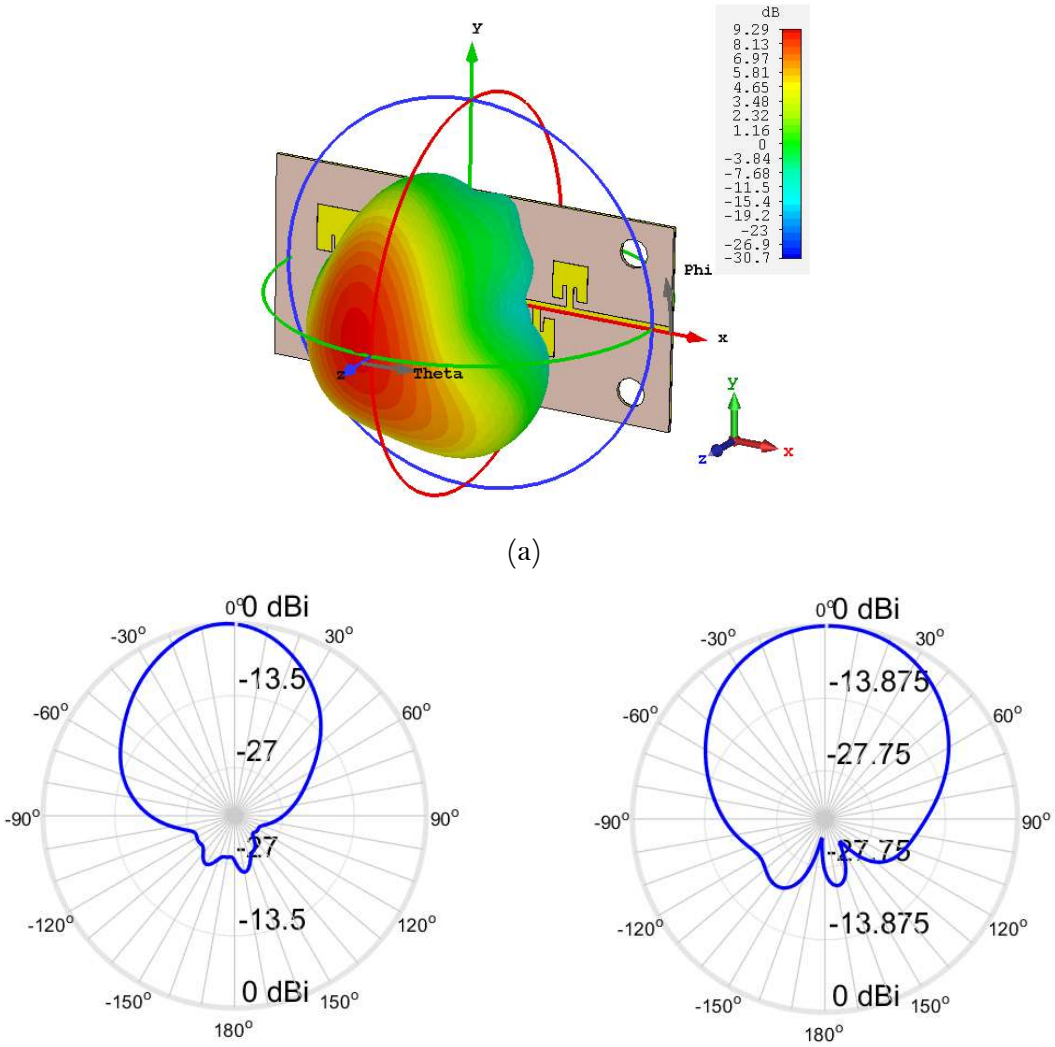

Figure 5.15: Radiation Patterns of the 7-element array at 28 GHz: (a) 3D representation; (b) φ = 0° plane; (c) φ = 90° plane.

Figure 5.15 presents radiation patterns at 28 GHz. When compared to the 5-element patterns, they are identical, with the difference that its direction is closer to 0°. Even the gain is like the one obtained at the same frequency in the 5-element array, being that maximum gain 9.29 dBi.

When compared with the 27 GHz pattern, the sidelobe level improves in this case, now its maximum value is -21.2 dB, which is wanted in the arrays.

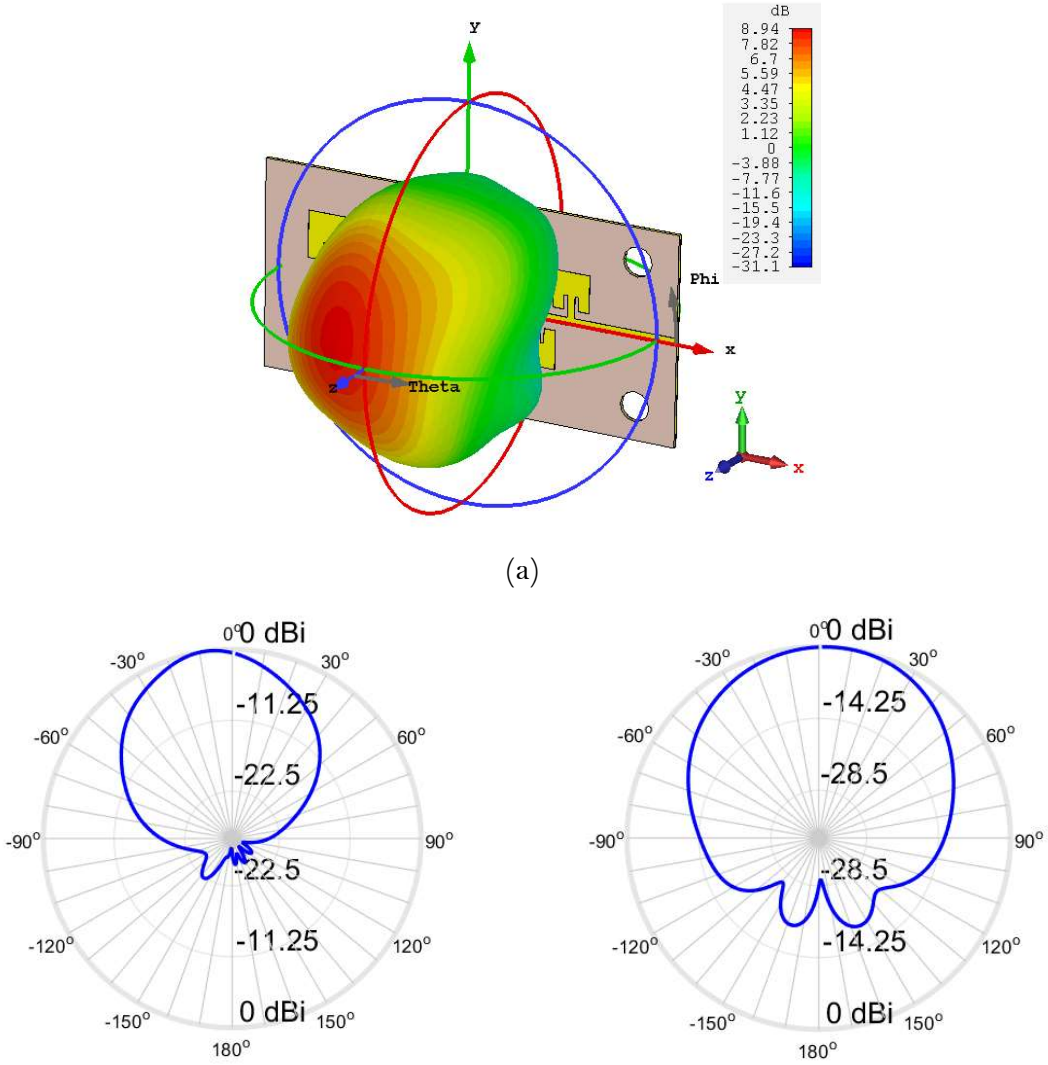

Figure 5.16: Radiation Patterns of the 7-element array at 29 GHz: (a) 3D representation; (b) φ = 0° plane; (c) φ = 90° plane.

To finalize the radiation patterns of this array, Figure 5.16 shows the radiation pattern at 29 GHz. Comparing these diagrams to both presented for this array a deviation on the direction is notice, previous patterns were closer to 0°, which is not beneficial since one of the components sought in log-periodic arrays is similar radiation patterns throughout all frequencies.

Nevertheless, looking into the gain, this value continues to be identical to the previous ones, as expected from these arrays, presenting a maximum gain of 8.94 dBi.

As a final consideration, the sidelobe is higher when compared with the one at 28 GHz, though, it still is a low value, -18.8 dB.

In spite of existing differences in the radiation, this array still seems a viable solution for mmWaves applications, even though it is necessary to be careful about is placement.

5.2.2.3 Maximum Gain and Efficiency over frequency

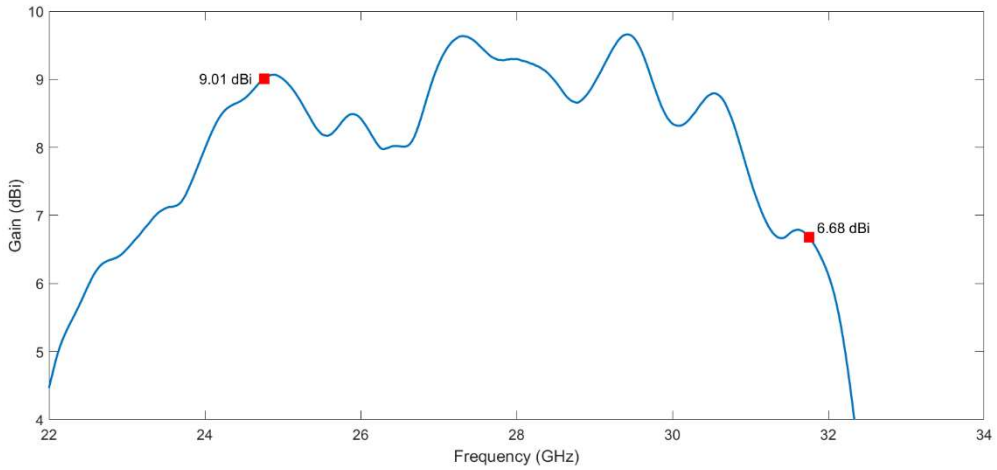

Figure 5.17: Maximum Gain over frequency behaviour in the 7-element array.

For the 7-element array, the gain is presented in Figure 5.17. In this case, there is a little more variation when compared with the 5-element array, especially at frequencies higher than 30 GHz. Nevertheless, from the start frequency until 30 GHz this array has a good performance, with a gain higher than 8 dBi, and the variations are not extreme.

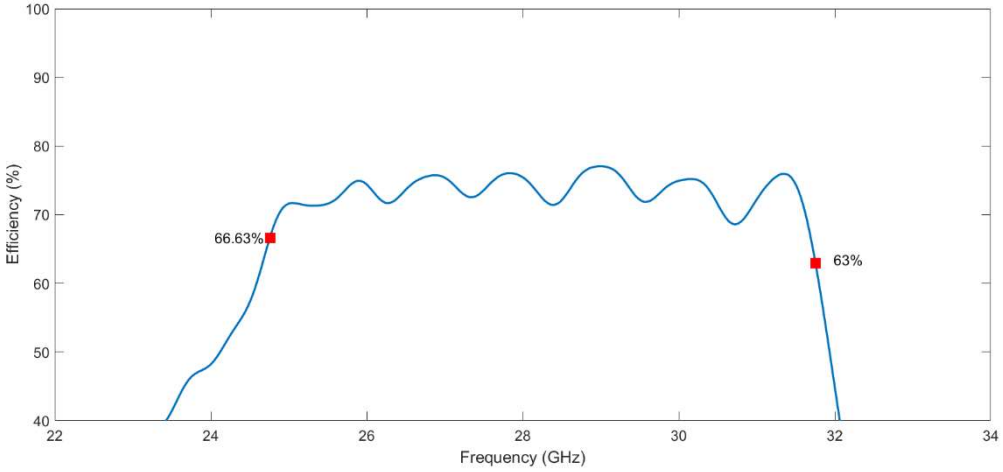

Figure 5.18: Total efficiency over frequency in the 7-element array.

As a final parameter, the efficiency is shown in Figure 5.18. This factor is constant in almost the entire frequency band. The markers help in the observation of this factor. In

average the efficiency seems to be higher than 70 %, and this is very similar to the 5-element array, which means that adding more patches does not influence the efficiency performance.

5.2.3 9-element array

5.2.3.1 Reflection coefficient

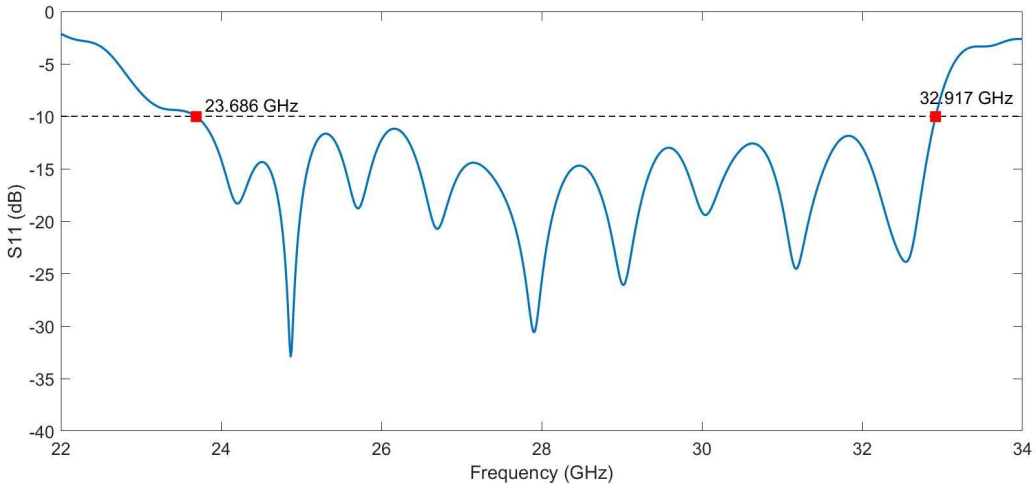

Figure 5.19: S11 of the 9-element array.

Figure 5.19 displays the S_{11} performance of the array. As expected, this array covers more bandwidth than the rest. Its frequency range of operation starts at 23.686 GHz and stops at 32.917 GHz. Such is equivalent to a fractional bandwidth of 0.326, meaning that this array can be considered an ultra-wideband array by the standards presented in Table 2.1. However, one characteristic deserves acknowledgement, at some points S11 value is very close to -10 dB, these points can pose as a problem when measuring because of imprecision upon printing and small losses in the substrate.

5.2.3.2 Radiation Patterns

To continue the appreciation on this array, its radiation patterns at 27 GHz, 28 GHz and, 29 GHz will be displayed and commented.

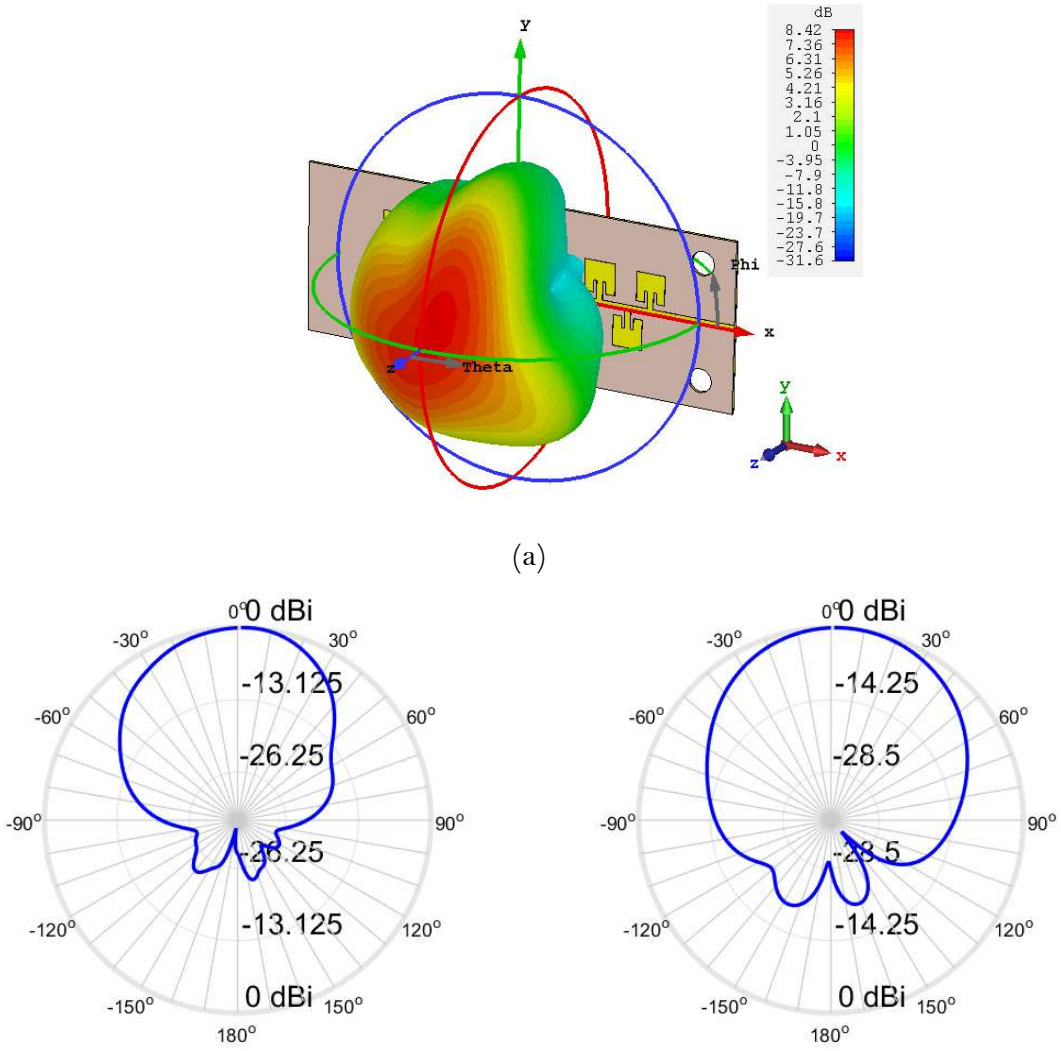

Figure 5.20: Radiation Patterns of the 9-element array at 27 GHz: (a) 3D representation; (b) φ = 0° plane; (c) φ = 90° plane.

Maintaining the logic, the first radiation pattern presented is 27 GHz and is shown in Figure 5.20.

The format of this pattern is a little different from the previous ones, because there are two direction points with maximum gain, instead of just one. Furthermore, the gain decreases, to 8.42 dBi, which is not desirable, especially in mmWaves applications because of the higher attenuations in the atmosphere.

The maximum value of sidelobe presented in CST is -19.4 dB which is good because it means that are fewer interferences in the transmission.

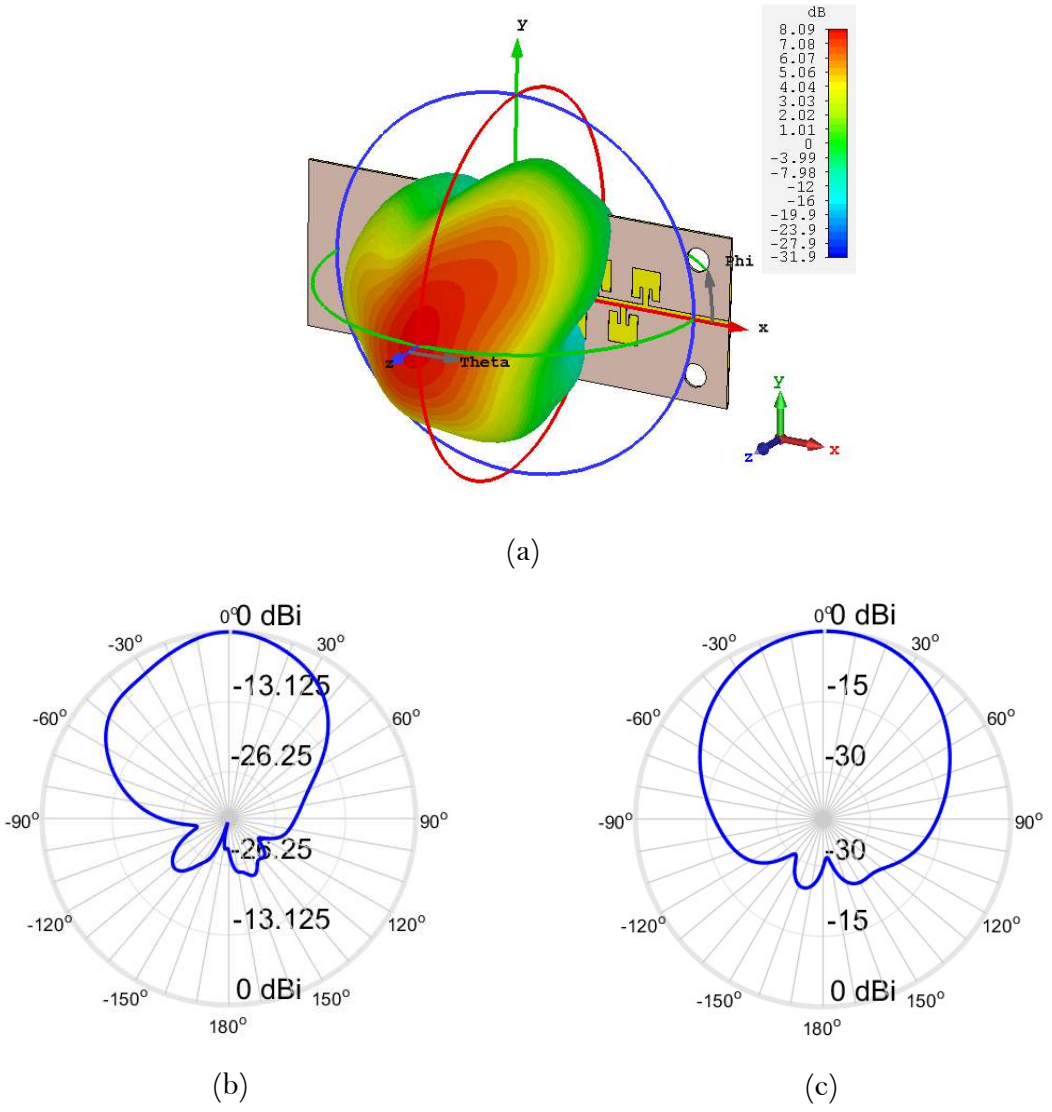

Figure 5.21: Radiation Patterns of the 9-element array at 28 GHz: (a) 3D representation; (b) φ = 0° plane; (c) φ = 90° plane.

Figure 5.21 presents the radiation patterns at 28 GHz. The direction of the main lobe is almost in the centre of the axes, meaning that the maximum transmission point is almost at 0° as intended.

The maximum gain in this frequency is 8.09 dBi. This value is lower than the one presented at 27 GHz. The value presented is lower than the gains presented by the previous arrays at the same frequency.

Using CST, the sidelobe values were obtained. In this case, the highest value presented in the simulation is -21.2 dB, meaning that this factor does not influence the operation of the array.

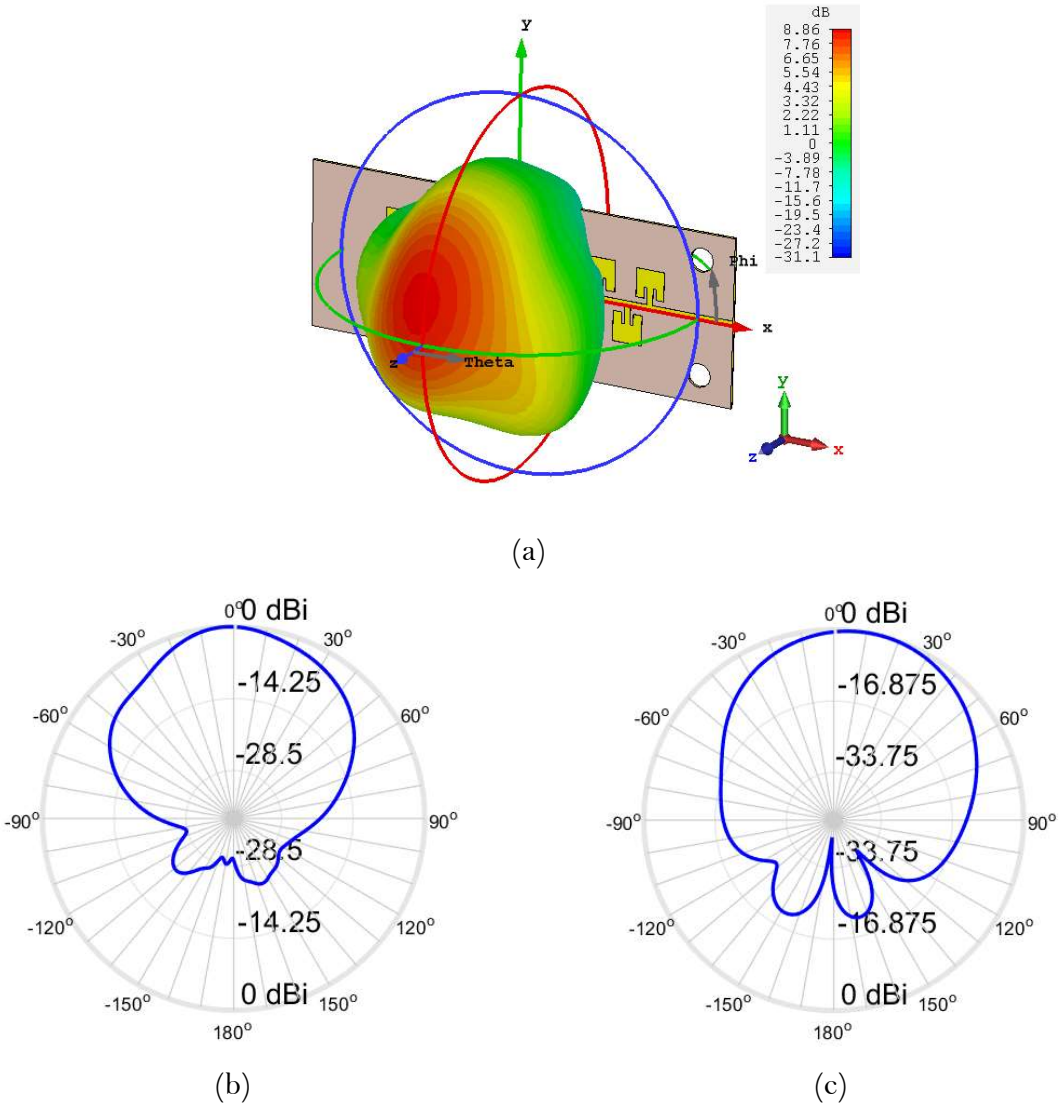

Figure 5.22: Radiation Patterns of the 9-element array at 29 GHz: (a) 3D representation; (b) φ = 0° plane; (c) φ = 90° plane.

Just like in the other arrays, the radiation pattern at 29 GHz was studied to characterize the operation of the array throughout the frequency, and it is presented in Figure 5.22.

The main lobe is very close to the centre of both polar patterns, which is desirable for this array since this is supposed to be a directional array.

A maximum gain of 8.86 dBi was acquired in the simulation. This indicates that the gain is identical throughout the operating band, which is a good characteristic for an wideband array.

In terms of sidelobe level, its highest value is -20.2 dB, which is good, since the value is low and is not going to interfere with the array behaviour.

5.2.3.3 Maximum Gain and Efficiency over frequency

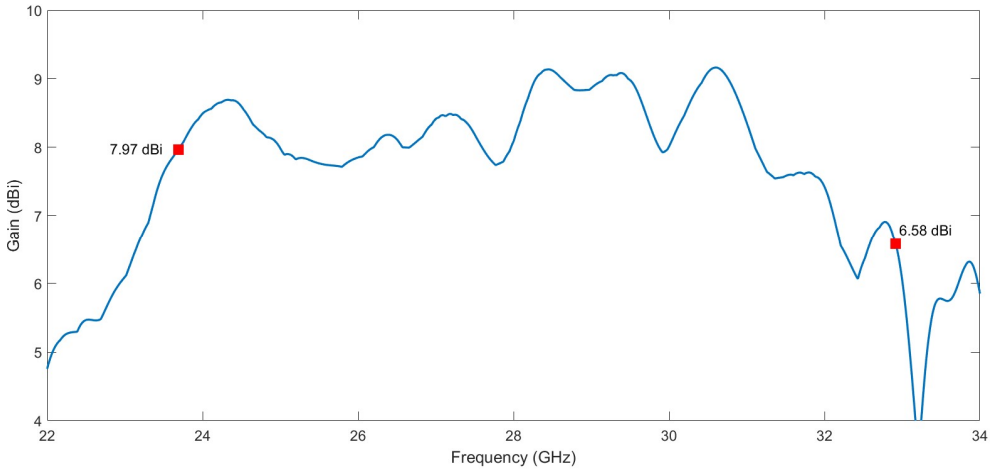

Figure 5.23: Maximum Gain versus Frequency in the 9-element array.

Figure 5.23 shows the maximum gain behaviour of the array. With the aid of the markers is visible that this array has a gain higher than 7 dBi in the majority of the band of operation. However, this indicates that the gain dropped when compared with both previous arrays, meaning that adding more patches can cause a decrease in the gain. Overall the gain is still good, despite having decreased.

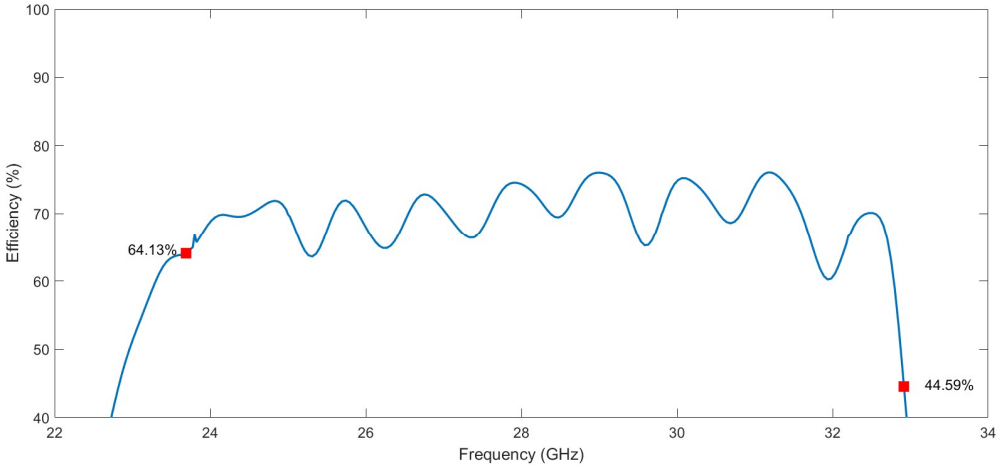

Figure 5.24: Efficiency versus Frequency in the 9-element array.

In terms of efficiency, and observing Figure 5.24, this array continues to have a similar behaviour when compared with the previous ones, but in the frequencies higher than 32 GHz this parameters decreases, which indicates that in high frequencies these kinds of arrays might have some problems in this aspect.

Altogether this array works well for mmWaves applications, even though that in higher frequencies these arrays might suffer a little more loss.

5.3 Wideband array at MmWaves: Thicker Substrate case

5.3.1 5-element array

To start the presentation of the several simulations made to characterize the arrays printed with a thicker substrate, the 5-element array is going to be the first to be presented, equally to the other set of arrays.

5.3.1.1 Reflection coefficient

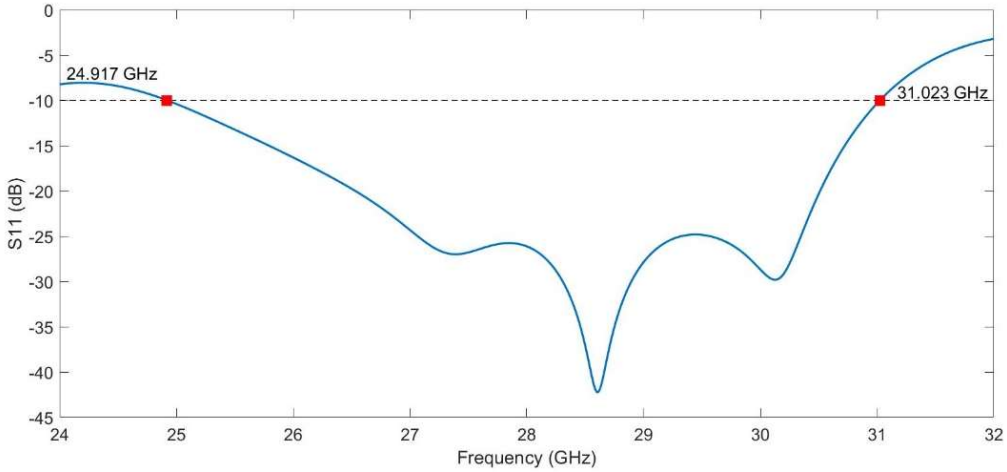

Figure 5.25: S11 response of the 5-element array.

Figure 5.25 displays the S11 performance of the 5-element array. As anticipated, introducing a quarter wavelength to the structure took away the log-periodic characteristic that the S11 presented in the previous arrays.

In the other perspective, the bandwidth covered by this array is higher when compared with the previous 5-element array simulated for mmWaves applications. Its frequency range begins at 24.917 GHz and stops at 31.023 GHz, corresponding to a fractional bandwidth of 0.218. This is a good factor in favour of this array when compared with the previous one designed, but without seeing the radiation patterns, this array cannot be considered better or worse than the previous since there are still factors to be accounted.

5.3.1.2 Radiation Patterns

To make a full comparison between arrays the radiation patterns at 27 GHz, 28 GHz, and 29 GHz will be presented.

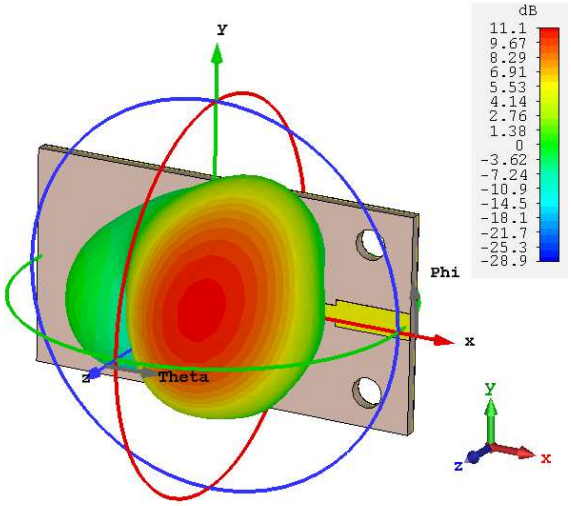

(a)

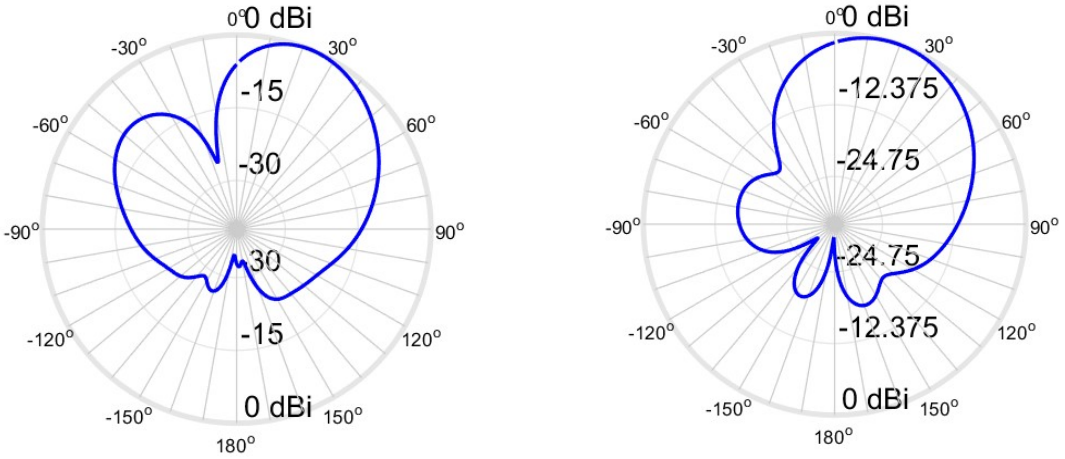

(b) (c)

Figure 5.26: Radiation Patterns of the 5-element array at 27 GHz: (a) 3D representation; (b) φ = 0° plane; (c) φ = 90° plane.

The radiation patterns at 27 GHz are displayed in Figure 5.26. When compared with the previous patterns, the maximum lobe of transmission suffers a deviation. This was expected since the 50 Ω line is very wide, being the main reason for the deviation on the pattern.

Comparatively, the gain enhances when compared with the other 5-element array. Such was expected because of the increase of thickness in the substrate. This is a good

factor in this array, considering that the attenuations in the mmWaves are much higher, having antennas with this characteristic upgraded is desirable.

One thing to consider when measuring this array gain is that the maximum lobe is not considered in both polar patterns presented, meaning that the gain measured is going to be different from the maximum value of 11.1 dBi, but instead it should present a value close to 9.88 dBi, maximum value of gain in the plane $\varphi = 0°$.

The last comment to this pattern is the fact that in this array, the sidelobe value is very high, which is an unwanted factor, and might influence the operation of the array at this frequency.

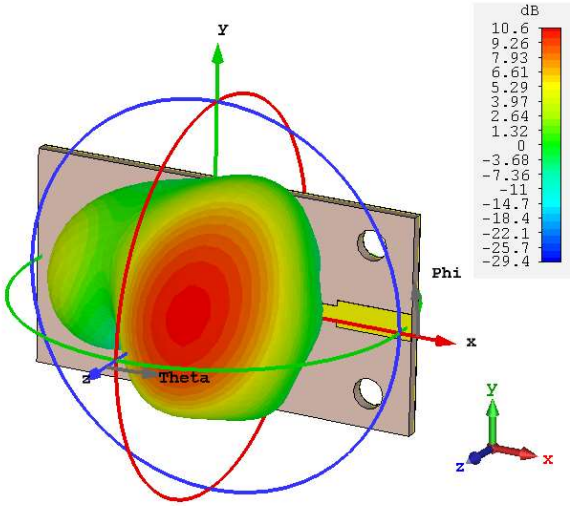

(a)

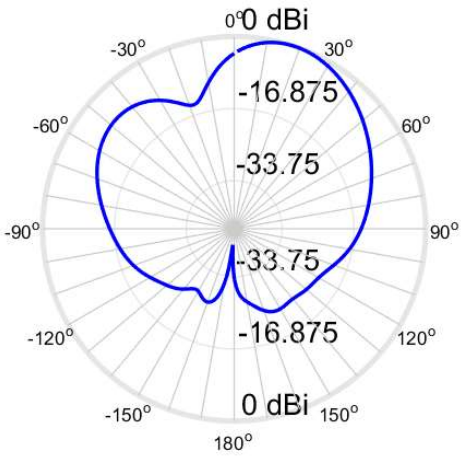

(b)

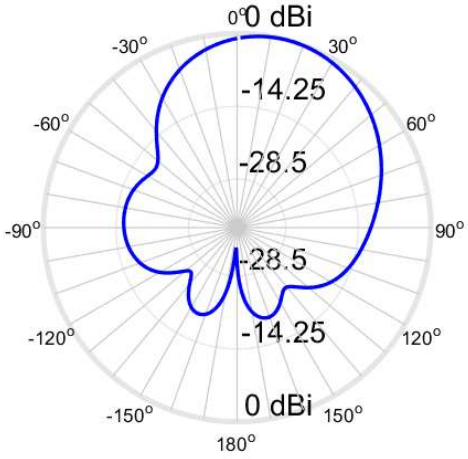

(c)

Figure 5.27:Radiation Patterns of the 5-element array at 28 GHz: (a) 3D representation; (b) $\varphi = 0°$ plane; (c) $\varphi = 90°$ plane.

Continuing to evaluate the performance of the array, Figure 5.27 presents its radiation pattern at 28 GHz. This pattern is similar to the one presented for 27 GHz. Therefore, some appreciations made for the previous pattern can be applied to this one, the deviation in the main lobe is almost the same, and the sidelobe level continues to present a high value that can influence the performance.

Looking into the gain, the maximum gain presented has a value of 10.6 dBi, which is 0.5 dBi less when compared with 27 GHz but continues to be higher than the gains presented previously in this dissertation. In the same manner as 27 GHz, the maximum lobe is not shown in both polar planes, and the maximum gain that the measurements should present is 9.61 dBi, from $\varphi = 0°$ plane.

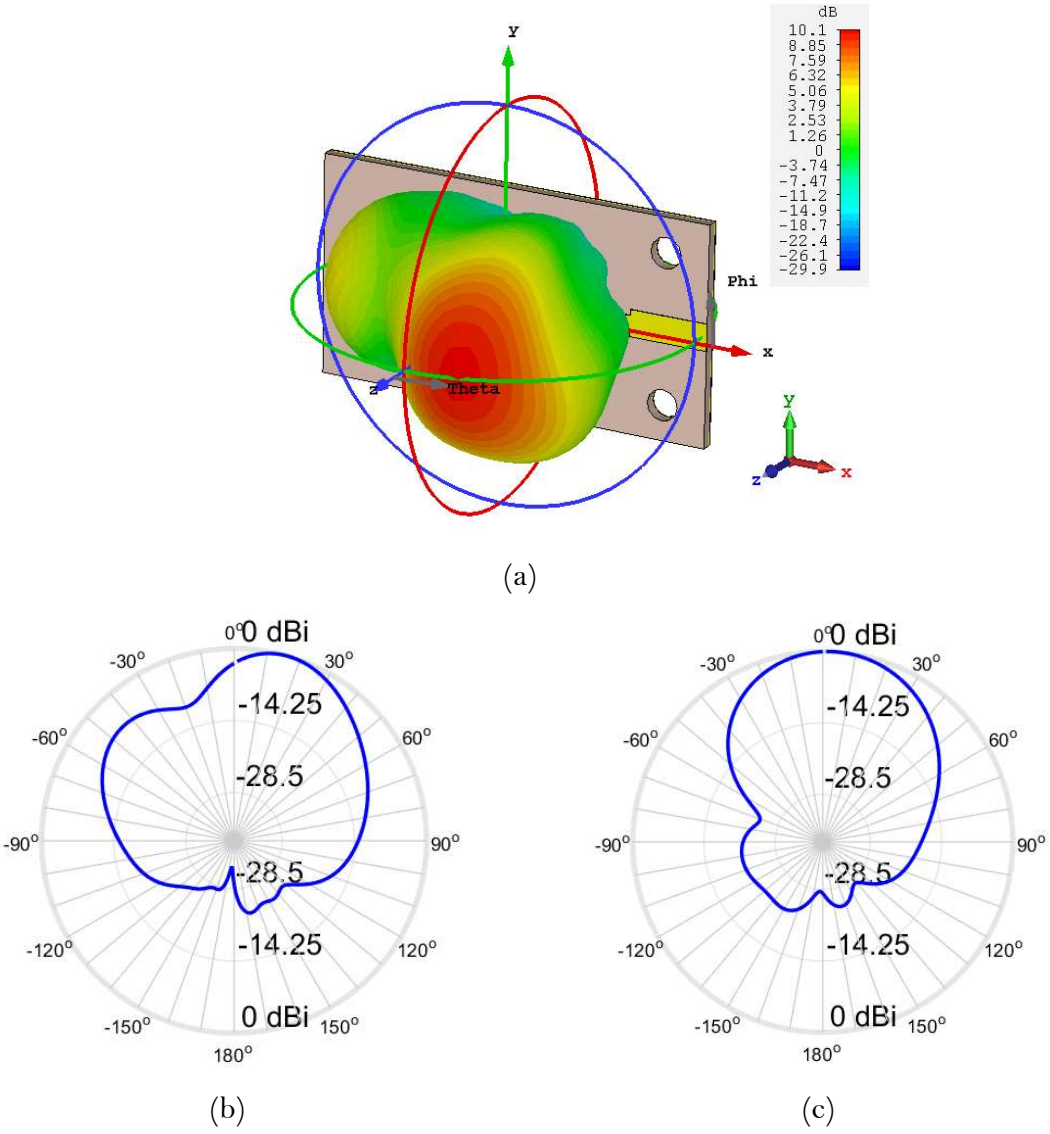

Figure 5.28: Radiation Patterns of the 5-element array at 29 GHz: (a) 3D representation; (b) $\varphi = 0°$ plane; (c) $\varphi = 90°$ plane.

To finalize the characterization of the wideband array, the pattern at 29 GHz is presented in Figure 5.28.

In comparison with previous patterns, the main lobe is closer to the centre point of the axes. However, the deviation towards the 50 Ω line is maintained.

Nonetheless, gain continues to decrease, now the maximum gain is 10.1 dBi, but in this case, the maximum gain can be measured since the gain at plane $\varphi = 0°$ is the maximum gain at the frequency.

One problem that persists is the fact that the sidelobe being at a high value, which is undesired and may influence the operation of the array.

In general, these patterns show some problems and some advantages when compared with ones presented for the previous arrays of this dissertation. Having a higher gain is the main factor in favour of this array. On the negative side, the sidelobe level increased and might pose a problem in the operation at specific frequencies. Nevertheless, the patterns of this array are going to be measured to have a comparison factor and further evaluate its performance.

5.3.1.3 Maximum Gain and Efficiency over frequency

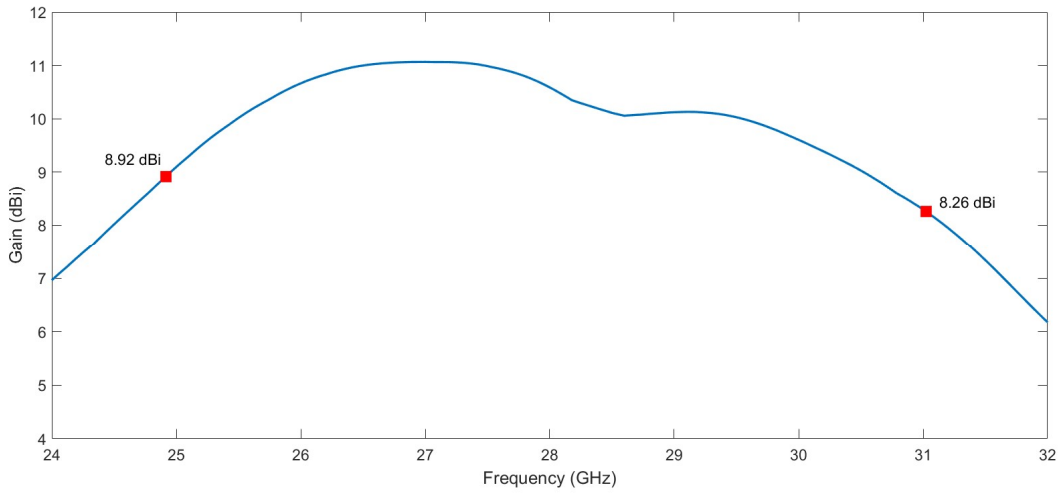

Figure 5.29: Maximum Gain versus Frequency in the 5-element array.

Through Figure 5.29 and comparing with both preceding 5-element arrays, it is possible to observe that in this array the gain increased, due to the thicker substrate used, and is a little more stable, here the gain increases in almost a constant manner and when the decrease starts it does not abruptly change. Another good point is that the gain is greater than 8 dBi throughout all the frequency range, the markers help to perceive that.

In general, the gain behaviour is a little better when compared with both 5-elements arrays earlier presented.

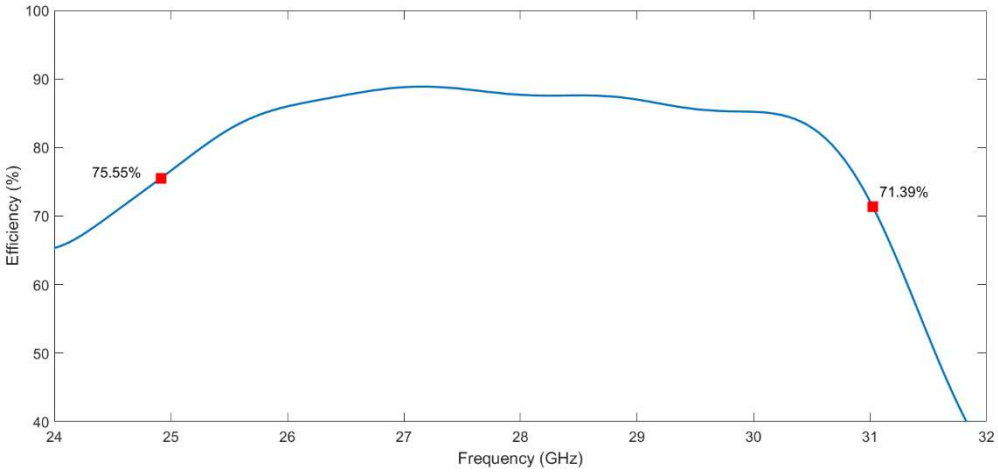

Figure 5.30: Efficiency versus Frequency in the 5-element array.

Using Figure 5.30 some conclusions can be taken regarding efficiency. First, the efficiency value increases when compared with all previous arrays, now the value presented is higher than 80% in almost the entire frequency band, meaning that this array does not have many losses. Second, in both delimiting points of the array frequency range, the values of efficiency increased, and the problem of efficiency presented in frequencies higher than 30 GHz does not present himself in this array.

To sum up, this array has a better performance in these parameters and makes him a viable solution for mmWaves applications.

5.3.2 7-element array

Continuing to present the arrays printed with the thicker substrate, now it is time to present the simulation results of the 7-element array. The idea of this array is to increase the bandwidth while maintaining a similar gain and efficiency throughout the frequency.

5.3.2.1 Reflection coefficient

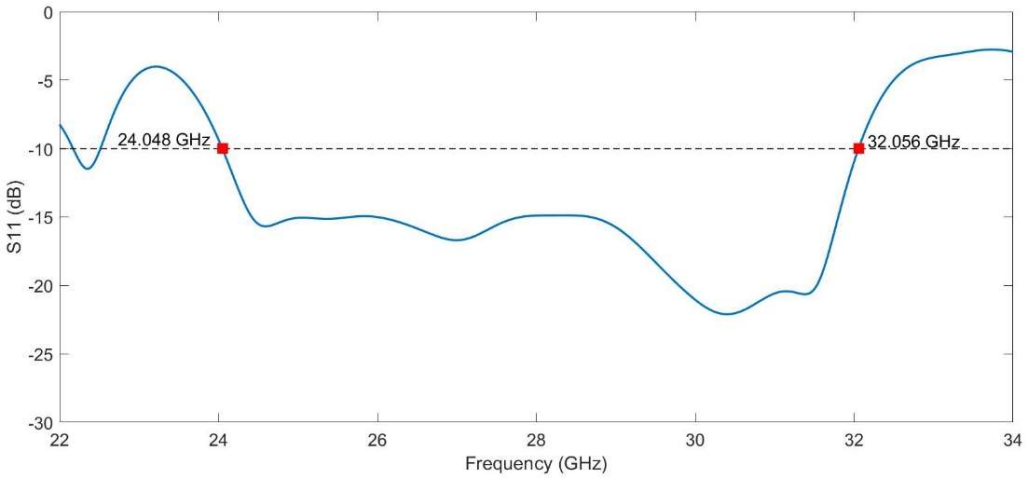

Figure 5.31: Simulated S11 of the 7-element array.

Figure 5.31 exhibits the S11 response of the array. In this case, the array loses its log-periodic properties

. In spite of losing that characteristic, its bandwidth covered is more substantial when compared with the previously designed 7-element array. The frequency of operation starts at 24.048 GHz and stops at 32.056 GHz, covering 8.008 GHz of bandwidth, which is equivalent to 0.286 in fractional bandwidth. Putting into context, this array is considered an ultra-wideband array.

5.3.2.2 Radiation Patterns

Identically, the radiation patterns for frequencies of 27 GHz, 28 GHz, and 29 GHz were studied to provide a better characterization of the 7-element array.

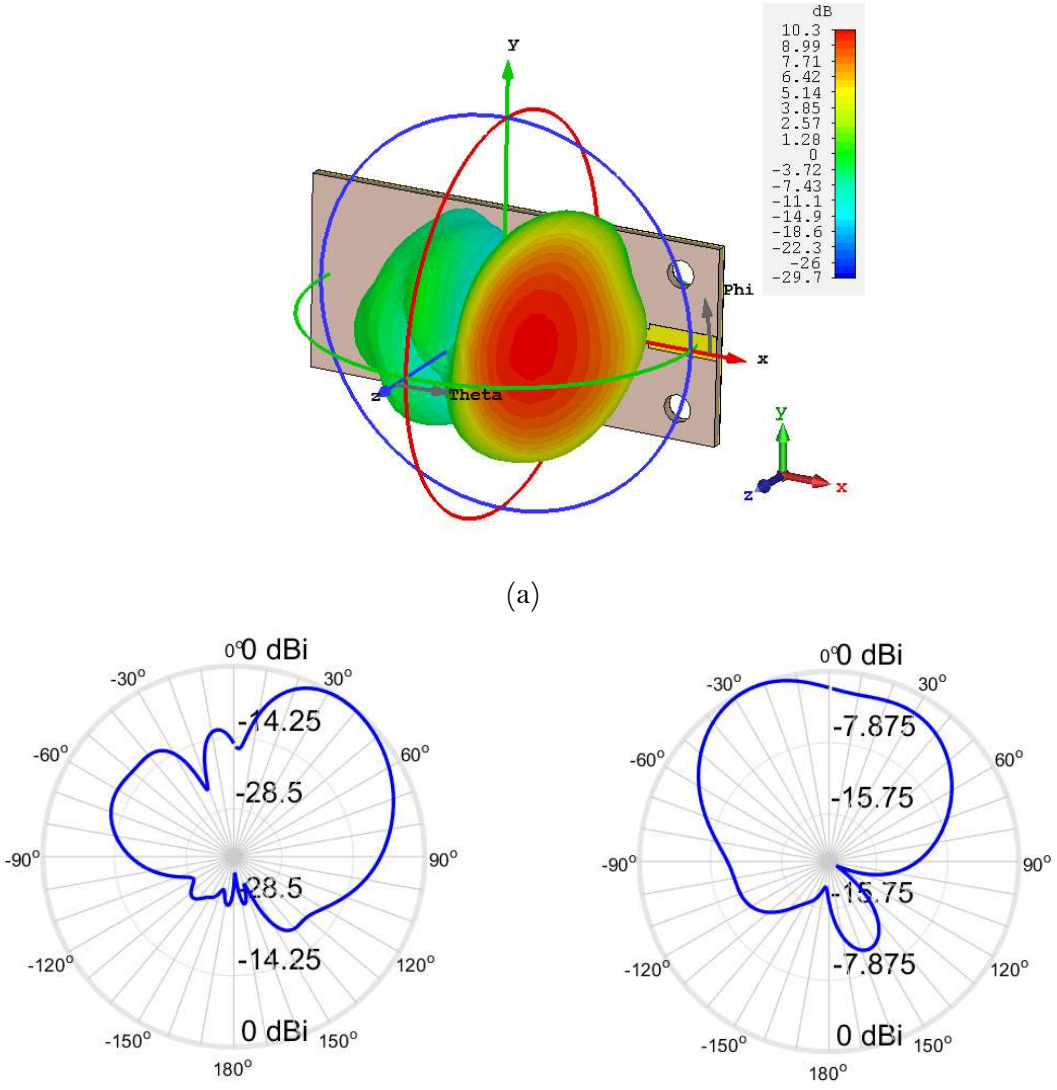

(a)

(b)

(c)

Figure 5.32: Radiation Patterns of the 7-element array at 27 GHz: (a) 3D representation; (b) φ = 0° plane; (c) φ = 90° plane.

Figure 5.32 exhibits the radiation patterns at 27 GHz. This pattern is similar to the one presented at the same frequency in the 5-element array. The 50 Ω line influence is still noticeable, and even a little more deviate towards the line.

Comparing the gain at this frequency with the presented for the 5-element array, a decrease occurs, the maximum gain presented is 10.3 dBi, which is a good value for this parameter.

However, since the planes that will be measured do not contain the maximum gain, the value to take into account when comparing the simulated and measured gain is 9.84 dBi, which is the maximum gain at the plane φ = 0°.

One last consideration should be made. The sidelobe level continues to increase, meaning that this effect tends to worsen as the number of elements increases.

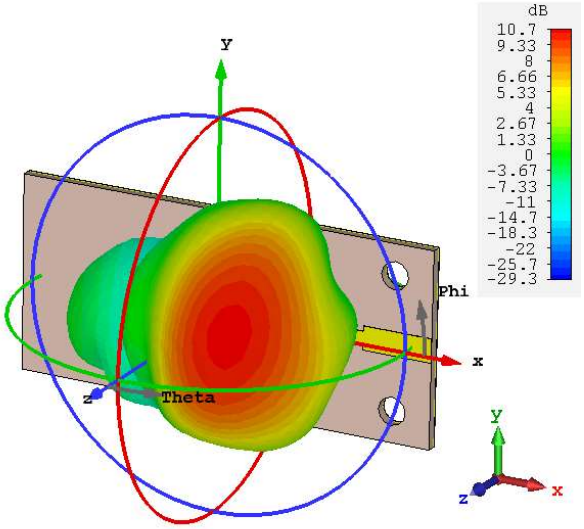

(a)

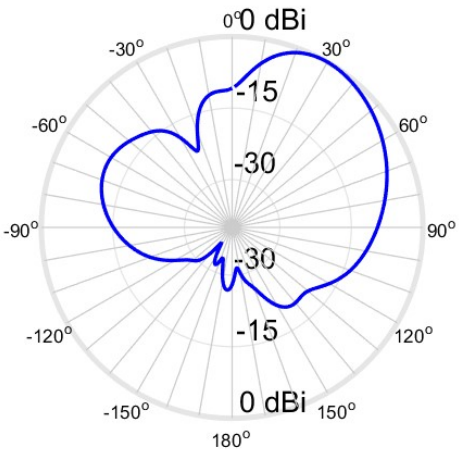

(b)

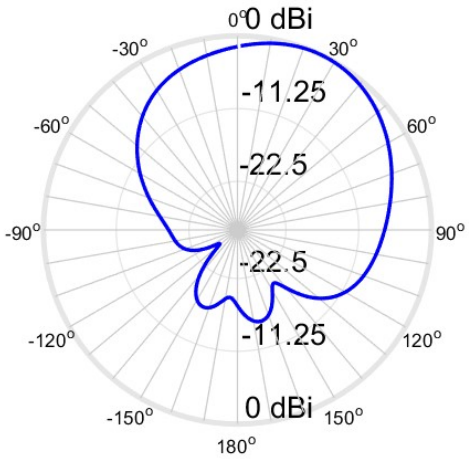

(c)

Figure 5.33: Radiation Patterns of the 7-element array at 28 GHz: (a) 3D representation; (b) φ = 0° plane; (c) φ = 90° plane.

At 28 GHz, Figure 5.33, the behaviour of the array is comparable with the pattern of 27 GHz. The main lobe direction deviates towards the patches, but only a few degrees it is not an extreme change of direction.

Comparing the gain at this frequency with the one presented for the 5-element array at this same frequency, they almost identical this gain is 10.7 dBi, while the other gain is 10.6 dBi. This means that at the frequency of the quarter wavelength transformer the gain performance is roughly the same.

Equally to the previous pattern, the maximum gain is not presented in both planes measured, so the reference gain upon measuring is 9.8 dBi presented in the φ = 0° plane.

The sidelobes at this frequency decrease, which is good because it causes fewer interferences in the array's operation.

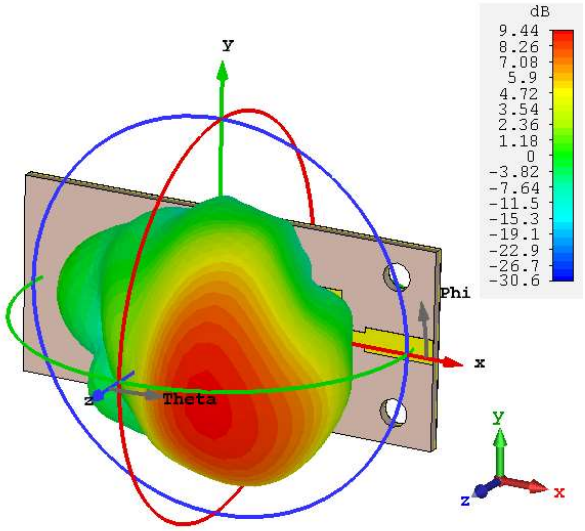

(a)

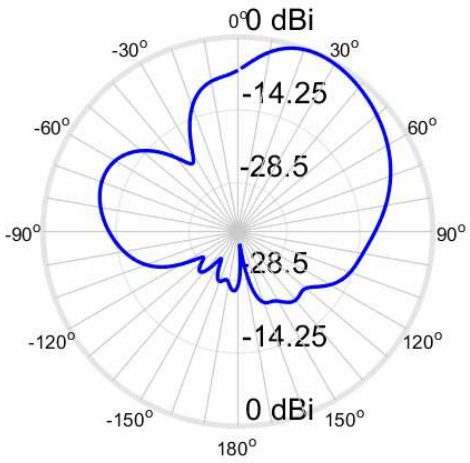

(b)

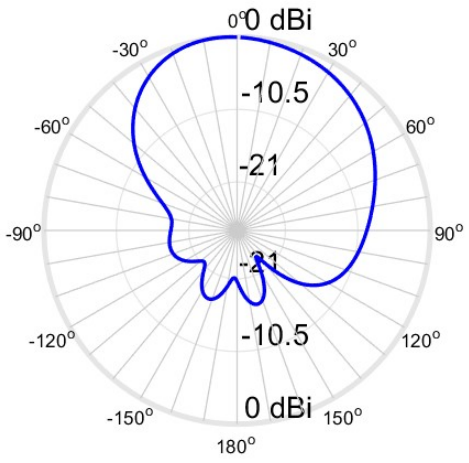

(c)

Figure 5.34: Radiation Patterns of the 7-element array at 29 GHz: (a) 3D representation; (b) φ = 0° plane; (c) φ = 90° plane.

As the last component of the characterization of this array, the 29 GHz radiation pattern is presented in Figure 5.34. In this case, the direction of the main lobe is almost centred in the plane φ = 0°. This will be good when measuring since the gain obtain is going to be similar to the maximum gain, although not the same.

The maximum gain at this frequency is 9.44 dBi, meaning that a 1 dBi decrease occurred which is not desired. However, the gain provided is still suitable for mmWaves applications.

The sidelobe level is high and might become a problem in the performance of the array at this frequency.

In general, these array radiation patterns are similar to the 5-element array, especially in the direction of the main lobe. On the other hand, this array provides less gain at some frequencies when compared with the 5-element array, which is undesirable.

5.3.2.3 Maximum Gain and Efficiency over frequency

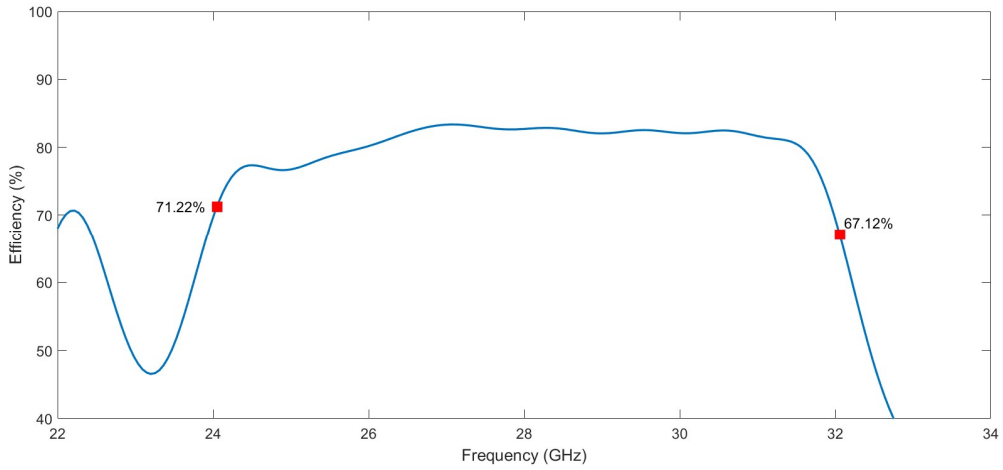

Figure 5.35: Maximum Gain versus Frequency int the 7-element array.

Figure 5.35 demonstrates the gain behaviour throughout the frequency. The gain has some variations, and when compared with the 5-element array, this characteristic is a little more deteriorated. The gain is higher than 7 dBi in the frequency band, that can be seen with the help of the markers. But the variations presented can be a factor that diminishes the operations of the array.

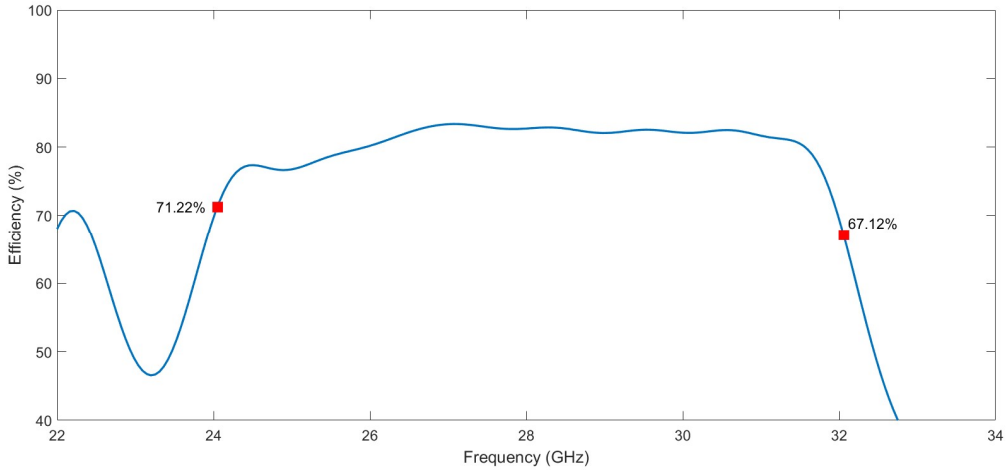

Figure 5.36: Efficiency versus Frequency in the 7-element array.

As a final parameter of this array, Figure 5.36 shows the Efficiency comportment in the frequency. In this regard, the efficiency increases when compared with the other 7-element array. Be that as it may, when compared with the 5-element array the efficiency lowered, even if slightly this must be pointed.

In conclusion, this array gain performance and efficiency are better than the previous 7-element array, however, when compared with 5-element array they worsen which is undesirable,

5.3.3 9-element array

To Finalize this set of arrays, the 9-element array simulations results will be presented. This array intends to enhance the bandwidth while maintaining, or even improve, the other characteristics of the array.

5.3.3.1 Reflection coefficient

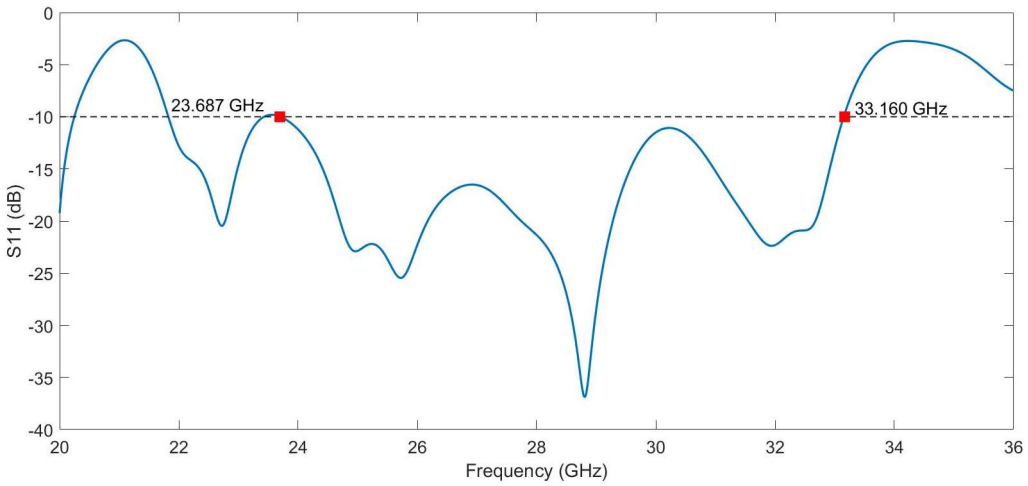

Figure 5.37: Simulated S11 of the 9-element array.

Like the previous arrays, the first parameter to be presented is the S11, and this can be contemplated by observing Figure 5.37.

The markers assist in perceive the bandwidth covered by this array. The frequency range starts at 23.687 GHz and stops at 33.160 GHz, that equals to 9.473 GHz of frequency covered and a fractional bandwidth of 0.333. Despite having more bandwidth lower than - 10 dB, this array start frequency is at 23.687 GHz because before that value of frequency the S11 is above -10 dB.

Having the fractional bandwidth in consideration and applying considering the classifications in Table 2.1, this array is classified as ultra-wideband array. This is great since the objective was to create a wideband array, and applying this technique was so successful that the objective was achieved and surpassed.

Nonetheless, the rest of the parameters need careful evaluation since the S11 performance is not the only thing that matters.

5.3.3.2 Radiation Patterns

Keeping the coherence, the radiation patterns shown for this array are 27 GHz, 28 GHz, and 29 GHz. By doing this a comparison between the patterns of each array can be made.

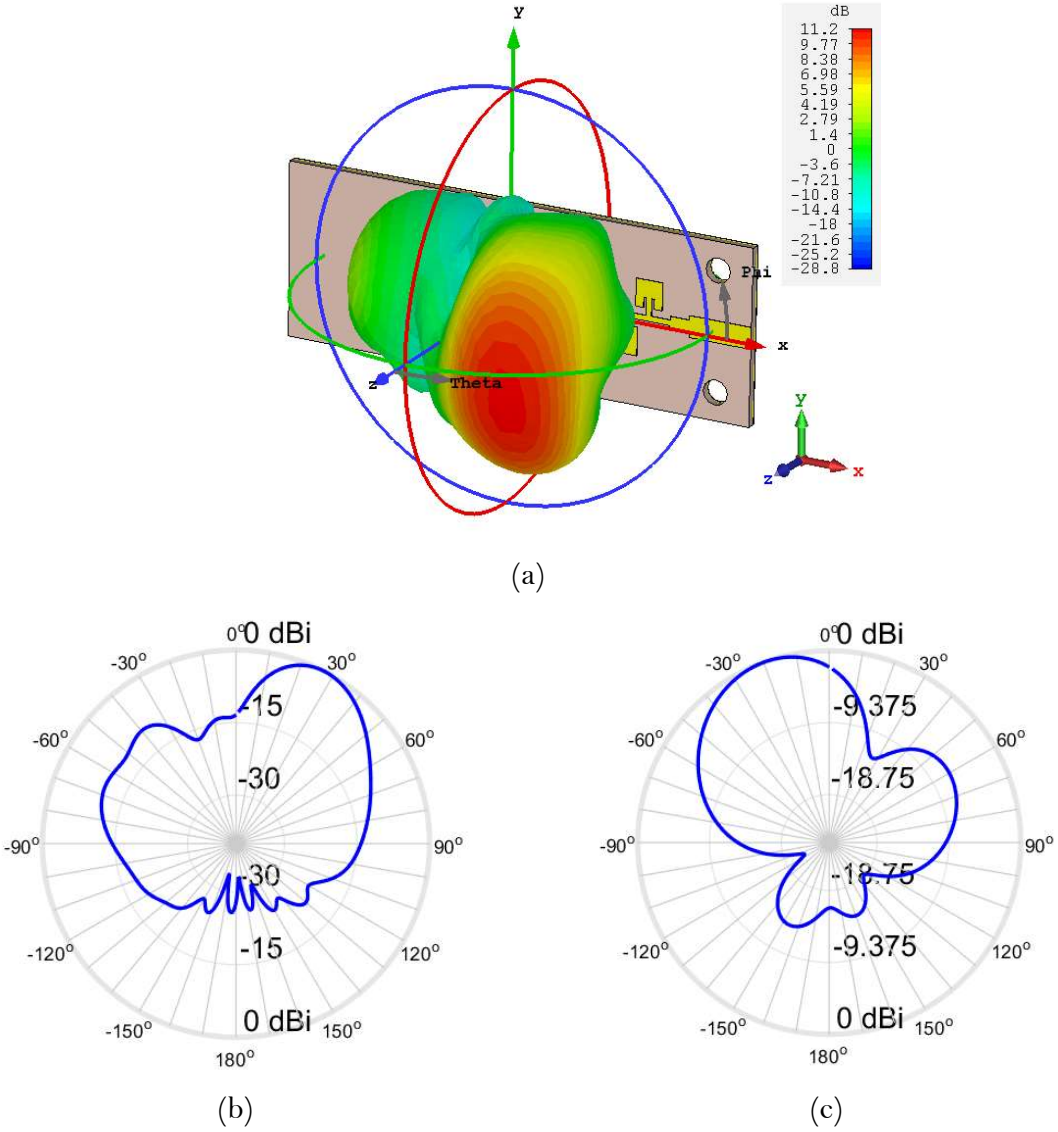

Figure 5.38: Radiation Patterns of the 9-element array at 27 GHz: (a) 3D representation; (b) φ = 0° plane; (c) φ = 90° plane.

Starting with the radiation patterns at 27 GHz, presented in Figure 5.38, in this case, the pattern maintains an identical form to the previous arrays made with the same 90 Ω structure. The only difference is that the main lobe is closer to the plane φ = 0°, which indicates that the gain obtained when measuring the plane will be similar to the maximum gain.

Nonetheless, the 50 Ω line still causes some problems since the best point of transmission is not in teh centre of the axes.

The maximum gain at this frequency is 11.2 dBi, though, the maximum gain that can be measured is 11 dBi, in the plane φ = 0°, this value is very close to the maximum gain.

The major problem in this array is the sidelobe level. The value of this parameter is -6.9 dB, which is not the best and might influence the transmission of the signal.

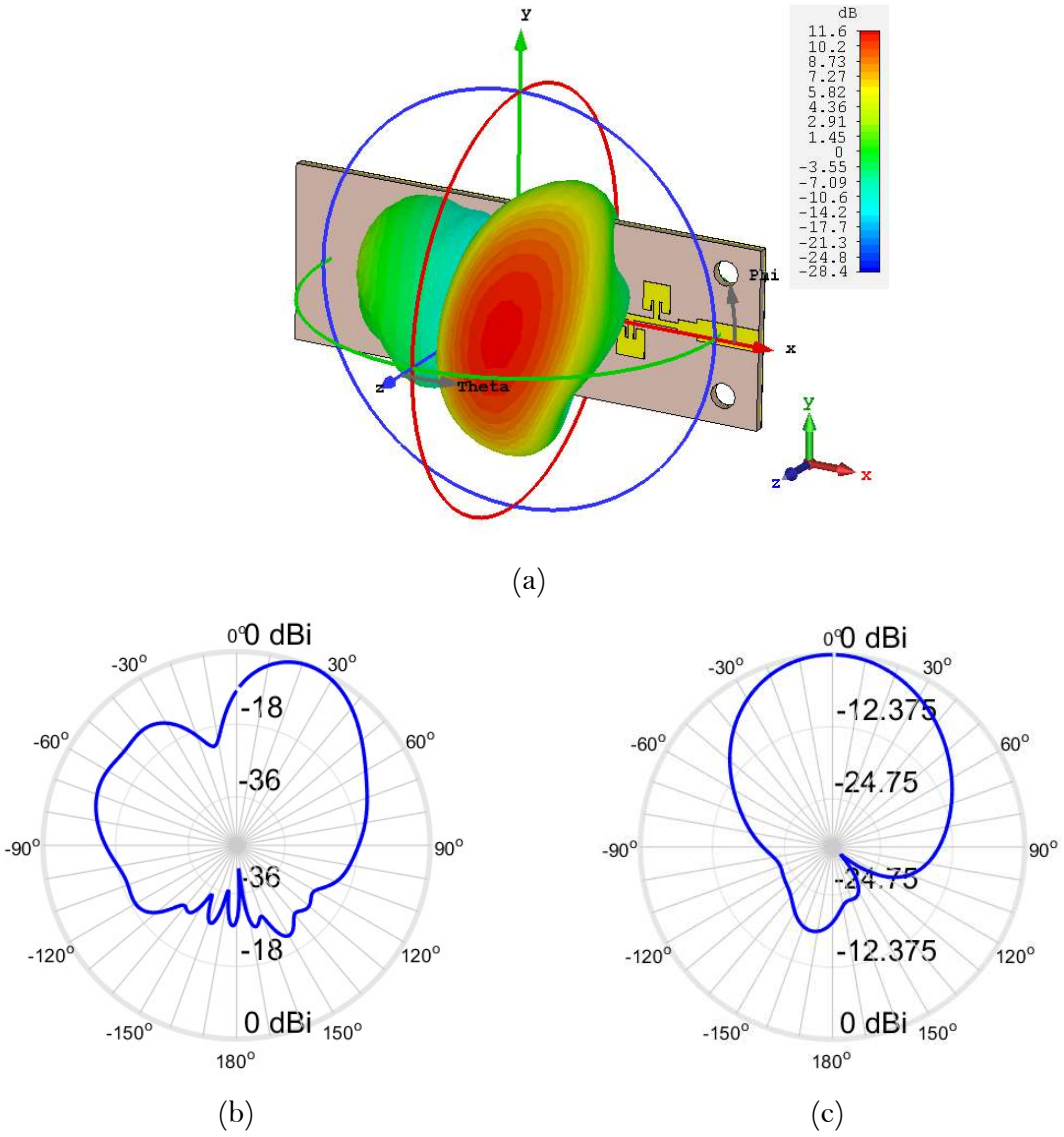

Figure 5.39: Radiation Patterns of the 9-element array at 28 GHz: (a) 3D representation; (b) φ = 0° plane; (c) φ = 90° plane.

Figure 5.39 shows the radiation pattern at 28 GHz. This case is comparable with the 27 GHz. The main lobe is not in any of the polar planes, so, the maximum gain of 11.6 dBi cannot be measured.

Since the maximum gain is not going to be measured, the maximum gain measured is the one presented in the plane φ = 0°, which is 11.2 dBi.

One point that improves in this pattern is the sidelobe level when compared with 27 GHz pattern. The maximum value presented is -10.9 dB, although this is not a perfect value, it is better than value presented at 27 GHz and will influence less in the transmission.

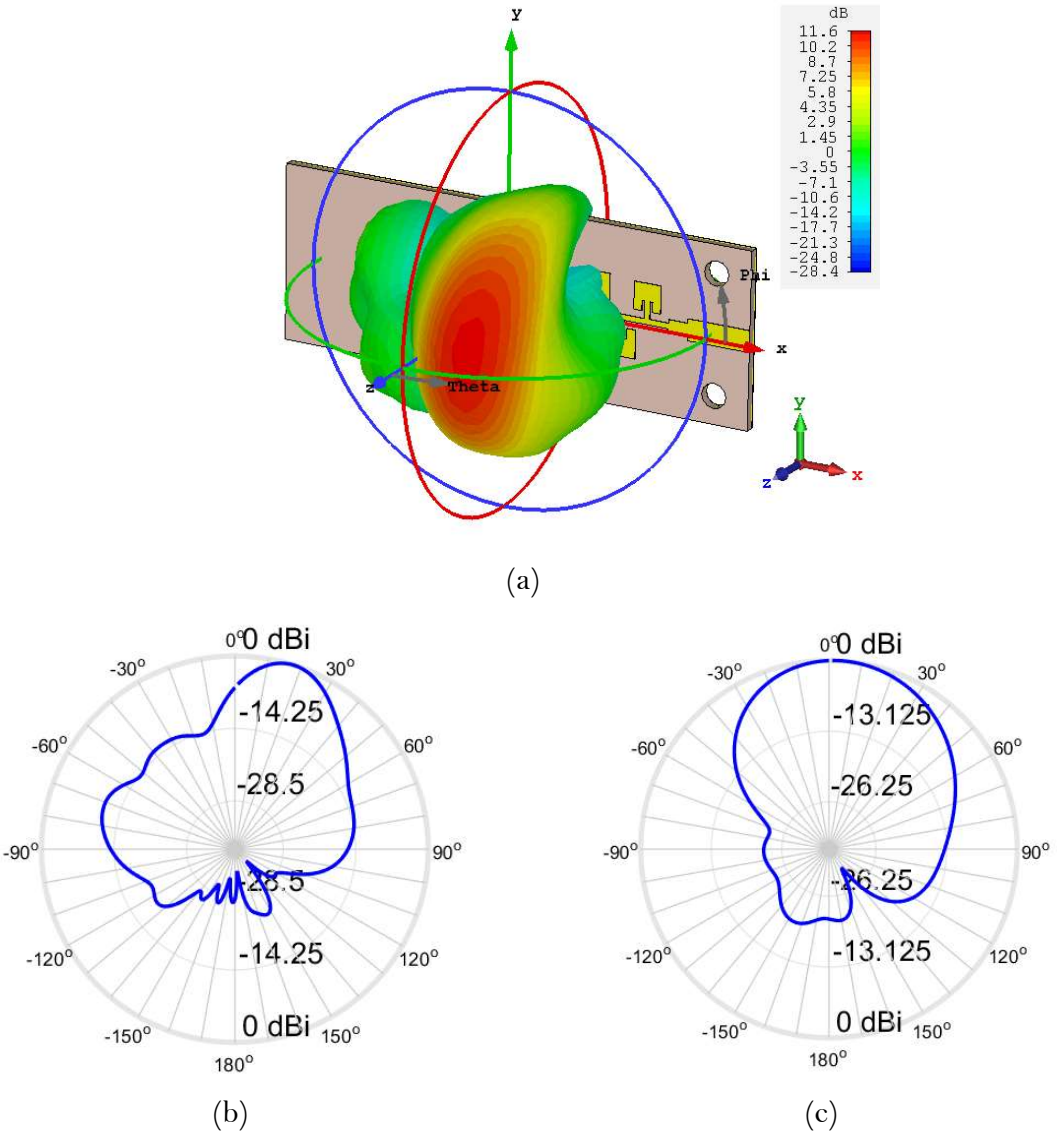

Figure 5.40: Radiation Patterns of the 9-element array at 29 GHz: (a) 3D representation; (b) φ = 0° plane; (c) φ = 90° plane.

The final array radiation pattern presented is the 29 GHz pattern, Figure 5.40. This pattern is similar to both previous patterns shown for this array characterization.

In the same manner as before the maximum gain, that has a value of 11.6 dBi, is not in either of the polar patterns presented. Therefore, the maximum gain that can be measured is 11.5 dBi, presented in the plane $\varphi = 0°$.

Lastly, the sidelobe level is -10.9 dB. This value shows that throughout the frequency band this characteristic improves and is less of problem, even so, this value is not exceptional, if compared with the other 9-element array simulated, it is worse but workable.

Briefly, the patterns of this arrays are more similar to each other, meaning that a point of ideal transmission can be found. The gain presented in the patterns is suitable for mmWaves applications since it can suppress free-space losses. However, these patterns present high values in the sidelobe level that may influence the transmission of the signal.

5.3.3.3 Maximum Gain and Efficiency over frequency

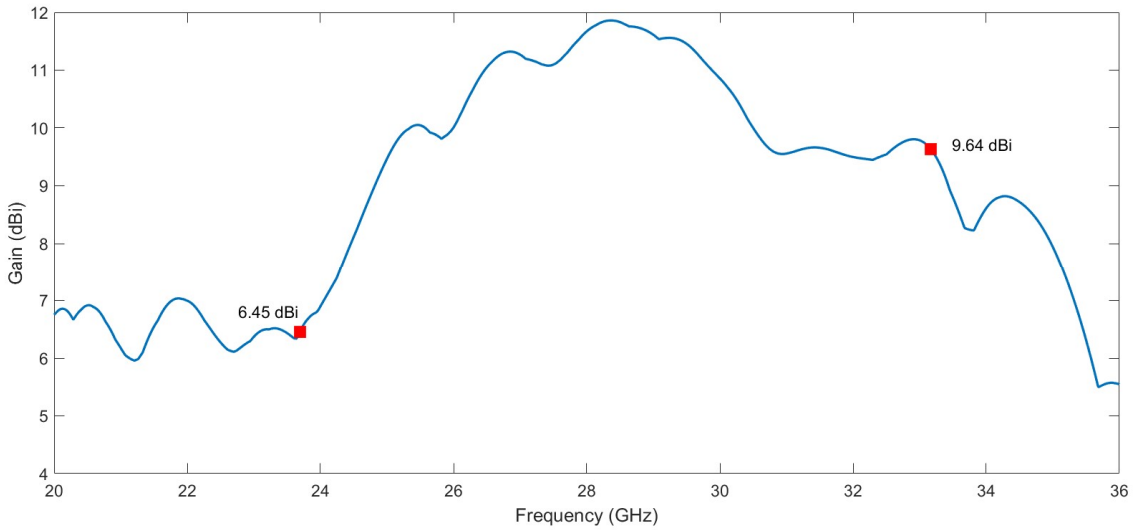

Figure 5.41: Maximum Gain versus Frequency in the 9-element printed array.

Figure 5.41 has a representation of the behaviour of the maximum gain throughout the frequency in the 9-element array. With the assistance of the markers, some points about the behaviour can be made, starting with the fact that the gain is not constant. The gain varies throughout the frequency and does not a fixed value, despite that the gain is greater than 9 dBi in the majority of the operating band which is good if we compare with the thinner arrays these values of gain are higher than the ones presented in all of those arrays.

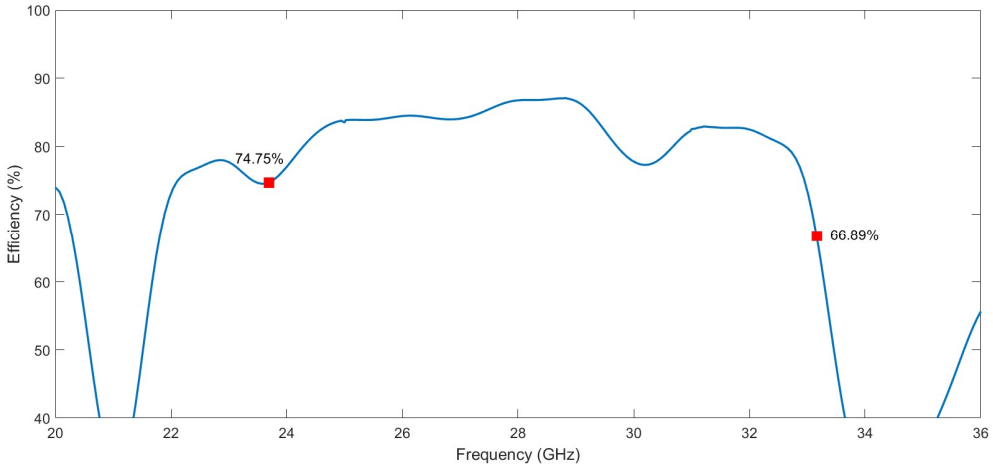

Figure 5.42: Efficiency versus Frequency in the 9-element printed array.

The final parameter shown is efficiency, and it is presented in Figure 5.42. In general, the array possesses a good efficiency, until 32 GHz the value is always greater than 75 %, which is better when compared with thinner arrays.

In conclusion, both gain and efficiency presented leave good indications about this array's operation, and overall this array seems adequate for mmWaves applications. Nonetheless, these are simulated values and some measurements need to be done to understand is real operation.

5.4 Comparison between MmWaves arrays results

. As previously mentioned, two different sets of arrays were designed. The main difference in their design is the substrate's height. Testing this characteristic helped to fully understand how to take advantage of log-periodic structures.

Even though these structures aim to have similarities in their results, the fact that in one case the characteristic impedance of the structure is 50 Ω, meaning that it is not necessary to make impedance transformations, and in the other is necessary to transform the characteristic impedance from 90 Ω to 50 Ω, using a quarter wavelength transformer, influence the various results of the simulations.

In the case of S11, one of the main components in the response disappears because of the usage of quarter wavelength transformer. This adaptation is necessary, however, by doing this the S11 is affected since only one frequency can be fully matched, that causes a change in the S11 and the typical log-periodic response is lost. From another point of view, by doing this adaptation the array covers more bandwidth than before which is a good

factor since this dissertation objective is to create arrays with as much bandwidth as possible

Table 5.1: Comparison of the fractional bandwidth presented by each array.

	5-element array Fractional Bandwidth	7-element array Fractional Bandwidth	9-element array Fractional Bandwidth
Thinner substrate	0.173	0.248	0.326
Thicker substrate	0.218	0.286	0.333

Table 5.1 confirms what was said before. By changing the impedance of the structure and then adapt using the quarter wavelength transformer higher bandwidth

In contrast, the radiation patterns of the thinner arrays are more directive, with the main lobe being close to the centre position of the axes, whereas the thicker arrays are more deviate due to the size of the 50 Ω line used in the adaption, this affects the main lobe direction. Another aspect in the patterns is the fact that, in the thicker arrays, the sidelobes possess higher power and can influence the transmission of the signal, while this does not happen in the thinner arrays.

Another point that deserves consideration is the gain. This factor benefits the printed arrays since they present a thicker substrate, which increases the gain. Nevertheless, all arrays presented a good gain, since it is higher than 8 dBi throughout the frequency in which the arrays operate.

Table 5.2: Comparison of the simulated gain for the 5-element arrays.

	Gain at 27 GHz (dBi)	Gain at 28 GHz (dBi)	Gain at 29 GHz (dBi)
Thinner substrate	8.82	9.09	8.62
Thicker substrate	11.1	10.6	10.1

Table 5.3: Comparison of the simulated gain for the 7-element arrays.

	Gain at 27 GHz (dBi)	Gain at 28 GHz (dBi)	Gain at 29 GHz (dBi)
Thinner substrate	9.12	9.29	8.94
Thicker substrate	10.28	10.66	9.44

Table 5.4: Comparison of the simulated gain for the 9-element arrays.

	Gain at 27 GHz (dBi)	Gain at 28 GHz (dBi)	Gain at 29 GHz (dBi)
Thinner substrate	8.42	8.09	8.86
Thicker substrate	11.17	11.64	11.61

Examining Table 5.2, Table 5.3 and Table 5.4, the antecedent facts are verified. All arrays that were printed using the thicker substrate present higher gain at the frequencies. In this point, using the thicker substrate is better since they can be work in systems with higher sensibility.

The last issue that deserves comment is the efficiency. By observing the several graphs presented for the efficiency of each array, it can be concluded that the arrays with more thickness have higher efficiencies overall throughout their operating band, becoming another point in favour of these arrays.

In conclusion, an ideal array constructed based on this structure should maintain a constant impedance, or at least similar impedances that do not influence the radiation patterns, provide a gain equivalent to the thicker arrays, have an efficiency close to the one presented in the thicker arrays, the S11 characteristics of the thinner arrays, and provide the fractional bandwidth of the thicker arrays. However, for this a new substrate should be used to provide these characteristics.

Chapter 6

6 Measurements and discussion

This chapter presents the results obtained when measuring the arrays that were printed. The measurements were made using a Vector Network analyzer (VNA). The radiation patterns of C band array were measured using the anechoic chamber of Departamento de Eletrónica, Telecomunicações e Informática (DETI). For the mmWaves arrays it was used the anechoic chamber of Instituto de Telecomunicações (IT).

6.1 Wideband array at C Band Results

Simulating an array shows is behaviour in a perfect environment. When the array is printed some variables, influence is performance. A few examples are the precision of machine printing the array, the losses in the substrate, or space where measurements are made. All these factors cause a change in the response of the array.

As said before an array operating at a lower band of frequencies was simulated to understand the various factors involved in the development of these arrays. Figure 6.1 demonstrates this array after being printed.

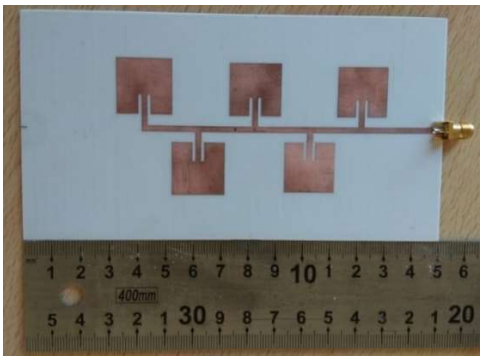

Figure 6.1: Image of the printed array.

To begin the measurements the S11 performance of the array was measured using a VNA.

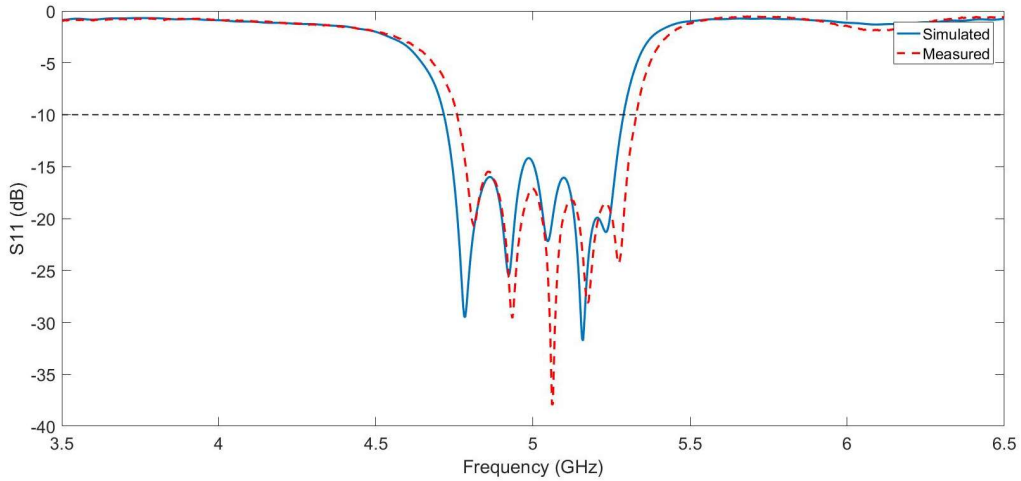

Figure 6.2: Comparison between simulated and measured S11 of the 5-element C band array.

Figure 6.2 demonstrates S11 Simulated and measured of the 5-element array. A minor frequency shift occurs. However, this is common in microstrip antennas. One thing noticeable is the fact that each peak changes its adaptation, in some improves but in others decrease, but in general the S11 has a great result.

To measure the radiation diagrams some characteristics needed to be taken in account. When measuring S_{21} parameters, needed to characterize the array, they are measured with an antenna of reference that possesses a specific gain at each frequency, G_{ref}. The values measured are not normalized and do not consider the reference antenna properties.

So, to calculate the gain of the antenna, it is necessary to measure the S21 value of the reference antenna at each frequency of operation, S_{21_ref}.

Lastly, the S_{21} of the printed antenna, S_{21aut}, is measured to calculate the gain and make the polar representations.

With all these factors, and using equation (6.1), the gain of the array is calculated for each frequency.

$$G_{AUT} = G_{ref} - \left(S_{21\_ref} - S_{21_{aut}}\right) \tag{6.1}$$

This equation is going to be used in every array of this dissertation to calculate the various gains.

Using all notions presented, the measured results for the frequencies of 4.8 GHz, 5 GHz, and 5.2 GHz where taken.

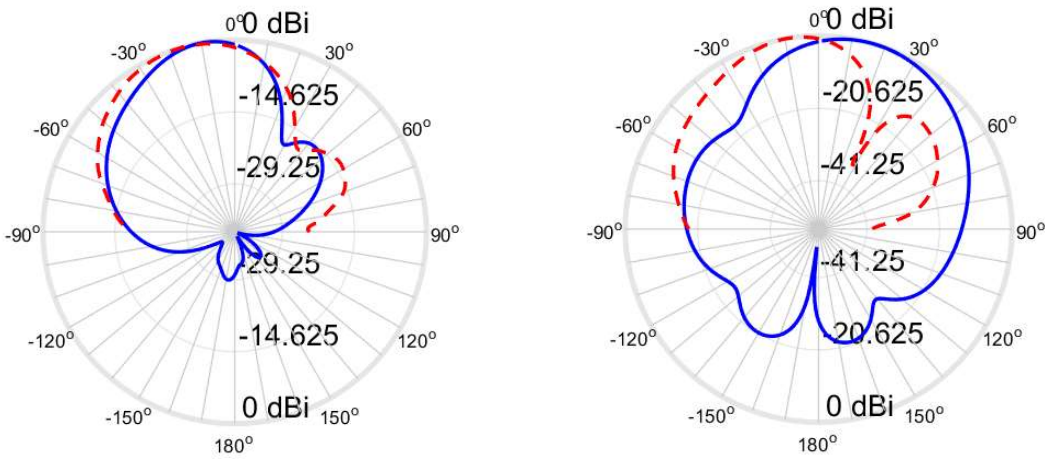

(a) (b)

Figure 6.3: Comparison between Simulated (Blue) and Measured (Red) radiation patterns at 4.8 GHz in the planes: (a) φ =0°; (b) φ =90°.

Figure 6.3 shows the polar representation of the radiation patterns. Comparing the simulated and measured results, in general their performance is similar. However, on plane φ = 90° a difference in between the simulated and measured value exists, this was not expected and the measurements should be repeated.

The maximum gain simulated at this frequency is 9.5 dBi. However, this gain is not represented in either of the planes measured. So, the reference gain when measuring was the gain in the plane φ = 0°, which is 9.12 dBi. Using equation (6.1) the gain was calculated. The value obtained was 9.1 dBi, meaning that, at this frequency, the gains are almost the same, which implies that this array operation is similar to the simulation.

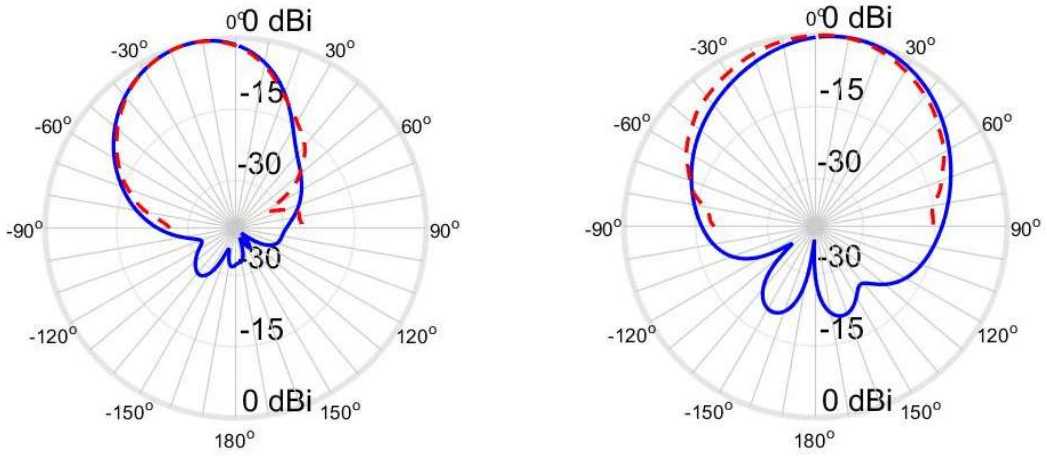

(a) (b)

Figure 6.4: Comparison between Simulated (Blue) and Measured (Red) radiation patterns at 5 GHz in the planes: (a) φ = 0°; (b) φ = 90°.

Figure 6.4 shows the patterns at 5 GHz. These diagrams are very similar, which means a good correlation exists between simulation and measurements, which is good.

The gain obtained was 9.74 dBi, which is less when compared with the maximum gain theoretical, 10.1 dBi. However, the best point of transmission is not represented in these graphs meaning that the maximum is not presented in these patterns.

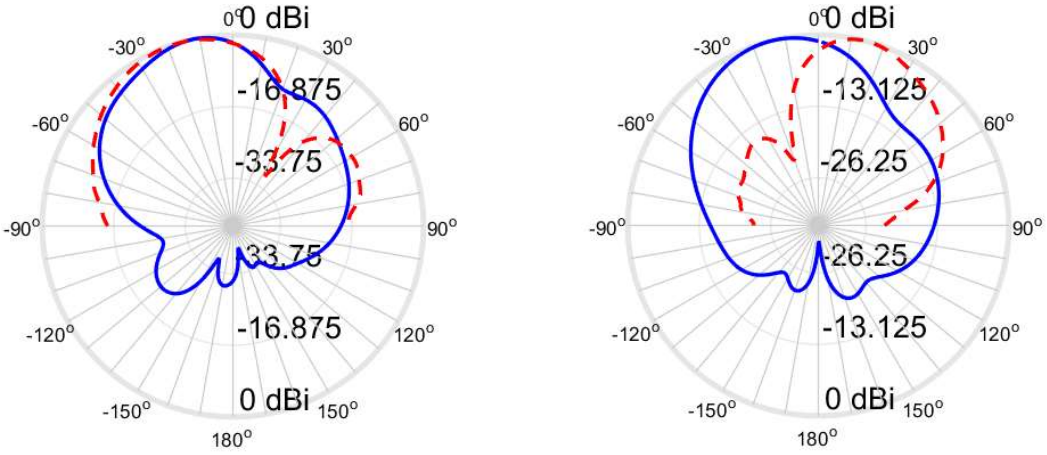

(a) (b)

Figure 6.5: Comparison between Simulated (Blue) and Measured (Red) radiation patterns at 5.2 GHz in the planes: (a) φ =0°; (b) φ =90°.

To finalize the characterization of this array, Figure 6.5 shows a comparison of the radiation patterns at 5.2 GHz.

In this case, some differences can be observed. First, in the φ = 90° the results do not match and at this plane the measurements should be repeated.

Second, in the plane φ = 0° a sidelobe level appeared when measuring, meaning that in this plane a misplacement occurred too.

Concerning the gain, the maximum gain point is contained in the plane φ =0°, 8.18 dBi, meaning that the gain calculated should be comparable. The gain measured was 8.58 dBi, which is higher. This difference is not substantial, and this indicates that the gain measured is more stable throughout the frequency.

To summarize, in some planes there were some errors upon measuring, in such cases the differences between simulated and measured values are noticeable. The gain values were similar at the frequencies, meaning that this factor behaves as expected.

With these values taken, in general, this array performance is good, which leaves useful insights for the following arrays.

6.2 MmWaves Arrays Results: Thinner substrate case

In the previous chapter, several simulations results helped to characterize the arrays made with a thinner substrate. Despite that, only the S11 measurements were performed in these arrays.

The main reason is the late arrival of the substrate, but another reason that caused some concerns is that the anechoic chamber in IT used to measure the radiation patterns may break the array, and that would be unpleasant.

So, this section is devised in three sub-sections, each one presenting the S11 measured of each array and comparing them with the simulation result.

6.2.1 5-element array

Figure 6.6: 5-element array printed for mmWaves applications using the thinner substrate.

Figure 6.6 shows the array after being printed. This proves that the array has a small and compact structure, as usual in a microstrip antenna. Using the VNA, the S11 was measured.

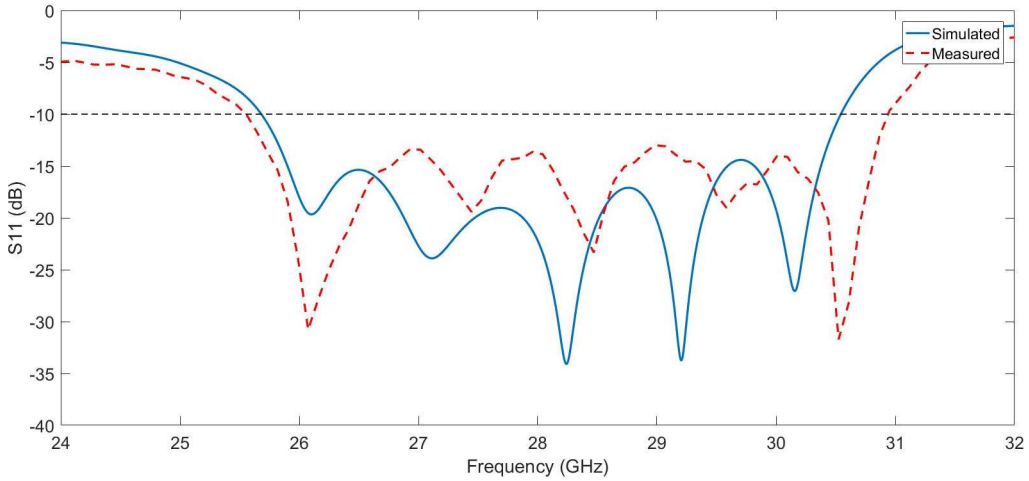

Figure 6.7: Comparison between the simulated and measured S11 of the 5-element array.

Through careful observation of Figure 6.7, some differences are found between the results. One functional difference is the fact that, in this case, the array covers more bandwidth than expected.

The measurements present a bandwidth of 5.388 GHz that starts at 25.551 GHz and stops at 30.939 GHz, such corresponds to a fractional bandwidth of 0.191This means that an increase of 0.018 occurred.

Another difference observed is that all the peaks at the respective frequency do not perform as expected. In some cases, the adaptation is lost, and in others enhanced.

A reason for this difference in the results is the fact that the machine used to print the arrays do not possess the necessary precision to make the array precisely as depicted in the simulation.

Overall, this array performance is better than anticipated in the simulations since more bandwidth is covered.

6.2.2 7-element array

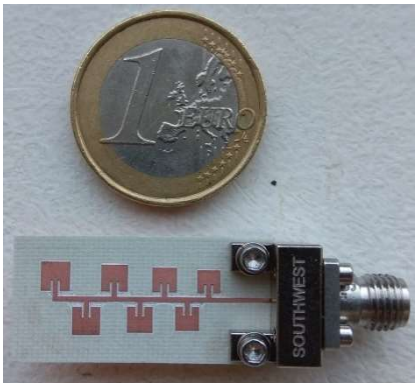

Figure 6.8: 7-element array printed for mmWaves applications using the thinner substrate.

In Figure 6.8, the 7-element used in the measurements is shown. This array is very similar to the 5-element array, the only difference between is the two elements added.

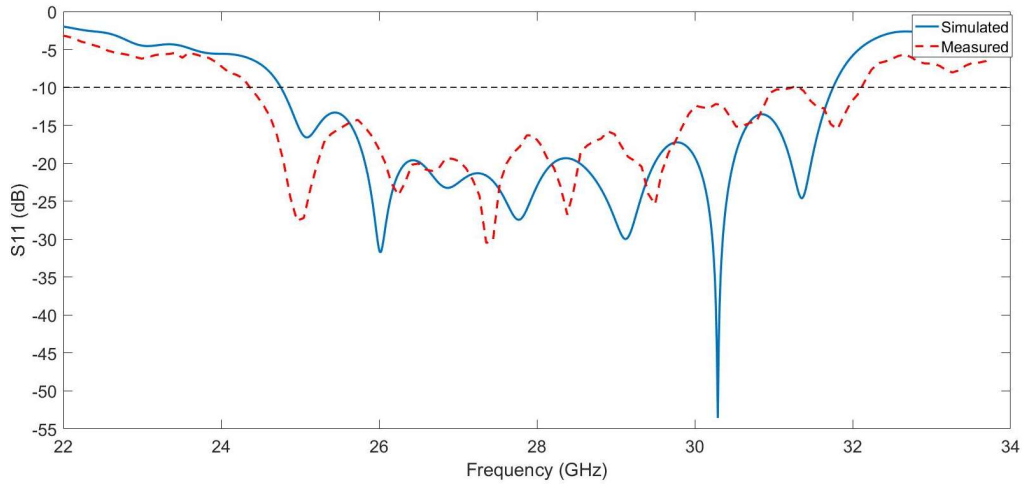

Figure 6.9: Comparison between the simulated and measured S11 of the 7-element array.

Using a VNA, the S11 of the array was measured, and the result obtained is shown in Figure 6.9.

In this case, the differences between the measured and simulated results are more accentuated. First, one of the peaks is no longer in the frequency band since there is a point

above -10 dB before that frequency. Second, the difference between adaptations is more noticeable.

Looking into the bandwidth covered, this array frequency range starts at 24.365 GHz and stops at 31.238 GHz. Therefore, the fractional bandwidth of this array is 0.247, which is similar to the 0.246 obtained in the simulation.

Even though this happens, the results acquired are not strange since the primary reason for this to happen is the fact that the machine that printed this array cannot print with the same precision used in the simulation, especially in the distances between patches.

6.2.3 9-element array

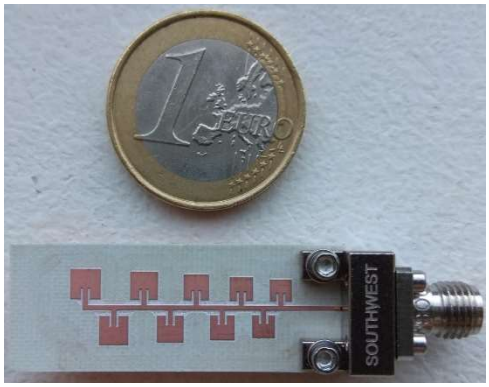

Figure 6.10: 9-element array printed for mmWaves applications using the thinner substrate.

The final array printed using this substrate was the 9-element array and is shown in Figure 6.10. Its size and structure are comparable with both previous arrays given that he is compact and small.

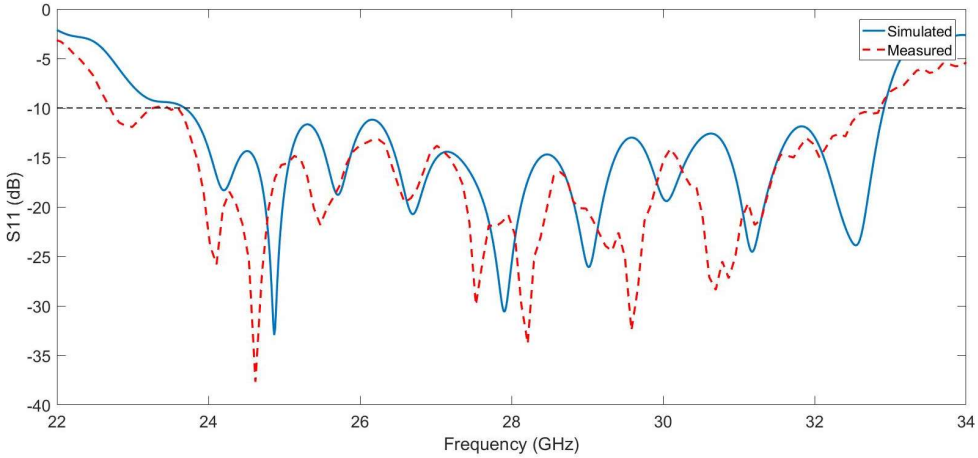

Figure 6.11: Comparison between the simulated and measured S11 of the 9-element array.

The 9-element S11 response is shown in Figure 6.11. Although the S11 responses are not the same, their overall response is reasonably equivalent.

The measurements indicate that the frequency of operation shifted. The bandwidth covered is 9.266 GHz, from 23.599 GHz to 32.865 GHz. In terms of fractional bandwidth, the value calculated is 0.328.

Making a comparison between the simulated fractional bandwidth, 0.326, and the measured one, the difference between them comes from the frequency shift since this means that the central frequency changes, altering this value.

In general, this S11 measured proves that this array works as intended and provides the desired capabilities for mmWaves applications.

6.3 MmWaves Arrays Results: Thicker Substrate case

To measure these arrays, and because the anechoic chamber of DETI does not work at this band of frequencies, it was used the anechoic chamber of IT. This chamber is not fully built, and due to this fact, the measurements taken on it have more inaccuracies.

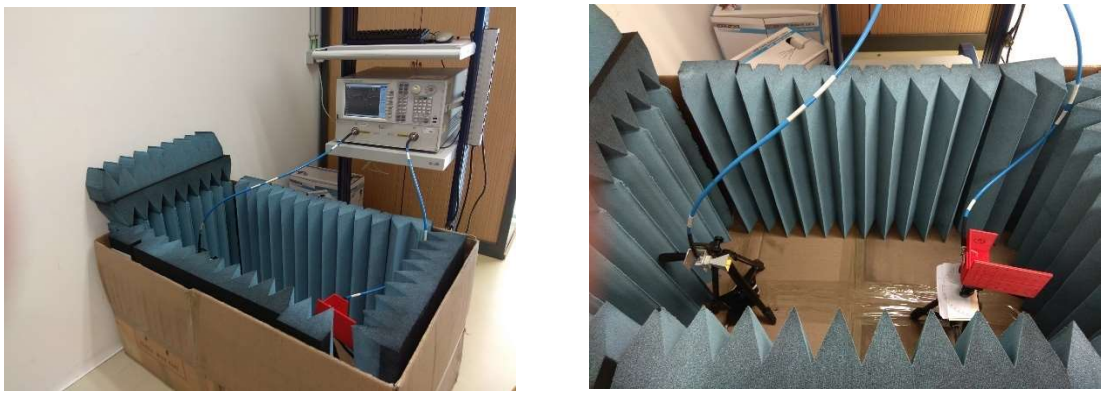

(a) (b)

Figure 6.12: Anechoic chamber used to measure the mmWaves arrays: (a) exterior view; (b) interior view.

Figure 6.12 displays the setup used to take the measurements. This is not the ideal system to measure the arrays. Regardless, this was the only setup available, so it had to be used. The range of angles measured started at -70° and stopped at 70° with an interval of 2° between points measured. The primary reason for this was the pressure that the cable imposes and that made it very difficult to rotate more the antenna.

6.3.1 5-element Array

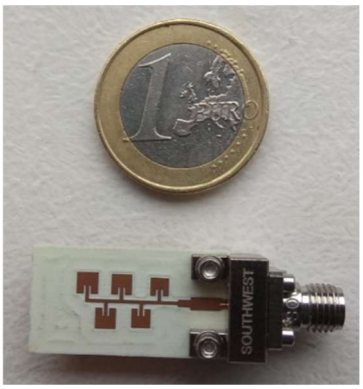

Figure 6.13: 5-element array for mmWaves applications made with the thicker substrate.

A demonstration of the 5-element is presented in Figure 6.13. Not surprisingly, the size of the structure is very small and compact, which is good to incorporate in everyday systems.

The first step to evaluate the performance of this array is to measure its S11 and compare with its simulated value to see if they correspond.

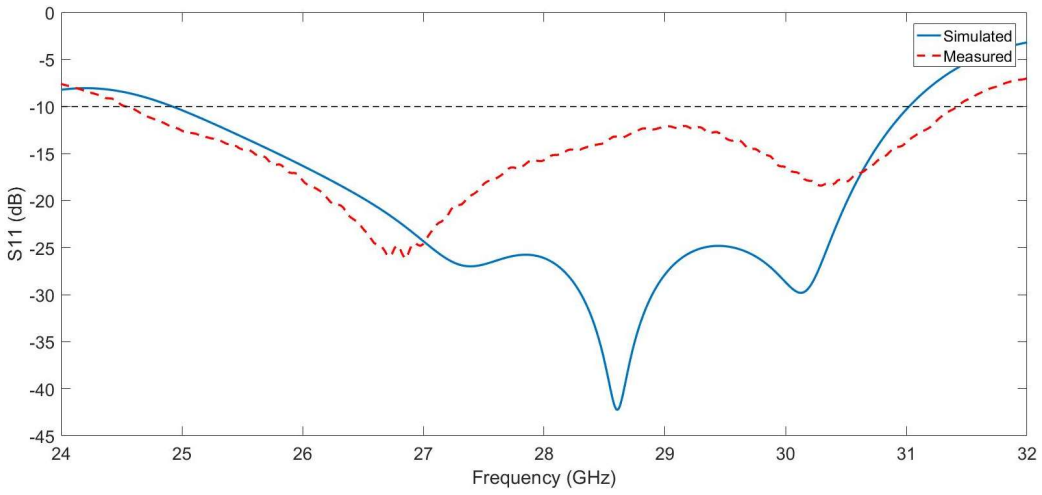

Figure 6.14: Comparison between Simulated and Measured S11 response of the 5-element array.

Through an examination of Figure 6.14, a difference in the S11 response is observed. One of the reasons for this to happen is the precision using in the simulation. During the simulations, the values used had four decimal points. However, this precision might not be achieved when printing the array, and this is the main reason for the difference in the S11 response.

Nonetheless, the measurement presents a good bandwidth, starting at 24.534 GHz and stopping at 31.423 GHz, which is equivalent to a fractional bandwidth of 0.246, meaning that is almost an ultra-wideband array.

This means that, in terms of bandwidth performance, the printed array has a better performance than the simulated, which is good since it is desired to cover as much bandwidth as possible.

Notwithstanding, the radiation patterns need to be measured to better characterize this array, in this case at 27 GHz, 28 GHz, and 29 GHz, since they were the values presented earlier.

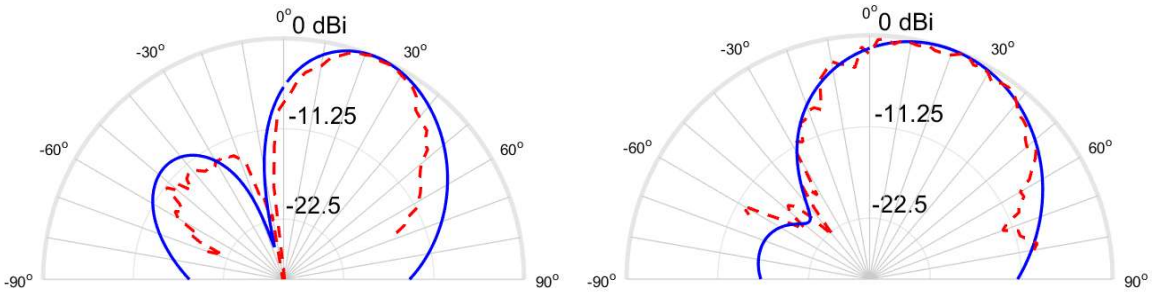

(a) (b)

Figure 6.15: Comparison between Simulated (Blue) and Measured (Red) radiation patterns of the 5-element array at 27 GHz in the planes: (a) φ=0°; (b) φ=90°.

Looking into Figure 6.15, it is seen that the measured and simulated polar diagrams at 27 GHz are similar, and because these measurements were made in an anechoic chamber that is not a perfect environment, these results are good, and a good match between simulation and practical results is observed.

When the patterns are measured, the gain can also be obtained using the equation (6.1). As explained before, the reference gain is the one presented in the plane φ = 0°, 9.88 dBi. Knowing this, the gain measured was 10.71. This indicates that the array has been misplaced relative to the reference antenna.

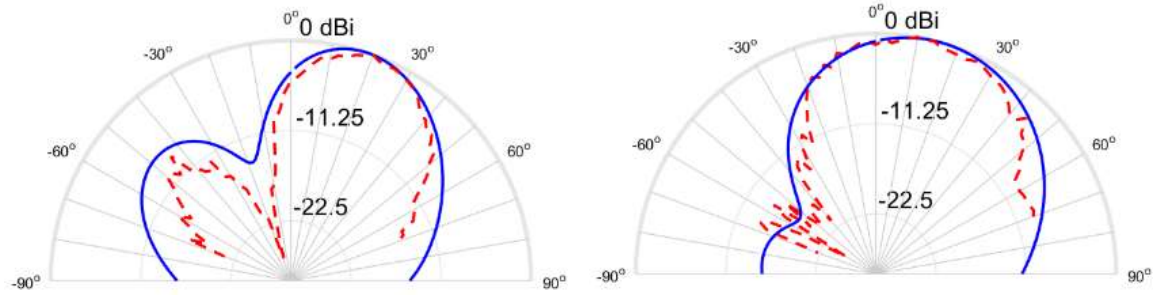

Figure 6.16: Comparison between Simulated (Blue) and Measured (Red) radiation patterns of the 5-element array at 28 GHz in the planes: (a) φ=0°; (b) φ=90°.

Figure 6.16 shows the behaviour at 28 GHz. As expected from the performance at 27 GHz, this array at 28 GHz continues to present an identical behaviour between simulated and measured values. This means that for both frequencies the array performs as intended.

At this frequency, the gain measured was 10.29 dBi, which is higher than the anticipated 9.61 dBi. After seeing the value measured at 27 GHz, this value is not abnormal since both patterns were measured at the same time, meaning that the same error occurred.

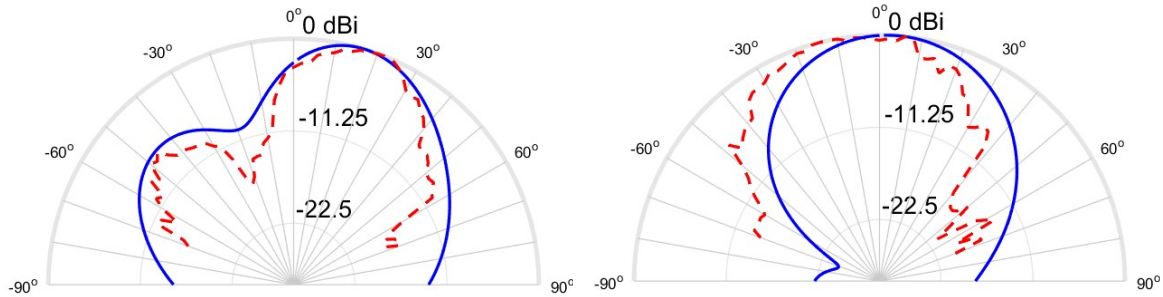

Figure 6.17: Comparison between Simulated (Blue) and Measured (Red) radiation patterns of the 5-element array at 29 GHz in the planes: (a) φ=0°; (b) φ=90°.

Lastly, Figure 6.17 demonstrates that in this array a correlation between simulation and measurements exists. Although the radiation patterns are not precisely matched, their behaviour is very similar. Maybe if the measurements have been taken in better environments this would be different.

Using equation (6.1) the gain was calculated. The value acquired was 9.48 dBi, meaning that a decrease happened, the expected value was 10.1 dBi happened. Since all gains were measured at the same time, the error in the measurements was similar.

In general, this array has good performance. The bandwidth is better than expected, the radiation patterns have a good similarity between simulation and measurements, and the gain obtained, although it is not exactly what was expected, is close to that value. Due to all this, the array performs very well and covers the expected needs that are intended for him.

6.3.2 7-element Array

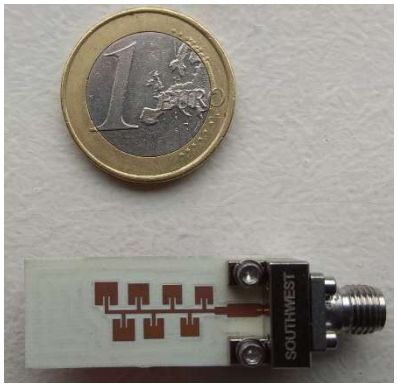

Figure 6.18: 7-element array for mmWaves applications made with the thicker substrate.

Figure 6.18 exhibits the 7-element array printed. In comparison with the previous structure this array is more extended, because of the two added elements, but a small and compact structure is maintained.

The evaluation of this array starts with measurements of S11 and compare this value with the simulation value provided by CST.

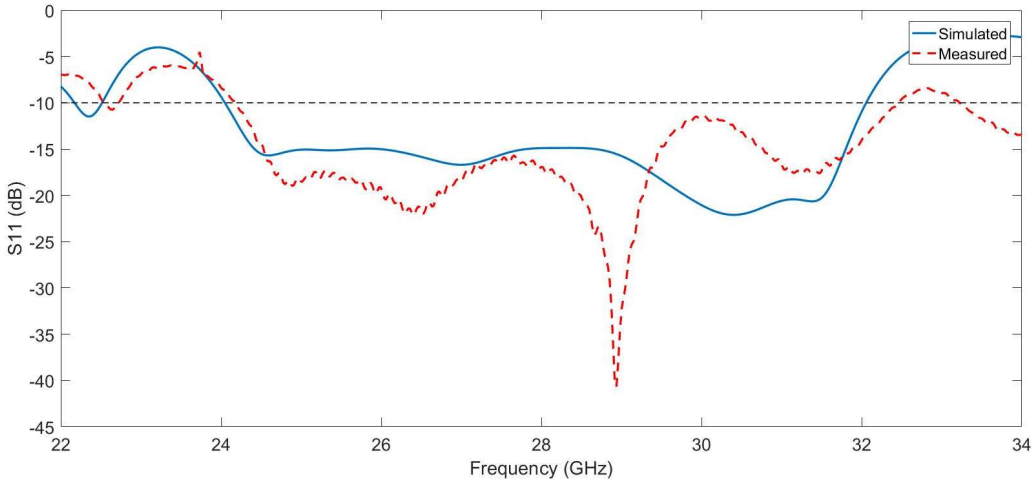

Figure 6.19: Comparison between Simulated and measured S11 responses of the 7-element array.

Observing Figure 6.19, some differences between the results are shown, beginning with a peak close to 29 GHz that did not appear before. Throughout the rest of the

frequency band the values vary, though these variations are normal. One last point observed is the fact that the upper limiting frequency is a lit bit higher.

The precision used in the simulation caused these factors. Just like in the previous case, the number of decimal points used in the simulation might not be achieved by the machine that printed the antenna, and that explains the difference.

Concerning the bandwidth covered, the measurements indicate that this array coverage starts at 24.183 GHz and goes until 32.465 GHz, that is equivalent to 0.292 of fractional bandwidth. This value is similar to the obtained in the simulation, it was 0.286, and the difference is caused by upper limiting frequency.

After seeing that the range of frequencies of this array has a match between simulated and measured values, it is time to observe its radiation patterns.

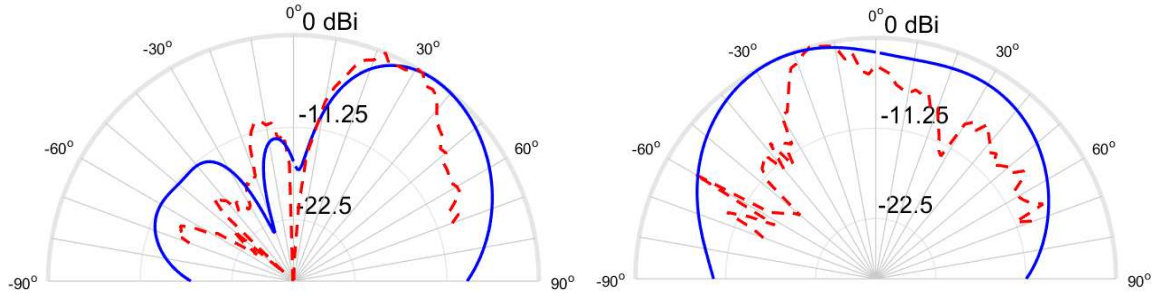

(a) (b)

Figure 6.20: Comparison between Simulated (Blue) and Measured (Red) radiation patterns of the 7-element array at 27 GHz in the planes: (a) φ=0°; (b) φ=90°.

In this case, there are some differences between results, especially in the case of the plane φ = 90°. The significant points of difference occur when the simulated values are low, meaning that in the peaks is when this is more noticeable.

For the plane φ = 0° there some similarities, and in general this plane seems to be comparable, the deviations exist due to an error when measuring.

On the other hand, the plane φ = 90° the difference between results is higher, since it can be seen in the 3D graph presented in Figure 5.32 that in this plane the values are very low, it is challenging to have this precision without a perfect anechoic chamber, and this is the principal fact causing the difference between the performances.

At this frequency, the maximum gain measured was 10.38 dBi. This value is higher than the expected 9.84 dBi from the plane φ = 0°, therefore, wrong positioning of the array

upon measuring explain this fact since this gain is closer to the maximum gain of the array at 27 GHz.

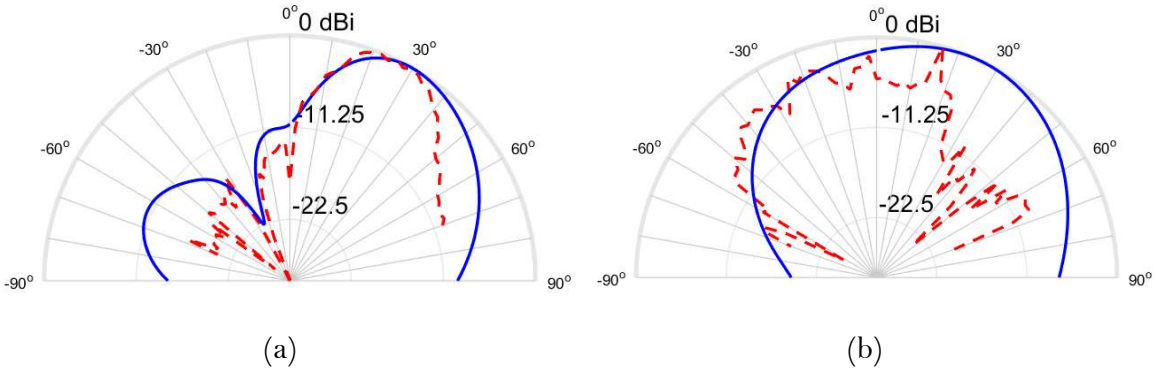

Figure 6.21: Comparison between Simulated (Blue) and Measured (Red) radiation patterns of the 7-element array at 28 GHz in the planes: (a) φ=0°; (b) φ=90°.

In Figure 6.21, the polar diagrams at 28 GHz are presented. These results seem to present similar problems like the ones at 27 GHz. When the value of the simulation is low, upon measuring a peak in that point occurs. Moreover, in the plane $\varphi = 90°$ the values measured are low throughout the plane, and this makes it difficult to measure. In general, the results at this frequency are similar to what was anticipated.

The measured gain was 10.09 dBi. This indicates that the array was not perfectly centred with the reference antenna since the gain measured is higher than gain in the plane $\varphi = 0°$, the gain should be 9.8 dBi.

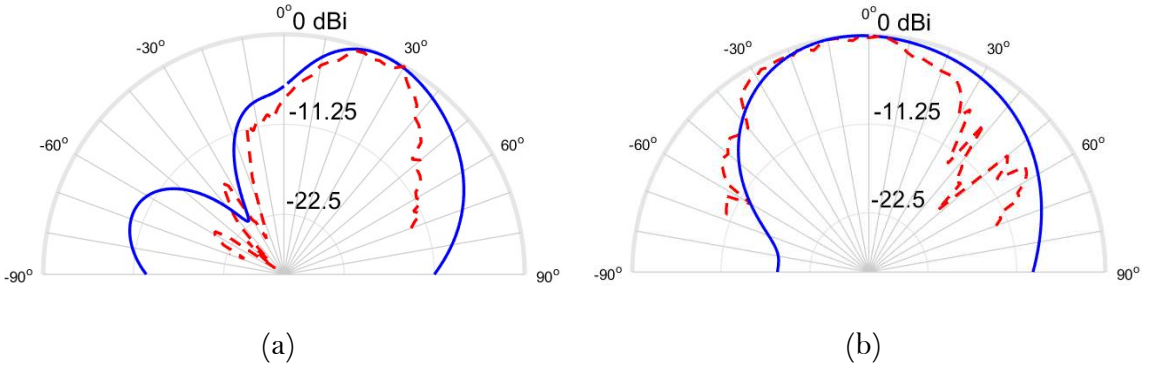

Figure 6.22: Comparison between Simulated (Blue) and Measured (Red) radiation patterns of the 7-element array at 29 GHz in the planes: (a) φ=0°; (b) φ=90°.

To finalize this array characterization Figure 6.22 presents the polar patterns at 29 GHz. Observing them one factor is confirmed, if the simulation results presented a low value, in the measurements a peak will appear.

In the plane φ =0° the results seem to have a match, and the array behaviour is identical to what was expected from him.

For the plane φ =90°, in this case, the values have a better match, and the format of the pattern is closer to what was the simulated pattern.

In general, these diagrams show a good resemblance taking into account the environment in which they were measured.

To finalize, the gain measured was 9.45 dBi. This value is higher than the gain in plane φ = 0°, 9.44 dBi. However, this value was anticipated since in both in both previous frequencies the same mistake occurred.

This array as excellent performance, even though some patterns differ from the simulated values, but the bandwidth covered is a little higher than expected, which is good, and the gain values are reasonable, their values are different from what was expected, but this happens due a bad positing of the array when measuring. Such a thing proves this array works as desired and is viable to be used.

6.3.3 9-element Array

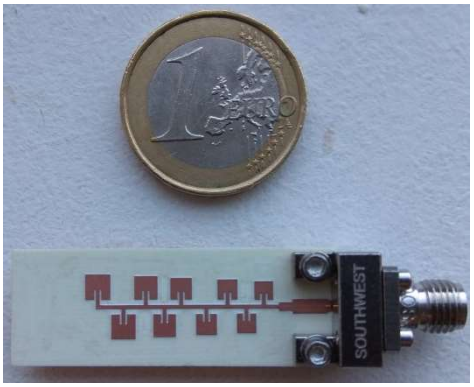

Figure 6.23: 9-element array for mmWaves applications made with the thicker substrate.

The 9-element array printed is presented in Figure 6.23. The structure is equal to the previous ones and maintains a small and compact composition.

As a starting point, the S11 of this array was measured and compared with its simulated performance, that representation is in Figure 6.24.

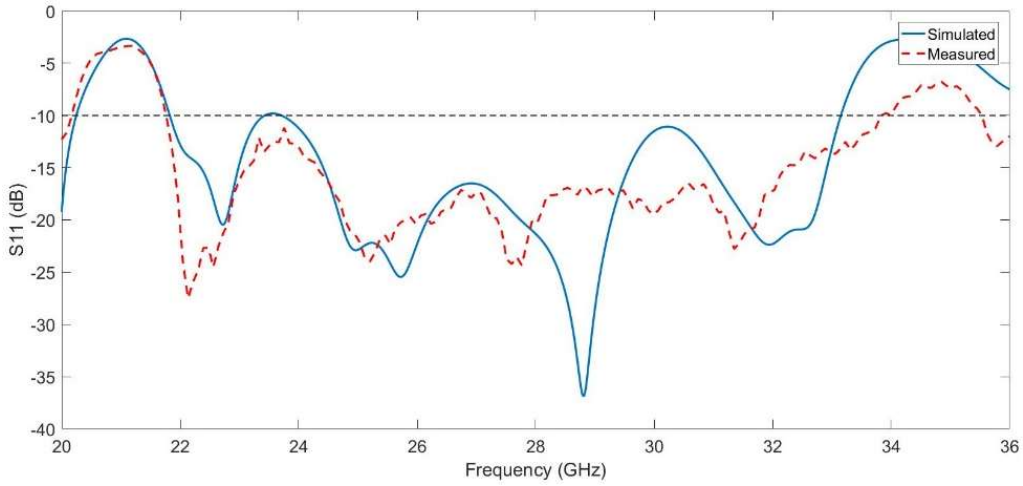

Figure 6.24: Comparison of the S11 simulated and measured of the 9-element array.

Comparing the results one thing is visible, the S11 measured covers more bandwidth than the simulated. This was expected since in both previous arrays of 5 and 7 elements the first half performance, lower than 28 GHz, improve in relation to the simulation. In this case, this improvement means that the peak that defined the start frequency is now below -10 dB. This is caused by imprecise printing.

The frequency range measured starts at 21.761 GHz and stops at 33.831 GHz, equivalent to 0.434 of fractional bandwidth, meaning that is an ultra-wideband array.

Since the array bandwidth was similar to what was simulated, the radiation patterns were measured to confirm if the array works appropriately. In the same manner as before, 27 GHz, 28 GHz and 29 GHz were the frequencies tested.

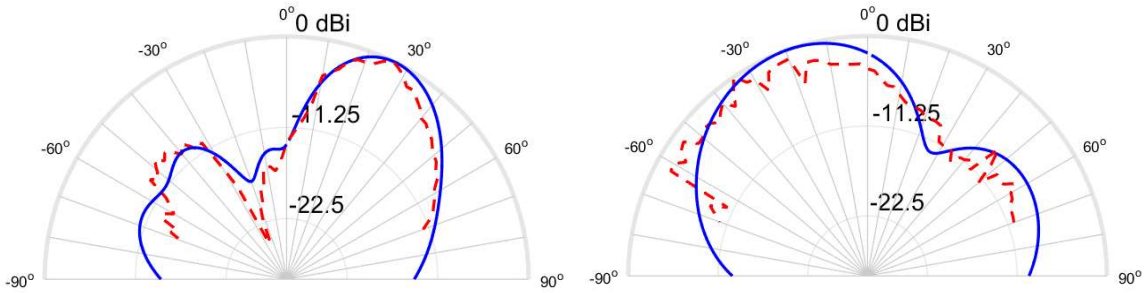

(a) (b)

Figure 6.25: Comparison between Simulated (Blue) and Measured (Red) radiation patterns of the 9-element array at 27 GHz in the planes: (a) φ=0°; (b) φ=90°.

Figure 6.25 shows the patterns of the array at 27 GHz. In this case, the patterns have a correspondence between simulated and measured values. This performance indicates that the array operates very similarly to the simulation.

Some points have a difference in the simulation value. Such a thing happens due to the imperfect environment upon measuring, that was demonstrated previously.

The maximum gain measured at this frequency was 10.72 dBi, which is close to the maximum gain of 11 dBi presented in the plane φ = 0°. This indicates that the measurements were performed accurately.

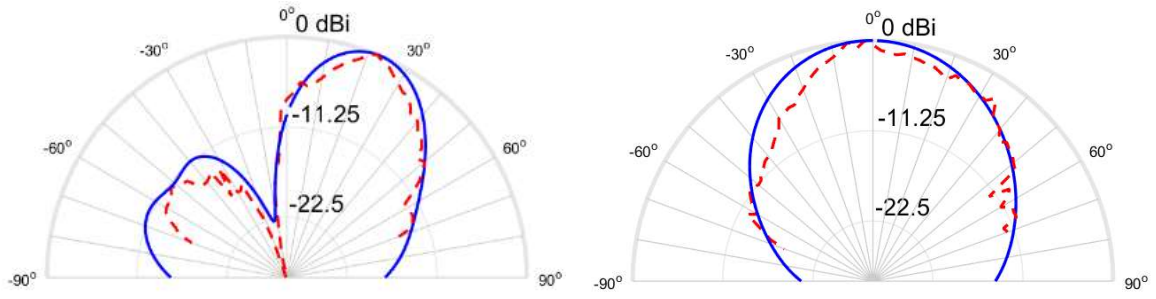

(a) (b)

Figure 6.26: Comparison between Simulated (Blue) and Measured (Red) radiation patterns of the 9-element array at 28 GHz in the planes: (a) φ=0°; (b) φ=90°.

At 28 GHz, Figure 6.26, a resemblance between the results is seen. One factor is still visible, if the pattern presents a peak, when measuring this aspect is accentuated, such is demonstrated in the plane φ = 0°.

The final issue in this pattern is the gain. At this frequency, the measurements gave a value of 11.1 dBi, which is close to the gain presented in the plane φ = 0°, 11.2 dBi. This indicates a similarity between the values measured and the ones simulated.

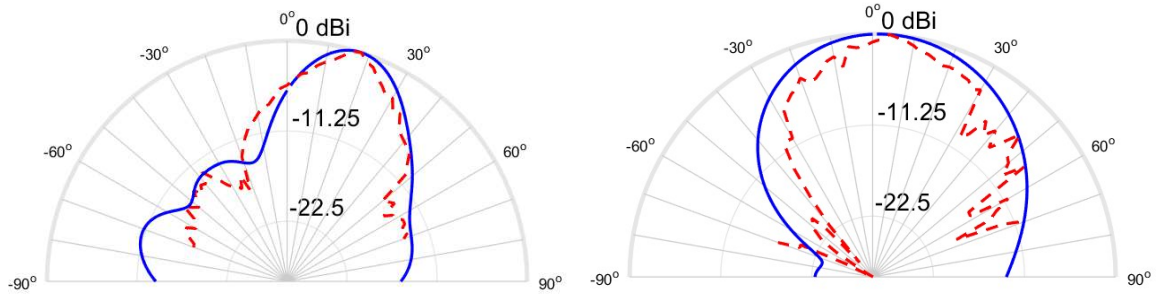

(a) (b)

Figure 6.27: Comparison between Simulated (Blue) and Measured (Red) radiation patterns of the 9-element array at 29 GHz in the planes: (a) φ=0°; (b) φ=90°.

To conclude, Figure 6.27 shows the radiation patterns at 29 GHz. In this case, the results seem to correspond. The difference between the format of the patterns is minimal, and only in the plane $\varphi = 90°$ there are some distinctive points.

The gain at this frequency is 10.71 dBi, meaning that is close to the maximum gain at the plane $\varphi = 0°$, 11.5 dBi.

In summary, these array simulation results are correspondent to the measured ones. Nonetheless, the S11 measured has a slight difference when compared with the simulated. This was expected since both previous arrays showed an improvement in the S11 in frequencies below 26 GHz.

Using this array in mmWaves applications is viable since a good gain performance is observed, covers a large bandwidth, and the patterns are adequate.

6.4 Discussion of the results obtained

During this dissertation, several arrays were produced with some differences in their implementation.

The first array was made as proof of concept. The intention behind this array was to create a designing method for the rest of the dissertation.

Nonetheless, the results obtained proved that the array designed can be applied in several wireless communication systems working in the C band, for example, with the gain presented and the bandwidth covered this array can be applied in satellite communications that exist in this band.

The results show excellent correspondence in terms of bandwidth and gain, although the polar patterns demonstrate a few differences between the simulation and measurements.

After validating the C band array and conceiving a logic methodology to construct arrays with this structure, the next step was to design arrays operating at mmWaves band.

For this band six arrays were made, three using a thicker substrate and three using a thinner substrate. Altering this parameter, and making a comparison between arrays, helped to fully understand the importance of the substrate in the design of microstrip antennas.

The objective behind making three arrays with each substrate was to see the effect caused by adding more patches to the array. Adding more patches should enhance the bandwidth while maintaining the other characteristics, or even improve them.

In the first case, when using the thinner substrate, the results were satisfactory since only the 7-element array had less bandwidth compared with the simulation results. The 5-element array achieved 0.191 of fractional bandwidth while the 7-element array had 0.247 and the 9-element array provided a bandwidth coverage of 0.328.

These results indicate that the array works as intend in their operation and, at least in terms of bandwidth, meets the requirements, in the case of the 9-element array surpasses the requirements because it is an ultra-wideband array.

Since these arrays were only evaluated in terms of bandwidth, there is not much more to say about them. With the late arrival of the substrate and the risk of breaking the arrays, some measurements were not performed. The major reason for this is the fact that the anechoic chamber is not the perfect environment to take measurements, with the significant difficulty being the pressure imposed by the cable in the structure.

In the second case, when using a thicker substrate, the results were very satisfactory, given that the bandwidth provided by each is higher than the one represented in the simulations. For instance, the 5-element array has a fractional bandwidth of 0.246, while the 7-element array covers 0.292, and the 9-element array achieves 0.434 of bandwidth.

Furthermore, the gain is similar to the expected from the simulations, even though in this case only the gains at the plane $\varphi = 0°$ at the frequencies of 27 GHz, 28 GHz, and 29 GHz were measured. The reason for this is that the main lobe of transmission varies in position throughout the frequency, and it is complicated to measure each specific frequency maximum gain.

Nevertheless, in the 5-element array, the gains measured were 10.71 dBi at 27 GHz, 10.29 dBi at 28 GHz, and 9.48 dBi at 29 GHz. The 7-element array presents a gain of 10.38 dBi at 27 GHz, 10.09 dBi at 28 GHz, and 9.45 dBi at 29 GHz. Finally, the 9-element array gains measured were 10.72 dBi at 27 GHz, 11.1 dBi at 28 GHz, and 10.71 dBi at 29 GHz.

Arrays and antennas with this gain characteristics and with the bandwidth coverage they possess are a good match for low earth orbit (LEO) constellations, especially the 9-element array since it is an ultra-wideband array with a good gain characteristic.

Comparing both structures in terms of bandwidth measured. It is seen that the array built with the thicker substrate covers more bandwidth than the others.

Table 6.1: Comparison between the fractional bandwidth measured values in both sets of arrays.

	5-element array Fractional Bandwidth	7-element array Fractional Bandwidth	9-element array Fractional Bandwidth
Thinner substrate	0.191	0.247	0.328
Thicker substrate	0.246	0.292	0.434

Using Table 6.1 to evaluate each substrate performance and analyze their behaviour. The thicker substrate is the best choice because the bandwidth covered is greater.

This factor should be the only comparing both structures. However, and seeing the gains measured in the thicker substrate case, these structures continue to provide a better characteristic in this factor since the gains calculated for them are higher than the ones presented in the simulations for the thinner substrate arrays.

Lastly, the array with the best overall performance is the 9-element array produced with the thicker substrate. The reason for this choice is the fact that this array behaves like an ultra-wideband array, meaning that surpasses the intended characteristics, and in terms of gain this array provides the necessary gain for several applications, for example, for LEO constellations.

One last consideration as to be pointed out, the fact that the environment where the measurements of the radiation patterns were performed is not ideal and repeating these measurements in a real anechoic chamber should be considered.

Chapter 7

7 Conclusions and Future Work

7.1 Conclusion

The principal objective of this dissertation was to design and test a wideband array operating in the mmWaves band. During this work, several aspects were considered to produce the best array possible.

Testing the various changes in the antenna arrays was necessary to understand all the implications that each component has in the array performance. In general, the alterations made pushed this structure close to its limit in terms of performance.

Recognizing that the migration to the mmWaves band is essential to implement the 5G systems, inside that topic, there are several applications where these arrays can be applied.

One topic that could benefit from them is the LEO constellations. Since these constellations intend to improve the speed of the communications, and in that sense, the use of wideband arrays means that more information can be transmitted, becoming a solution to be implemented in these systems.

From all the arrays produced the 9-element array produced with the thicker substrate is the best match to the applications mentioned above. The reason for choosing this array is the fact that it can cover 12,07 GHz of bandwidth, 0.434 of fractional bandwidth, and in most of its operating band the efficiency is good, implying that there are low losses in its operation, joining this with its workable gain values, turns this array into an proper match to LEO systems.

Nonetheless, all the other arrays possess good attributes, especially the ones produced with the thicker substrate. In the simulations, all of them fulfil the objective of being wideband arrays, and the measured S11 confirm this. In the case of the thicker

substrate, the polar diagrams measured are relatable to the simulation results, indicating that they also perform well in real life and not only in the simulation.

Overall, the results were successful and the primary goal of this dissertation was achieved. Several arrays were built to show various ways to improve their characteristics, and in the end, an ideal array was produced. Ultimately, these structures proved that they should be considered when designing antennas for LEO constellations operating in the mmWaves band.

7.2 Future Work

To further improve this work, four suggestions are made to enhance the results obtained:

- Repeat the radiation patterns measurements in a proper anechoic chamber to verify the results obtained.
- Development of a mathematical expression to calculate the distance between patches in this kind of structures, the expression would have as variables the central frequency, scaling factor and number of patches. Creating this expression would diminish the time necessary to produce an array with this structure.
- Test another substrate in which the antenna array can have a 50 Ω structure and maintain the gain values presented in the thicker substrate antenna arrays.
- Add more patches to improve the bandwidth further, while diminishing the scaling factor to guarantee a more constant gain and efficiency throughout the entire frequency range.

References

[1] Y. Huang and K. Boyle, *ANTENNAS : From theory to Practice.* .

[2] "Different Types of Wireless Communication Technologies." [Online]. Available: https://www.watelectronics.com/different-types-of-wireless-communication-technologies/. [Accessed: 29-Oct-2019].

[3] "What is Wireless Communications? - Definition from Techopedia." [Online]. Available: https://www.techopedia.com/definition/10062/wireless-communications. [Accessed: 29-Oct-2019].

[4] "Advantages of wireless communication,disadvantages of Wireless Communication." [Online]. Available: https://www.rfwireless-world.com/Terminology/Advantages-and-Disadvantages-of-wireless-communication.html. [Accessed: 29-Oct-2019].

[5] C. Balanis, *Antenna Theory Analysis and Design*. 2016.

[6] R. Cicchetti, E. Miozzi, and O. Testa, "Wideband and UWB antennas for wireless applications: A comprehensive review," *Int. J. Antennas Propag.*, vol. 2017, 2017.

[7] "First mobile phone: World's first call was an epic brag." [Online]. Available: https://www.news.com.au/technology/innovation/inventions/inside-story-of-the-worlds-first-mobile-phone-call/news-story/8f25cd59d136e2d6c3cbb0e4961de278. [Accessed: 29-Oct-2019].

[8] "Making 5G NR a reality Leading the technology innovations for a unified, more capable 5G air interface," 2016.

[9] "What Is 5G? What You Need to Know About the Next-Gen Network | Digital Trends." [Online]. Available: https://www.digitaltrends.com/mobile/what-is-5g/. [Accessed: 29-Oct-2019].

[10] "What is 5G? The business guide to next-generation wireless technology | ZDNet." [Online]. Available: https://www.zdnet.com/article/what-is-5g-the-business-guide-to-next-generation-wireless-technology/. [Accessed: 29-Oct-2019].

[11] "5G and smart cities: everything you need to know | TechRadar." [Online]. Available: https://www.techradar.com/news/5g-and-smart-cities-everything-you-need-to-know. [Accessed: 29-Oct-2019].

[12] "5G: A transformation in progress | ZDNet." [Online]. Available: https://www.zdnet.com/article/5g-a-transformation-in-progress/. [Accessed: 29-Oct-2019].

[13] "5G mmWave: facts and fictions you should definitely know." [Online]. Available: https://www.androidauthority.com/what-is-5g-mmwave-933631/. [Accessed: 29-Oct-2019].

[14] J. Xu, J. Yao, L. Wang, K. Wu, L. Chen, and W. Lou, "Revolution of Self-Organizing Network for 5G MmWave Small Cell Management: From Reactive to Proactive," *IEEE Wirel. Commun.*, vol. 25, no. 4, pp. 66–73, 2018.

[15] "Path Loss at Millimeter Wave Frequencies | RAYmaps." [Online]. Available: http://www.raymaps.com/index.php/path-loss-at-millimeter-wave-frequencies/. [Accessed: 29-Oct-2019].

[16] "NYU Wireless Director Theodore Rappaport Addresses Millimeter Waves And Engineering Education." [Online]. Available: https://www.electronicdesign.com/communications/interview-nyu-wireless-director-theodore-rappaport-addresses-millimeter-waves-and-eng. [Accessed: 29-Oct-2019].

[17] "Antenna Theory - Antenna Arrays - Tutorialspoint." [Online]. Available: https://www.tutorialspoint.com/antenna_theory/antenna_theory_arrays.htm. [Accessed: 30-Oct-2019].

[18] Aerospace and Electronic Systems IEEE Society, "IEEE Standard for Ultrawideband Radar Definitions IEEE Aerospace and Electronic Systems Society," no. May, 2007.

[19] "Antennas: Lecture two." [Online]. Available: http://bu.edu.eg/portal/uploads/Engineering, Shoubra/Electrical Engineering/2443/crs-12091/Files/me-lect2.pdf. [Accessed: 30-Oct-2019].

[20] "Understanding antenna gain – RCExplorer." [Online]. Available: https://rcexplorer.se/projects/2009/06/understanding-antenna-gain/. [Accessed: 30-Oct-2019].

[21] F. Sabath, E. L. Mokole, and S. N. Samaddar, "Definition and classification of ultra-wideband signals and devices," *Radio Sci. Bull.*, vol. 313, no. 313, pp. 12–26, 2005.

[22] M. Abri, F. T. Bendimerad, and M. Bousahla, "A Log Periodic Series-Fed Antennas Array Design Using A Simple Transmission Line Model," vol. 2, no. 3, pp. 161–169,

2009.

[23] M. Abri, H. Abri Badaoui, M. A. Belhadi, and I. Kalai, "Log periodic bow-tie antennas (LPA) design using the transmission line model," *J. Radio Electron.*, no. 7, p. 19-p., 2012.

[24] K. Pojang and P. Rakluea, "The Design of Log Periodic Dipole Array Antenna for WLAN/LTE/UWB Applications," *Isc. 2018 - 18th Int. Symp. Commun. Inf. Technol.*, vol. 7, no. Iscit, pp. 16–21, 2018.

[25] E. Li, X. J. Li, B. C. Seet, and X. Lin, "Flexible Ink-printable Wideband Log-periodic Dipole Array Antenna for 5G Applications," *Proc. 2018 IEEE 7th Asia-Pacific Conf. Antennas Propagation, APCAP 2018*, no. 2, pp. 206–207, 2018.

[26] Z. Tu, G. Q. Zhang, D. F. Zhou, and F. Xing, "A wideband elliptic printed dipole antenna array," *Proc. - 2011 4th IEEE Int. Symp. Microwave, Antenna, Propag. EMC Technol. Wirel. Commun. MAPE 2011*, pp. 68–70, 2011.

[27] A. Kakkar, R. Singh, N. Nirdosh, and M. R. Tripathy, "A Wideband U-Slotted 1×2 Array Antenna for Energy Harvesting," *2018 5th Int. Conf. Signal Process. Integr. Networks, SPIN 2018*, pp. 232–235, 2018.

[28] M. H. B. Ucar, A. Sondas, and Y. E. Erdemli, "Design of 2x2 UWB printed antenna array for see-through-wall imaging," *CEM 2013 - Comput. Electromagn. Int. Work.*, pp. 26–27, 2013.

[29] H. Aslani and A. Radwan, "Modified step size patch array antenna for UWB wireless applications," *Int. Conf. Multimed. Comput. Syst. -Proceedings*, pp. 765–769, 2017.

[30] F. N. M. Isa and P. V. Brennan, "Design of a high gain and Ultra Wideband Microstrip Array Antenna for Avalanche Radar," 2011, pp. 1–38.

[31] L. Yang, J. D. Zhang, and W. Wu, "Wideband microstrip series-fed magnetic dipole array antenna," *Electron. Lett.*, vol. 50, no. 24, pp. 1793–1795, 2014.

[32] C. Deng, Y. Li, Z. Zhang, and Z. Feng, "A wideband sequential-phase fed circularly polarized patch array," *IEEE Trans. Antennas Propag.*, vol. 62, no. 7, pp. 3890–3893, 2014.

[33] M. Karahan, E. Aksoy, and D. S. A. Sahinkaya, "Design of wideband conformal antenna array at X-band for satellite applications," *RAST 2015 - Proc. 7th Int. Conf. Recent Adv. Sp. Technol.*, pp. 397–400, 2015.

[34] S. F. Jilani and A. Alomainy, "Millimeter-wave conformal antenna array for 5G wireless applications," *2017 IEEE Antennas Propag. Soc. Int. Symp. Proc.*, vol. 2017-

Janua, pp. 1439–1440, 2017.

[35] M. Khalily, R. Tafazolli, P. Xiao, and A. A. Kishk, "Broadband mm-Wave Microstrip Array Antenna with Improved Radiation Characteristics for Different 5G Applications," *IEEE Trans. Antennas Propag.*, vol. 66, no. 9, pp. 4641–4647, 2018.

[36] A. Hassanien, W. Swelam, and M. H. A. El Azeem, "16x8 wideband microstrip planar array antenna for E-band millimeter-wave 5G high speed WLAN and broadband internet applications," *2017 IEEE Antennas Propag. Soc. Int. Symp. Proc.*, vol. 2017-Janua, pp. 2613–2614, 2017.

[37] M. K. A. Rahim and P. Gardner, "Active microstrip log periodic antenna," *2004 RF Microw. Conf. RFM 2004 - Proc.*, pp. 136–139, 2004.

[38] M. K. A. Rahim and P. Gardner, "Microstrip log periodic antenna using circuit simulator," *ISAPE 2003 - 2003 6th Int. Symp. Antennas, Propag. EM Theory, Proc.*, pp. 202–205, 2003.

[39] "Log Periodic Antenna | LPDA Aerial Array | Electronics Notes." [Online]. Available: https://www.electronics-notes.com/articles/antennas-propagation/log-periodic-lpda-antenna/log-periodic-basics.php. [Accessed: 13-Nov-2019].

[40] "Automatic optimization | CST Studio Suite." [Online]. Available: https://www.3ds.com/products-services/simulia/products/cst-studio-suite/optimization/. [Accessed: 18-Nov-2019].

[41] A. Pcr and L. Kit, "RO4725JXR™ RO4730JXR™ & RO4730G3™ Antenna Grade Laminates," 2012.

[42] R. C. Advanced Circuit Materials Division, "RO4000 ® Series High Frequency Circuit Materials Some Typical Applications :," 2006.